NASA CR-72408

AN INVESTIGATION OF FLUORINE-HYDROGEN MAIN TANK INJECTION PRESSURIZATION

by

E. C. Cady

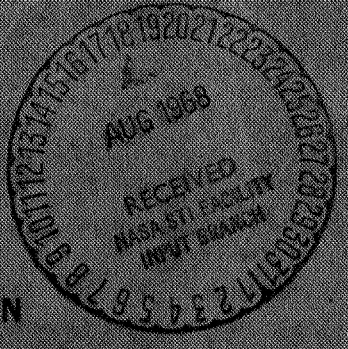

prepared for

NATIONAL AERONAUTICS AND SPACE ADMINISTRATION

CONTRACT NAS 3-7963

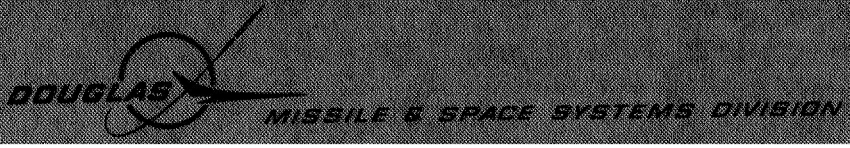

NASA CR-72408
DAC-62233

FINAL REPORT

AN INVESTIGATION OF FLUORINE-HYDROGEN MAIN TANK INJECTION PRESSURIZATION

by

E. C. Cady

prepared for

NATIONAL AERONAUTICS AND SPACE ADMINISTRATION

30 April 1968

CONTRACT NAS 3-7963

Technical Management
NASA Lewis Research Center
Cleveland, Ohio
Erwin A. Edelman

Douglas Aircraft Company
Missile and Space Systems Division
Santa Monica, California

FOREWORD

This report was prepared by the Douglas Aircraft Company under Contract NAS 3-7963. The contract is administered by the National Aeronautics and Space Administration, Lewis Research Center, Chemical and Nuclear Rocket Procurement Section, Cleveland, Ohio. The NASA Project Manager for the contract is Mr. E. A. Edelman. This is the Final Report on the contract, and it summarizes the technical effort from 31 July 1967 to 30 April 1968.

The contribution of W. G. Black and W. J. Wachtler, Douglas Aircraft Company, to the technical effort described in this report is gratefully acknowledged.

ABSTRACT

An experimental program is described that determined the feasibility and operating characteristics of Main Tank Injection of a LH_2 tank with F_2. A small-scale test program determined hypergolicity limits and is reported in an interim report. The large-scale test program to evaluate four and to design and test three F_2 injectors is described. Both pressurization and LH_2 expulsion were performed with a 105-gallon high-pressure LH_2 tank. The injector efficiency, design criteria, and performance limitations were determined. Reliable ignition, effective tank pressure control, and feasibility of the F_2-H_2 MTI pressurization technique were demonstrated.

CONTENTS

FIGURES

TABLES

SYMBOLS

A = Area

C = Orifice flow coefficient

C_A = Coefficient defined as (βA_{g_1}) actual/(βA_{g_1}) ideal

C_d = Discharge coefficient

C_p = Molar specific heat at constant pressure

C_v = Molar specific heat at constant volume

C_w = Coefficient defined as $(\dot{W}_L)$ actual/$(\dot{W}_L)$ ideal

d = Characteristic dimension in the injector or diameter

g = Gravitational constant

h = Heat transfer coefficient

K = Flow resistance coefficient

$\overline{K}$ = Thermal conductivity

L = Length

M = Mach number

$\overline{M}$ = Mass

m = Molecular weight

p = Pressure

$\dot{\Delta}P$ = Pressure rise rate

Q = Heat

Q_R = Heat of reaction

Q_V = Heat of vaporization

R = Gas constant

t = Time

T = Temperature

U = Velocity

V = Volume

$\dot{W}$ = Weight flow rate

Y = Compressible flow expansion factor

ΔZ = Head difference

β = Pumping area ratio - A_{L_1}/A_{g_1}

γ = Ratio of specific heats

λ = Pumping flow rate ratio - $\dot{W}_L/\dot{W}_g$

ρ = Density

μ = Viscosity

Subscripts

o = Total conditions

1 = Conditions at Station 1

2 = Conditions at Station 2

g = Gas conditions

L = Liquid conditions

b = Ullage conditions

r = Orifice conditions

SUMMARY

A comprehensive program was performed to design and test F_2 injectors for Main Tank Injection (MTI) of the LH_2 tank of a space vehicle. A series of 131 tests in small (5-in. diam x 10-in.) glass Dewars defined the limits of hypergolicity and the reaction product freezing. A series of 21 tests was performed with full-scale injectors in a 105-gal LH_2 tank to demonstrate the feasibility of the pressurization technique, to determine pressurization efficiency of three injector configurations: (1) ullage/simple (US), (2) submerged/aspirated (SA), (3) submerged/simple (SS), and to define tank pressure control limits. The tests were performed with tank expulsion pressures from 30 to 170 psig, F_2 flow rates from 0.001 to 0.01 lb/sec, and ullage fractions from 8 to 97% for multiple prepressurization and expulsion cycles.

The following results were noted:

(1) The US injector exhibited reliable ignition and efficient pressurization through ullage heating. Heat transfer losses reduced the pressurization efficiency at large ullage fractions.

(2) The SA injector did not properly pump (aspirate) sufficient LH_2 to provide pressurization through LH_2 vaporization. Rather, it operated very oxidizer-rich and hot; this led to severe injector damage. The pressurization efficiency was generally lower than the US mode, although at large ullage fractions (empty tank) the SA efficiency approached that of the US mode.

(3) The SS injector exhibited very low pressurization efficiency with a full tank, but efficiency approached that of the US mode as the tank emptied. At high injection pressures, the efficiency approached that of the US mode at lower ullage fractions (40% empty). The submerged injectors experienced occasional injectant freezing and detonation; these problems were eliminated by injector redesign.

(4) The pressurization data was correlated to simple pressurization models and injector design requirements were established. The feasibility and controllability of the MTI pressurization technique was demonstrated.

INTRODUCTION

Main Tank Injection (MTI) is a technique for rocket-vehicle propellant-tank pressurization in which a hypergolic reactant is injected into a propellant tank, and the resultant reaction heat release pressurizes the tank. Although much previous work had been done with MTI as applied to hypergolic storable propellants, little has been done with the hypergolic cryogenic propellants fluorine and hydrogen. The objective of the NASA-sponsored (Contract NAS 3-7963) program described herein was to determine, analytically and experimentally, the feasibility, limitations, and operating characteristics of a propellant tank pressurization system that uses the injection of fluorine into a liquid hydrogen tank to generate pressurizing gas by hydrogen vaporization. The program was in two phases: small-scale glass apparatus testing, and large-scale pressurization and expulsion testing.

The initial phase was reported in an interim report, NASA CR-72253. * This phase was an experimental study (encompassing a comprehensive series of 131 tests) of two problems peculiar to this cryogenic hypergolic system: 1) the effect that a number of physical and chemical variables have on the hypergolicity of fluorine injected into a liquid hydrogen tank and 2) the characteristics and behavior of the reaction products as they freeze in the hydrogen tank. The physical variables included injector location (ullage-space injection and submerged injection); F_2 phase (ambient gas, liquid, and saturated vapor), temperature (140° to 520°R), and pressure (65 to 195 psia); and H_2 condition (saturated at 25 to 55 psia). Chemical variables included propellant contaminants and catalytic effects. The tests were performed in small (5 in. diam by 10 in.) glass Dewars, with pressure and temperature measurements and Fastax movies (at 4000 pictures/sec) taken of each test. Expulsion of the LH_2 from the tank was not performed. The apparatus for the small-scale tests in shown in fig. 1.

The results of this initial effort led to the following conclusions:

(1) Fluorine and hydrogen are generally hypergolic under the conditions that are present when MTI is used to pressurize a hydrogen tank. These propellants normally ignite reliably and have a smooth pressure rise; however, in the simple ullage injection mode (US),

*Cady, E. C. Hypergolicity of F_2-H_2 and Reaction Product Freezing Under Main Tank Injection Pressurization Conditions. NASA CR-72253 (DAC-60975) 15 September 1967.

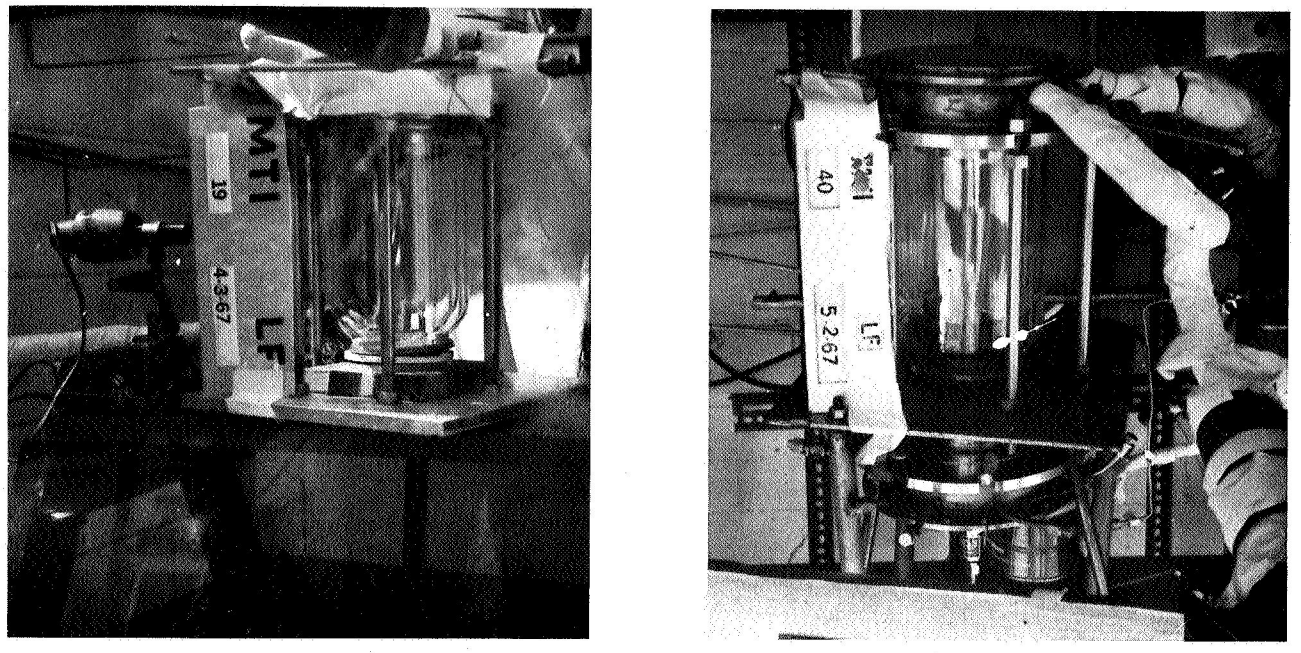

(A) ULLAGE INJECTION

(B) SUBMERGED INJECTION

Figure 1. Small-Scale Test Setups

it was found that the addition of about 1 % vol oxygen to the injectant fluorine caused reaction inhibition. An increased injectant total enthalpy (warming) was required to overcome this inhibition and enable ignition before the injectant could freeze. In the simple-submerged (SS) and simple-aspirated (SA) injection modes, a helium pre-injection purge gave an inhibition that was similar to that of US, but helped to alleviate the problem of HF freezing in the injector. With the helium pre-purge omitted, the hydrogen-fluorine ignition was reliable in these modes even when oxygen was added to the injectant.

(2) Injection of fluorine in the low-total-enthalpy state (liquid or cold gas) in any injection mode was hazardous, because of reaction inhibition, fluorine freezing, and destructive detonation. Particularly in the submerged mode, frozen HF tended to plug the injector. Despite these problems, the reliability of this pressurization technique was demonstrated in the small-scale glassware tests to the extent that full-scale tests of MTI pressurization could be undertaken with confidence.

(3) Preliminary vessel pressurization results indicated that the ullage injection mode tended to pressurize the tank by ullage heating rather than by vaporization of hydrogen (as specified in the program objectives). The submerged injection mode, however, did tend to pressurize the tank by hydrogen vaporization.

This report presents the results of the large-scale injector design, fabrication, and testing in a 105-gal, high-pressure, liquid-hydrogen tank. This phase of the program had the following requirements:

(1) Injector Design and Fabrication — Based on the data obtained from the small-scale glassware tests, evaluate the large-scale injection concepts that are suitable for a rocket liquid-hydrogen tank. These concepts included submerged injection with and without the use of aspiration of liquid hydrogen for combustion control and vaporization and ullage-space injection with and without the use of aspirators. Based on consideration of all pertinent injection and system variables, four injection system designs are to be selected and submitted for NASA approval and, upon approval, are to be fabricated and tested.

(2) Injector Testing — Test each of the approved injection concepts to demonstrate reliable ignition, pressurization, and LH_2 expulsion. The test variables are to include reactant flow rate, initial ullage pressure, and amount of ullage. Tank pressure control limitations, quantity of fluorine required, and expulsion rate for partial and complete expulsions are to be determined. Injector design parameters are to be varied to assure reliable operation.

The specific test requirements for the injector testing included a matrix of tests with each injector at conditions including:

Tank pressures from 30 to 170 psig for prepressurization and expulsion

Fluorine flow rates from 0.001 to 0.010 lb/sec

Initial and intermediate ullage levels from 8 to 97%

Multiple expulsions and prepressurizations (1 to 4 draining cycles)

INJECTOR DESIGN

General Considerations--Each of the injection concepts described in the Introduction was tested during the small-scale test program, and the results formed the foundation for the full-scale injector design. The concepts are described as (1) simple ullage-space injection (US), (2) aspirated ullage-space injection (UA), (3) simple submerged injection (SS), and (4) aspirated submerged injection (SA). "Aspirated," as used here, means that the injected fluorine is used to jet-pump hydrogen into a combustion zone that is separate from the pumping region.

Specific small-scale test results that are applicable to each of the concepts are described below, but other criteria, applicable in general, were also determined. Principal among these was the problem of injectant detonation noted in the small-scale tests, which gave rise to a basic rule: every reasonable technique must be used to avoid injectant freezing and detonation. A basic consequence of this requirement was that the fluorine injectant for the full-scale program be limited to the use of high-pressure, ambient-temperature gas. Although this requirement may restrict the eventual vehicular application of the system, it is necessary from a safety standpoint; further, some injectant warming can be readily obtained in a vehicular application with only a small cost to system performance (weight).

The pressurization data from the small-scale tests was also of particular interest, even though it was highly volume-dependent and was based on "slug-injection" of a specific quantity of fluorine rather than steady-flow injection of fluorine. It was found that the maximum small-scale pressurization rate, when computed for continuous injection into a full-scale tank (with ullage volume of 5.8 ft^3) gave a predicted pressure-rise rate in the full-scale tests of 10 psi/sec. This rate was high enough to simulate advanced vehicle requirements, yet low enough for effective manual control, and meant that the same injector valve, orifices, and plumbing configuration used for the small-scale glassware tests could be used for full-scale tests.

Ullage Injector Design--The US injection technique was extensively tested in the small-scale tests, because it showed pressurization system advantages for advanced vehicle missions. For example, it was found that US injection effectively heats the ullage gases, gives maximum pressure rise per weight of injectant and, for the final engine burn of a mission, leaves the LH_2 tank full of hot GH_2, which results in minimum residual propellant weight. The US injector, as used for the full-scale tests, is shown in fig. 2. The injector is a simple tube, on the tank centerline, with no diffusers or "splash plates." This configuration was used because the injected fluorine occasionally ignited

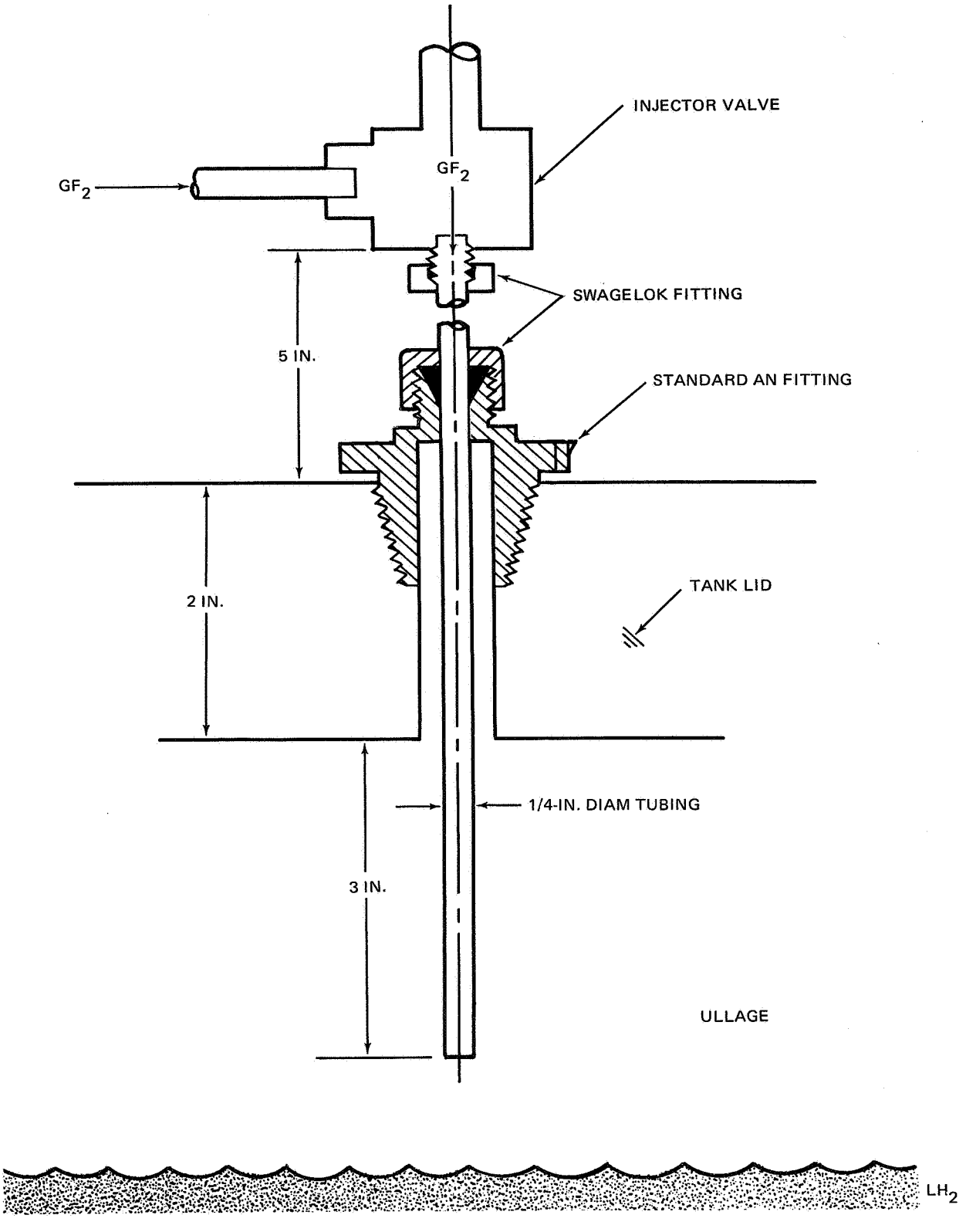

Figure 2. US Injector Configuration

at the LH_2 surface during the small-scale tests, and it was initially thought that the presence of a splash-plate might inhibit reliable ignition.

The UA injection technique (fig. 3a) was designed to pump (by aspiration) the proper amount of GH_2 to mix with the injectant and burn so that hot GH_2 of the proper temperature would be generated to pressurize the tank. The dimensions of the configuration shown were determined from the aspirator analysis of Appendix A. If the reaction flame occurs at the fluorine injector tip, aspiration cannot occur, and the injection is indistinguishable from the US mode. Several tests with this UA injector configuration were included in the small-scale glass tests to evaluate this mode. In these tests, there was no tendency for the injector to aspirate and the injector behaved exactly as a US injector. This injection mode was not recommended for full-scale testing because it demonstrated no pressurization or system advantages when compared to the US mode.

Submerged Injector Design--The concepts of submerged injection, including SS and SA, were extensively evaluated during the small-scale tests, and the results showed that both these techniques tended to provide tank pressurization by vaporizing hydrogen, which was a fundamental requirement of the program. However, during these small-scale tests, the SS mode appeared to have the following disadvantages when compared to the SA mode:

(1) The injectant burns at an uncontrollable mixture ratio that produces indeterminate ullage heating levels, and unpredictable pressurization rates.

(2) Subsurface burning creates large bubbles that may interfere with normal propellant draining.

(3) The large bubbles (2, above) may also severely disturb (slosh) the propellant and cause an undesirable transfer of large quantities of heat to the bulk liquid.

Based on these considerations, the SS configuration (shown in fig. 3b) was not initially recommended for full-scale testing; however, a number of SS-mode tests were made that are discussed further in Results.

Proper design of the SA injector for the full-scale testing presented a difficult problem. The initial SA injector small-scale test data and the motion pictures indicated that there was considerable reverse flow of fluorine through the pumping annulus into region A (fig. 3c) in this configuration. This reverse flow caused ignition and burning in this base region with a subsequent interruption of aspiration (pumping) of the LH_2. This effect was attributed to two causes. First, the pumping area for the LH_2 was apparently too large, allowing the F_2 static pressure to overcome the LH_2 static pressure in the annulus and reverse the LH_2 flow direction. Second, the flow tube was too large; this allowed an expansion and slowing of the injectant to a velocity that was less than the flame velocity, and this caused the flame to persist in the base region. To eliminate fluorine reverse

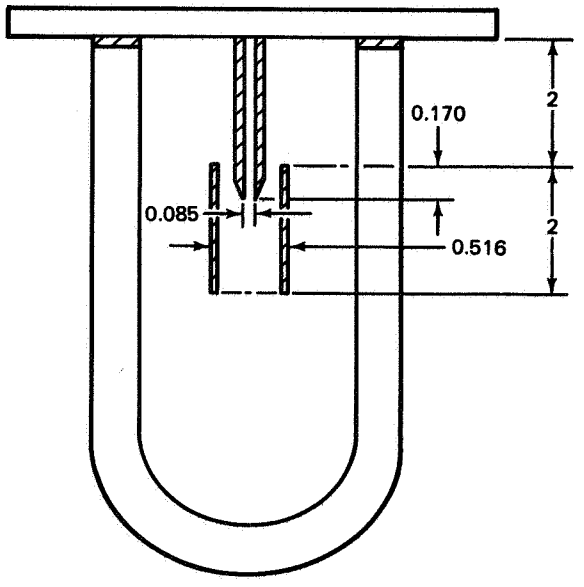

(a) UA INJECTOR CONCEPT

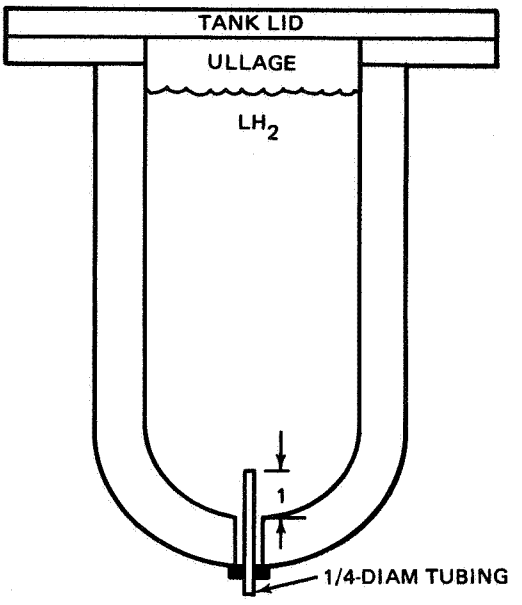

(b) SS INJECTOR CONFIGURATION

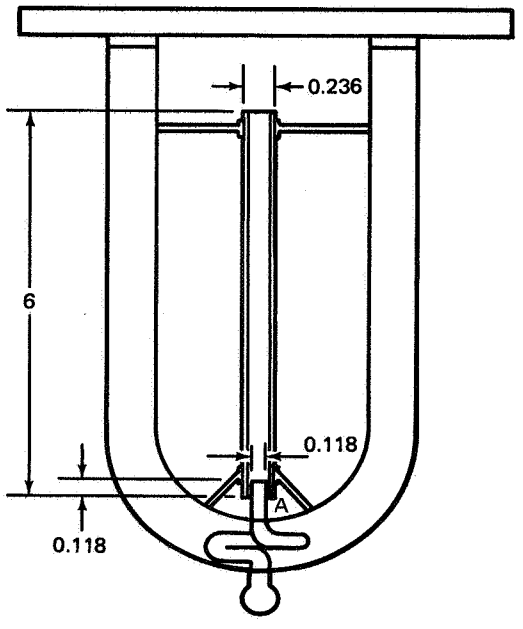

(c) SA INJECTOR – CONFIGURATION NO. 1

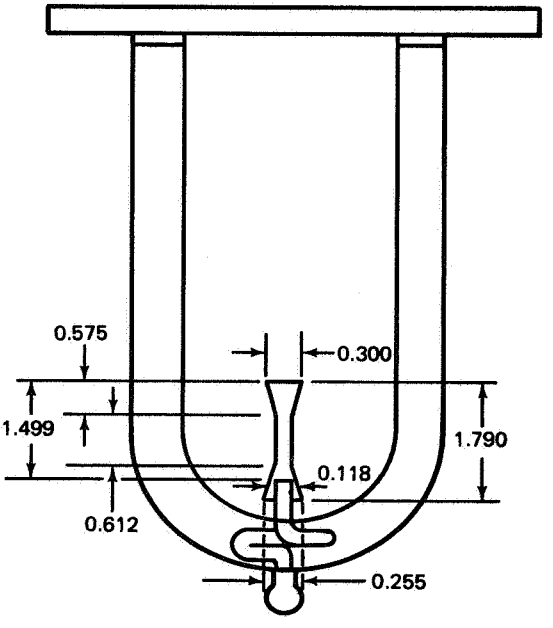

(d) SA INJECTOR – CONFIGURATION NO. 2

NOTE: ALL DIMENSIONS ARE IN INCHES

Figure 3. **Other Injector Configuration**

flow, and thus eliminate base burning, a separation of the burning region from the pumping region was necessary. This separation could be accomplished by three means:

(1) Changing the size and ratio of the F_2 and LH_2 flow areas to provide proper pumping.

(2) Decreasing the area of the aspirator tube so that the injectant flow velocity was higher than the flame velocity. (This would cause the flame to be ejected from the pumping region.)

(3) Increasing the area of the aspirator tube near the ullage to decelerate the flow velocity to match the flame velocity. (The flame should be stable at the point where the velocities are matched.)

A modified aspirator was designed according to these principles and tested in the small-scale tests. The configuration is shown in fig. 3d. The diameter of the straight section was made the same as that of the F_2 inlet, because it was known that under all test conditions the gas velocity in the F_2 inlet tube was higher than the flame velocity. (Subsequent analysis of all small-scale tests showed that the flame velocity was approximately 130 ft/sec.)

The small-scale tests with this injector design gave very encouraging results. Fluorine reverse flow was minimized (although it occurred to some degree, particularly at high injection pressures) and base burning was limited to about 5 msec, when the flame was in transit through the aspirator. As planned, the flame passed through the tube to the expanding section, where it was stable for the duration of the injection. The small amount of reverse F_2 flow that occurred was attributed to inaccurate fabrication in this small scale and to a transient high-pressure surge at the start of injection.

The success of these small-scale tests indicated that a full-scale SA injector could probably be designed that would aspirate and pump enough LH_2 to provide fuel-rich operation and thus ensure effective vaporization and pressurization. To this end, the fluid dynamics of the SA injector were analyzed to provide basic design data for the full-scale injector.

Previous analyses of aspirators or jet pumps in the literature* were unsuitable, because they consider only gas-pumping-gas in a different configuration. An approximate analytical model was developed, therefore, to predict the performance of a gas-pumping-liquid aspirator. Based on the initial analysis, the full-scale SA injector was designed and fabricated. The analysis was modified to reflect the actual injector configuration, and the injector was tested with simulated propellants (gaseous nitrogen and water) to map the actual injector pumping performance. Appendix A describes the

*Van Der Lingen: A Jet Pump Design Theory. Transactions of the ASME, Journal of Basic Engineering. December 1960, pp 947-960.

complete SA injector analysis and development, including the initial analysis, the water test results, the modified analysis, and the predicted injector performance.

Based on the initial results of the analysis and on the small-scale testing results, an SA injector was designed for the full-scale testing. The injector configuration is shown in fig. 4. The salient features of the design are as follows:

(1) The pumping region is capable of adjusting the pumping area ratio (β) from 0 to about 3. This is accomplished by turning the retainer on the threaded stem to move the external cone closer to or farther from the internal fluorine nozzle cone, thus varying the LH_2 flow area. The retainer can be locked at a given setting with a jamnut.

(2) The 10° cones used for the LH_2 flow path give minimum practical flow impingement and can be fabricated in either pyrex or metal injector configurations (10° is the standard taper angle for pyrex laboratory ware). The retainer also accurately centers the cones.

(3) Small diameter tubing connects the pumping region to the expansion cone so that the injectant velocity stays above the flame velocity. Initially, the pumping region was at the bottom of the tank, but the burning region and flameholder were 36 in. away in the ullage. The advantages of this configuration are as follows:

(A) The pumping zone is in the bottom of the tank where a constant supply of LH_2 is assured.

(B) The burning region is in the ullage, giving unchanging and predictable pressurization characteristics as the tank empties.

Further analysis of this configuration showed that the long, thin fluorine flow tube was such a good heat exchanger that even warm fluorine (>500°R) would be frozen solid before reaching the burning region. It was therefore necessary to shorten the distance from the pumping region to the burning region to 6 in. (compared to the 36 in. used previously) to ensure that the injected fluorine would remain well above 200°R, which is the temperature at which the total enthalpy becomes marginal and the fluorine tends to nonignition and subsequent detonation. This meant that the burning region would be below the surface of the LH_2 for virtually all liquid levels. The hot hydrogen created in the burning region would also be cooled as it flowed up to the ullage, but only by about 150°R (e. g., from 650° to 500°R). This condition would, unfortunately, lead to less predictable pressurization characteristics during outflow because of (1) variation of gas temperature into the ullage and (2) variation of heat transfer to the bulk liquid. On the other hand, this configuration could give possible mission advantages: it could give higher ullage temperatures as the tank empties, and thus minimize the residual gas weight. Eventually, to further alleviate the injectant freezing

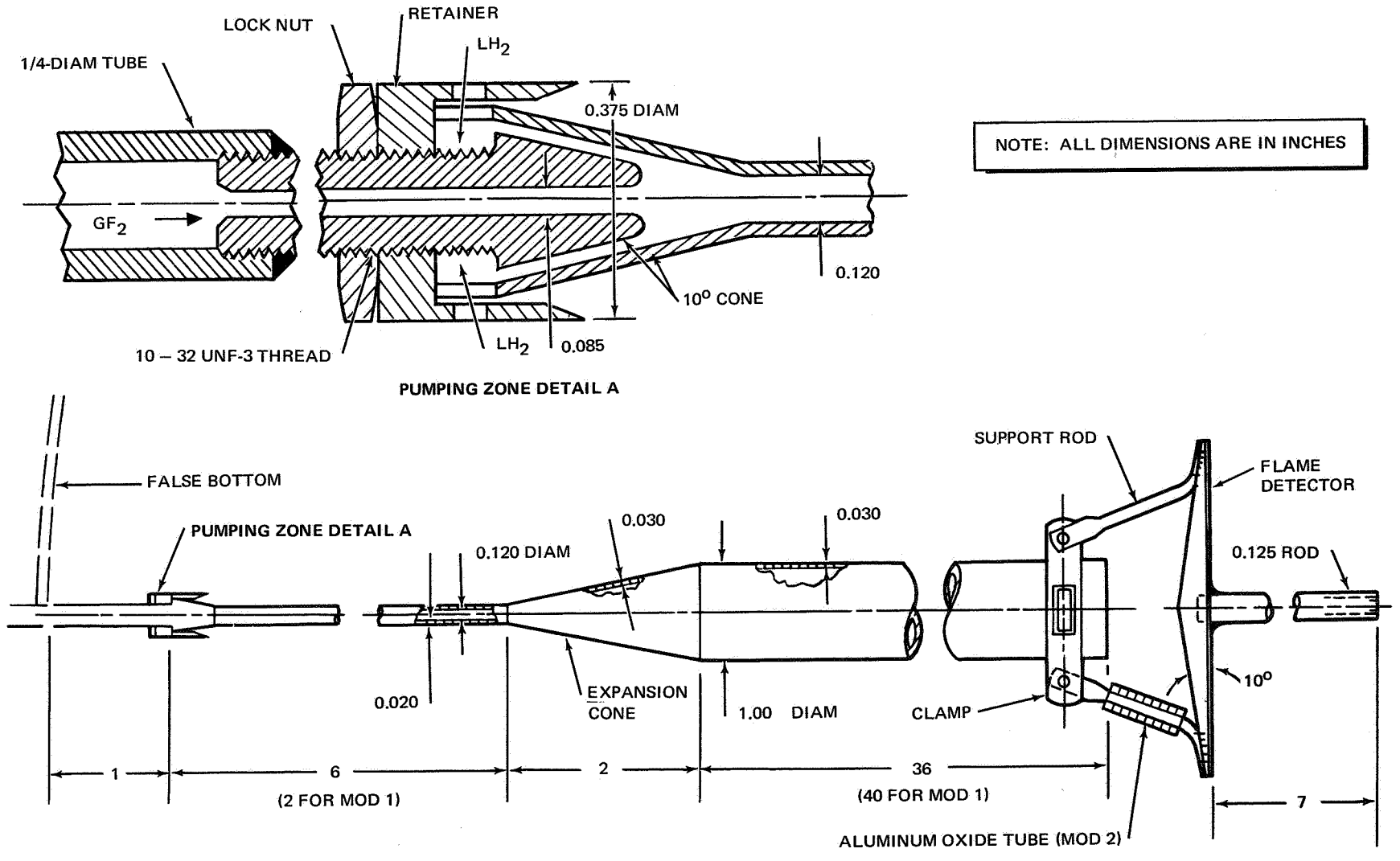

Figure 4. SA Injector Design

problem, it became necessary to reduce the pumping-region-to-burning-region distance from 6 in. to 2 in., as discussed in Results.

(4) The injector was initially fabricated of pyrex, to make it possible to see the flame pattern, etc.; later injectors were made of both stainless steel and aluminum.

(5) A flame deflector was used to distribute the hot hydrogen throughout the ullage and prevent flame impingement on the test tank cover or other equipment. It was designed to be clamped to either pyrex or metal injectors by its supporting legs. As discussed in Results, these legs tended to burn off and eventually had to be protected by a sheath of alumina (Al_2O_3) tubing, which is extremely flame and fluorine resistant.

(6) The entire injector was supported laterally (at the top and bottom), but not vertically, so that differential thermal contraction between the tank and the injector could be accommodated. The entire injector assembly was removable in two pieces from outside the test tank.

Test Apparatus Design--The apparatus that was used to test the injector concepts consists of a high-pressure (200 psi), 105 gal., vacuum-jacketed and superinsulated LH_2 Dewar, with appropriate fill, vent, and drain systems. A fluorine injection supply system with provisions for F_2 purging and disposal was connected to the LH_2 test tank. The overall test facility layout is shown in fig. 5. In the right foreground is the fluorine supply cylinder enclosure and barricade, with the fluorine valves mounted to it. Behind the barricade is the emergency shower and eyewash. In the right background is the LH_2 storage tank. The test tank is inside the test bay, center. The A-frame and hoist, mounted directly above the tank, was used to raise and lower the test tank cover, which weighs about 500 lb. Between the A-frame and the tank the motion-picture camera is mounted in place (without the purge box installed). In the left foreground is the helium bank that was used for test tank pressurization and purging, and in the left background is the LH_2 vent/drain line and vent stack. Complete details of the injector test facility, instrumentation, control system, experimental technique, and propellants are given in Appendix B.

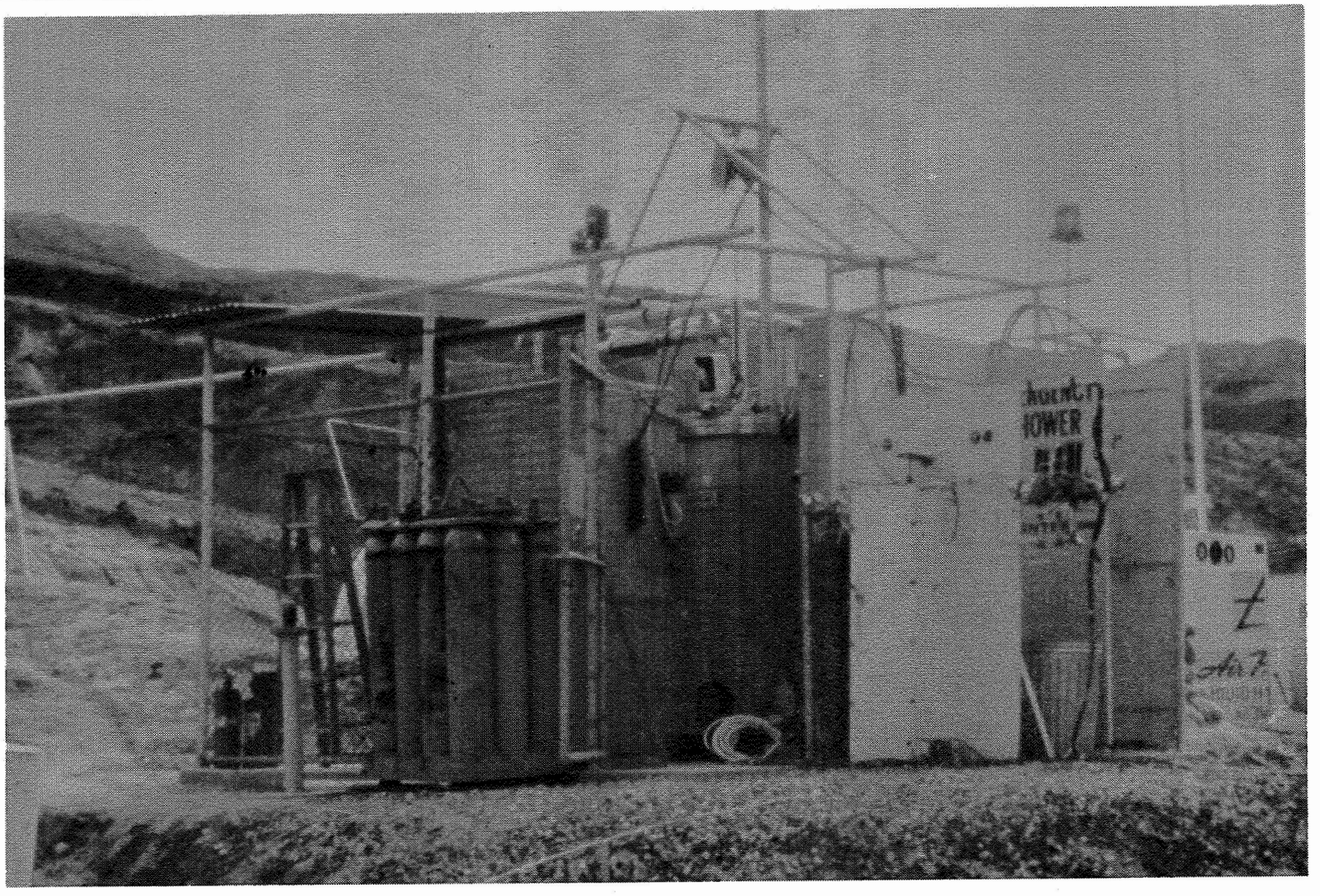

Figure 5. View of M T I Injector Test Facility

INJECTOR TESTING

General Results

Preliminary Tests--Prior to the full-scale MTI tests, a number of preliminary tests were performed to check out the operational aspects of the test facility, especially the LH_2 fill, vent, and drain system. Following the successful checkout of the LH_2 systems, and the correction of a number of minor problems, the initial fluorine injection tests were performed. In these two tests, the fluorine cylinder was opened, then closed, so that the fluorine that was injected was only the amount trapped upstream of the prevalve (approximately 0.0033 lb); the prevalve and injector valve were opened to allow injection into the hydrogen. The pressure and temperature rose after these injections, and this indicated that ignition had occurred. After these successful preliminary tests, the full-scale test program was performed. The first three tests were submerged tests (discussed later) and were followed by the US test series. The results are summarized in Table I, and the individual tests are discussed in detail in the following paragraphs.

US Injector Tests--Eleven US tests were made (Tests 4 through 14) and in general, the US mode gave rapid pressure rise, ullage heating, and pressure collapse following pressurization. Fig. 6 is an oscillograph record of a high-pressure US test that shows the general characteristics of the US injection mode. The pressure rises very rapidly to 103 psig, then, when the LH_2 expulsion first starts, the ullage volume increases so rapidly that the pressure peaks, drops somewhat, then stabilizes to almost keep up with the expulsion rate. Finally, the pressure drops again as the ullage volume gets very large and the heat transfer and the collapse occur (particularly between injections). The LH_2 flow rate ΔP trace overshoots (because of the smaller 1.375-in. orifice diameter) and some of the thermocouples move as the LH_2 draining proceeds. In these tests, the fluorine flow rate could be readily varied, with no injectant freezing problem at low flow (as in the submerged tests discussed later). In fact, an injector burning problem occurred. The initial US injector was of 304 stainless steel and it burned off at the point where it passed through the test tank lid as did the next two US injectors, also of 304 stainless steel (Tests 4, 5, and 6). Examination of these injectors indicated that a hot spot apparently formed where the injector tube passed through the lid because of insufficient cooling capacity in that area. The failure mechanism seemed to be that molten metal fluoride was formed, and this molten fluoride flowed

TABLE I
INJECTOR TEST SUMMARY

Test No.	Injection Mode	Expulsion Mode	% Ullage	P_T During Drain psig Initial	P_T During Drain psig Avg.	Avg. $\dot{W}_{LH_2}$ lb/sec	Avg. P_{F_2}-P_T psi	Avg. $\dot{W}_{F_2}$ lb/sec	t Inj. sec	Avg. Tullage °R	W_{F_2} Inj. lb	Movies	Remarks
1	(SS)	Complete	8.2	21.3	24.6	1.23 H	(180.6)	~0.0075	(16.5)	67	~0.124	O.K.	Glass SA injector broke at injection - SS mode
	1st Inj.						144.4		3.3				
	2nd Inj.						211.0		9.5				
	3rd Inj.						161.4		3.7				
2	SA	Partial 1st Exp.	8.3	34.4	14.4	0.78 H	(288.6)	0.01035	(26.2)	184	0.271	Poor	316 SA injector - flame in ullage, injector warped. Flame defl. damaged - no injection possible. For second expulsion - frozen HF plugged injector
	1st Inj.						275.5		9.4				
	2nd Inj.						293.2		10.1				
	3rd Inj.						302.3		1.9				
	4th Inj.						299.3		4.8				
		2nd Exp.	53.2	-	-	No Exp.	-	No Inj.	0				
3	SA	Complete	8.3	110	20.1	~1.3 H	(26.3)	0.0022	(29.6)	109	0.065	Poor	316 SA injector - ignition, then extinction. F_2 froze in injector, detonated at end of first injection - destroyed injector. Remaining injection burned remaining injector. No injection possible for second expulsion.
	1st Inj.						30.4		9.4				
	2nd Inj.						9.0		10.1				
	3rd Inj.						39.7		10.1				
4	US	Partial 1st Exp.	8.3	53.2	30.4	1.55 H	(30.7)	0.00255	(38.3)	301	0.078	None Camera Jammed	304 US injector - injector burned off at lid at 0.5 sec. of second injection of second expulsion.
	1st Inj.						7.75		9.4				
	2nd Inj.						26.0		10.0				
		2nd Exp.	86	15.2	14.0	1.06 H				528			
	1st Inj.						48.0		8.9				
	2nd Inj.						41.6		10.0				
5	US	Complete (Planned Partial) 1st Exp.	8.3	173.0	128.9	3.77* H	(195.3)	0.0096	(29.4)	407	0.282	Poor	304 US injector - injector burned at tip, plugged, no second injection possible - complete drain first expulsion - *With possible pull-through.
	1st Inj.						158.8		9.4				
	2nd Inj.						177.7		10.0				
	3rd Inj.						247.1		10.0				
		2nd Exp.	100.0	-	-	No Exp.	-	No Inj.	0				
6	US	Partial 1st Exp.	8.3	61.0	113.7	3.47* H	(202.2)	0.00978	(38.8)	302	0.380	Poor	304 US injector - injector burned off at lid - through lid - external fire after run. *Essentially complete drain on first drain with pull-through.
	1st Inj.						154.5		9.4				
	2nd Inj.						176.0		9.9				
	3rd Inj.						237.8		10.0				
		2nd Exp.	94.3	18.1	18.1	~1.15 H				356			
	1st Inj.						237.6		7.6				
	2nd Inj.						248.7		1.9				
7	US	Partial 1st Exp.	8.3	80.9	32.6	~1.68 H	(26.2)	0.00214	(60.8)	181	0.130	Good	A-286 US injector - injector burned off at lid, during third injection of second drain.
	1st Inj.						6.1		9.5				
	2nd Inj.						9.66		10.0				
	3rd Inj.						20.5		10.0				
	4th Inj.						34.85		5.7				
		2nd Exp.	~52.5	7.7	9.7	U							
	1st Inj.						34.1		2.0				
	2nd Inj.						37.82		8.7				
	3rd Inj.						43.77		4.9				
	4th Inj.						42.28		10.0				

TABLE I. - (Cont'd)
INJECTOR TEST SUMMARY

Test No.	Injection Mode	Expulsion Mode	% Ullage	P_T During Drain psig Initial	Avg.	Avg. $\dot{W}_{LH_2}$* lb/sec	Avg. P_{F_2}-P_T psi	Avg. $\dot{W}_{F_2}$ lb/sec	t Inj. sec	Avg. T_{ullage} °R	W_{F_2} Inj. lb	Movies	Remarks
8	US	Partial 1st Exp.	8.3	32.1	23.5	~1.38 H	(17.3)	0.00158	(48.2)	328	0.076	Fair	A-286 US injector - burned off at lid.
	1st Inj.						9.4		9.4				
		2nd Exp.	48.6	29.3	24.1	~1.40 H				242			
	1st Inj.						17.7		9.4				
		3rd Exp.	75.8	20.8	13.7	~1.05 H				172			
	1st Inj.						21.3		9.4				
	2nd Inj.						15.6		10.0				
	3rd Inj.						22.5		10.0				
9	US	Partial 1st Exp.	8.3	31.2	28.3	~1.48 H	(14.4)	0.0017	(38.3)	311	0.065	Fair	Aluminum US injector - very mild melting at tip. No fluoride formation.
	1st Inj.						6.9		9.4				
		2nd Exp.	37.8	28.3	23.4	~1.32 H				256			After run 10A, with a total of 63.6 sec and 0.282 lb of F_2, aluminum injector showed severe tip melting.
	1st Inj.						16.3		9.4				
		3rd Exp.	65.2	27.4	17.2	~1.10 H				244			
	1st Inj.						18.0		9.5				
	2nd Inj.						16.4		10.0				
10	US	Complete	8.3	110.0	97.0	3.51* L	(84.0)	0.00716	(19.7)	256	0.141	Poor	Copper US injector - no damage. *Possible pull-through.
	1st Inj.						56.9		9.7				
	2nd Inj.						110.0		10.0				
11	US	Partial 1st Exp.	8.3	102.9	96.6	~3.50* L	(102.9)	0.00678	(28.8)	266	0.195	Good	Same copper US injector - no damage. *Possible pull-through.
	1st Inj.						83.9		9.4				
		2nd Exp.	64.5	88.5	77.8	~3.00* L							
	1st Inj.						136.1		9.4				
	2nd Inj.						89.5		10.0				
12	US	Partial 1st Exp.	8.3	150.0	92.3	~3.40* L	(76.4)	0.00546	(45.7)	253	0.250	Fair	Same copper US injector - no damage. *Possible pull-through.
	1st Inj.						87.7		4.3				
	2nd Inj.						72.3		8.2				
		2nd Exp.	51.2	142.2	94.6	~3.45* L				320			
	1st Inj.						119.5		9.3				
	2nd Inj.						65.2		9.9				
	3rd Inj.						37.2		10.0				
	4th Inj.						98.7		4.0				
13	US	Partial 1st Exp.	8.3	51.7	49.6	~2.45* L	(62.1)	0.00426	(48.4)	284	0.206	Fair	Same copper US injector - no damage. *Possible pull-through - essentially empty on first drain.
	1st Inj.						13.3		9.4				
	2nd Inj.						60.0		9.9				
	3rd Inj.						71.8		10.0				
		2nd Exp.	92.2	28.3	25.4	~1.70* L				268			
	1st Inj.						86.7		9.4				
	2nd Inj.						77.5		9.7				
14	US	Partial 1st Exp.	8.3	67.0	66.1	~2.60* L	(68.6)	0.00434	(57.4)	289	0.250	Poor	Same copper US injector - after total of 200.0 sec and 1.042 lb of F_2 showed no damage. *Possible pull-through - essentially empty after third drain.
	1st Inj.						8.7		9.5				
	2nd Inj.						54.0		2.2				
		2nd Exp.	53.9	34.5	38.0	~1.90* L				312			
	1st Inj.						76.2		9.4				
	2nd Inj.						76.9		3.6				
		3rd Exp.	87.8	34.5	30.8	~1.65* L				341			
	1st Inj.						82.3		9.4				
	2nd Inj.						83.9		7.6				
		4th Exp.	97.0	25.6	21.8	~1.25* L				365			
	1st Inj.						83.4		9.4				
	2nd Inj.						87.2		6.3				

TABLE I. - (Concluded)

INJECTOR TEST SUMMARY

Test No.	Injection Mode	Expulsion Mode	% Ullage	P_T During Drain psig Inital	Avg.	Avg. $\dot{W}_{LH_2}$ lb/sec	Avg. $P_{F_2} - P_T$ psi	Avg. $\dot{W}_{F_2}$ lb/sec	t Inj. sec	Avg. $\delta_{Tullage}$ °R	W_{F_2} Inj. lb	Movies	Remarks
15	SA	Complete (Planned Partial)					(78.3)	0.00397	(16.4)		0.065	Good	Aluminum SA injector baffle on drain, F_2 froze in injector, exploded, no second injection and drain possible.
		1st Exp.	8.3	28.4	22.5	~1.49 L				162			
	1st Inj.						66.7		6.3				
	2nd Inj.						84.0		10.1				
		2nd Exp.	62.9	-	-	No Exp.	-	No Inj.	0	-			
16	SA	Partial					(263.4)	0.0104	(44.9)		0.466	Good	Aluminum SA injector CU injector tube, shortened injector length, removed false bottom. Used heated injector and helium post-purge between drains - No F_2 freezing. Burned off flame deflector, injector collapsed and injector nozzle and expulsion cone burned.
		1st Exp.	8.3	39.2	48.4	~1.80 L				250			
	1st Inj.						223.8		10.1				
	2nd Inj.						249.9		10.0				
		2nd Exp.	65.2	10.3	17.7	~1.14 L				126			
	1st Inj.						288.2		9.4				
	2nd Inj.						284.5		9.2				
	3rd Inj.						259.5		3.5				
	4th Inj.						271.4		2.7				
17	SA	Partial					(182.3)	0.00868	(45.0)		0.391	Fair	SS SA injector CU injector tube - shortened injector length - no false bottom - used helium post-purge between drains - no F_2 freezing. Used AL_2O_3 protected flame deflector - no damage, burned injector tube and nozzle.
		1st Exp.	8.3	34.4	42.3	~1.85 L				175			
	1st Inj.						138.8		9.4				
	2nd Inj.						189.5		10.0				
	3rd Inj.						200.6		1.0				
		2nd Exp.	70.5	36.5	47.5	~1.95 L				209			
	1st Inj.						200.0		9.4				
	2nd Inj.						200.4		2.6				
	3rd Inj.						180.5		2.6				
	4th Inj.						194.4		10.0				
18	SS	Complete	8.3	17.9	47.6	~1.43 L	(237.7)	0.0120	(36.0)	132	0.434	Poor	SS injector with CU injector tube - no false bottom - no F_2 freezing. No damage to injector.
	1st Inj.						281.5		9.3				
	2nd Inj.						266.2		10.1				
	3rd Inj.						211.9		10.1				
	4th Inj.						170.7		6.5				
19	SS	Partial					(164.2)	0.00923	(82.2)		0.759	Fair	SS injector with CU injector tube - no false bottom. No F_2 freezing with multiple drains. No damage to injector.
		1st Exp.	8.3	112.0	72.7	~2.50 L				74			
	1st Inj.						151.5		10.1				
	2nd Inj.						164.5		10.1				
	3rd Inj.						175.2		4.7				
		2nd Exp.	43.8	108.8	107.3	~3.00 L				140			
	1st Inj.						217.0		9.4				
	2nd Inj.						161.9		10.0				
	3rd Inj.						114.2		9.3				
		3rd Exp.	87.0	111.0	89.6	~2.80 L				258			
	1st Inj.						162.9		8.5				
	2nd Inj.						152.4		10.1				
	3rd Inj.						185.6		10.0				
20	SS	Complete (Planned Partial)					(61.1)	0.00354	(24.5)		0.087	Poor	SS injector with CU injector tube - no false bottom. Low pressure F_2 froze in injector, exploded. F_2 pressure increased but no further injection possible; no second expulsion possible. No injector damage from explosions.
		1st Exp.	8.3	50.0	33.7	~1.56 L				94			
	1st Inj.						2.2		1.9				
	2nd Inj.						13.5		6.7				
	3rd Inj.						9.1		7.9				
	4th Inj.						51.8		0.2				
	5th Inj						169.3		7.8				
		2nd Exp.	30.1	-	-	No Exp.	-	No Inj.	0	-			
21	SS	Partial					(134.9)	0.0068	(55.9)		0.380	Fair	SS injector with CU injector tube - no false bottom. No F_2 freezing with multiple drains. No damage to injector.
		1st Exp.	8.3	53.4	46.0	~1.73 L				88			
	1st Inj.						152.3		9.4				
	2nd Inj.						130.1		10.1				
		2nd Exp.	39.4	30.8	35.6	~1.50 L				U			
	1st Inj.						153.6		9.4				
	2nd Inj.						129.6		7.6				
		3rd Exp.	64.4	35.9	46.9	~1.75 L				131			
	1st Inj.						138.7		9.4				
	2nd Inj.						106.9		10.0				

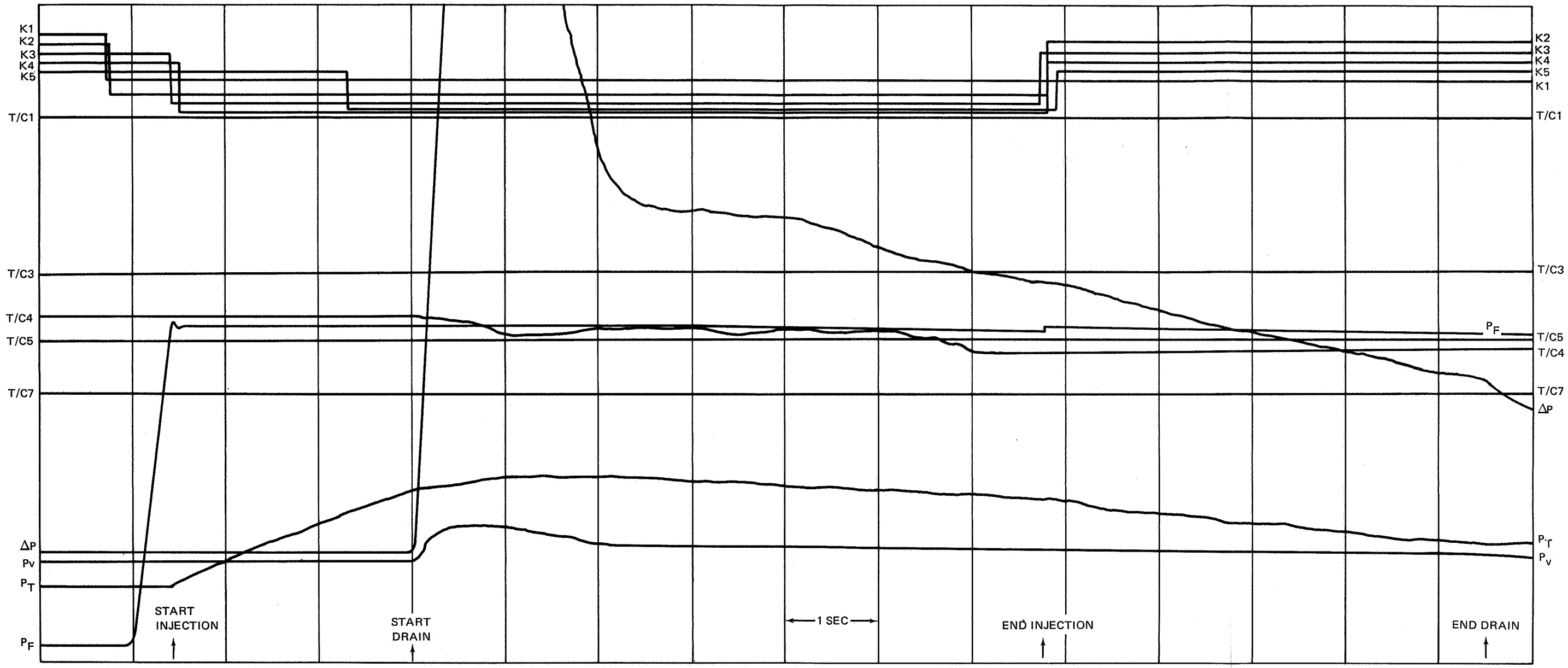

Figure 6. US Oscillograph Record (Test 11)

Foldout FRAME I

Fold out FRAME II

down the injector and plugged it, causing burnoff of the injector at the lid. Often, the bottom 3 in. or so of the injector was found in the tank bottom.

Two approaches to solve the problem were tried: to avoid melting by using high-temperature nickel alloy (A-286), and to avoid hot spots by using a higher-conductivity material such as aluminum or copper. A-286 injectors were used for Tests 7 and 8, and burned off exactly as did the 304 stainless steel injectors. An aluminum injector was used for Test 9 and showed only mild damage at the tip, and some discoloration where it passed through the lid. It was used again for Test 10A, and showed rather severe melting at the tip (but no fluoride formation) after it had been used for 63. 5 sec and 0. 282 lb of fluorine had passed through it. Since it was apparent that high thermal conductivity materials were beneficial, a copper injector was next used. This injector showed no damage after five runs (Tests 10 through 14); it had then been used for a total of 200 sec and 1. 042 lb of fluorine flow. The relative injector material resistance to the MTI testing environment is shown in fig. 7.

The pressurization efficiency of the US mode is discussed in more detail later; however, the injector burnout did not significantly affect tank pressurization and explusion (Compare Tests 8 and 9.), because the US injection mode essentially just heats the ullage gas. Injector burning is extremely undesirable, both because of the chance of burning through the tank lid to the outside, as in Test 6, and also because the burned injector contaminates the tank with a combination of metal fluorides, molten metal particles, and HF attack. This effect required cleaning of the tank after every two or three runs until the problem was solved.

The oscillograph records of the tests provided the most important data. The quality of the high-speed motion pictures was generally poor, and these motion pictures were much inferior to those taken during the small-scale tests. Fig. 8 shows a frame of the high-speed motion pictures as they showed the interior of the tank during a US mode test (Test 7). The basic problem in most of the motion pictures was that the lights that illuminated the tank interior were much dimmer than the light that was generated by the reaction. Further, immediately after injection, a vapor cloud was formed in the ullage; this could have been caused by LH_2 being splashed into the ullage. This cloud blacked out all view of the tank interior, and worse, when the flame was burning in the ullage, the cloud (and the liquid below it) reflected so much light that the picture was completely overexposed from the glare. As the tank emptied, the cloud formation subsided, and some detail inside the tank could be seen. The photograph shown was taken at the start of the second drain with the tank more than half empty. The white crescent at the bottom of the photo is the tank wall, and the white diagonal bars are the light tubes stretching downward into the tank. The false bottom can be seen as a faint circle at the center of the photograph. The LH_2 level is at the area where the tubes disappear and seem to bend. The vapor cloud, just starting to form, can be seen at the top. Shortly afterward, the cloud covered the picture and obscured all further view. This photo was taken by the light of the US reaction that was occurring in the ullage.

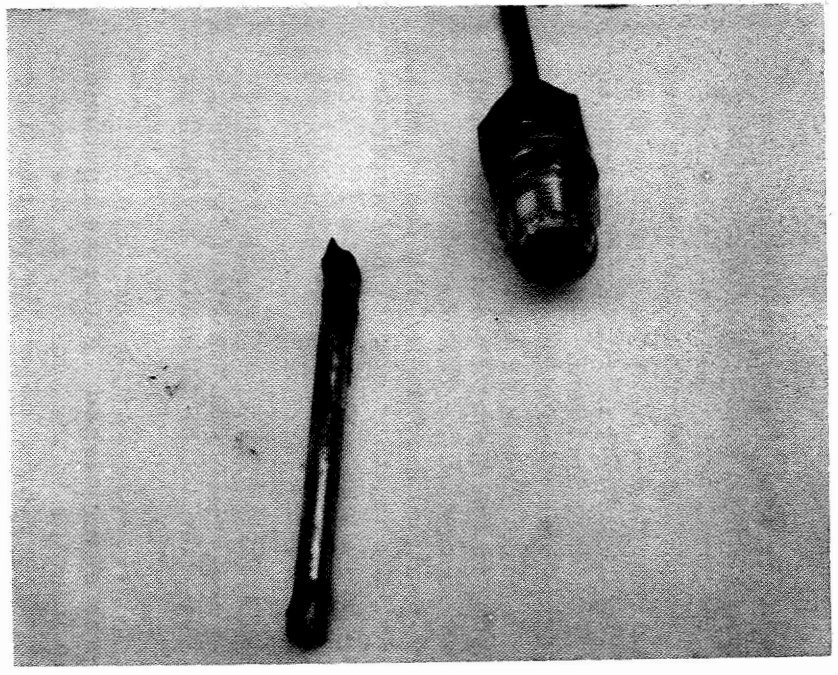

(a) 304 STAINLESS STEEL INJECTOR

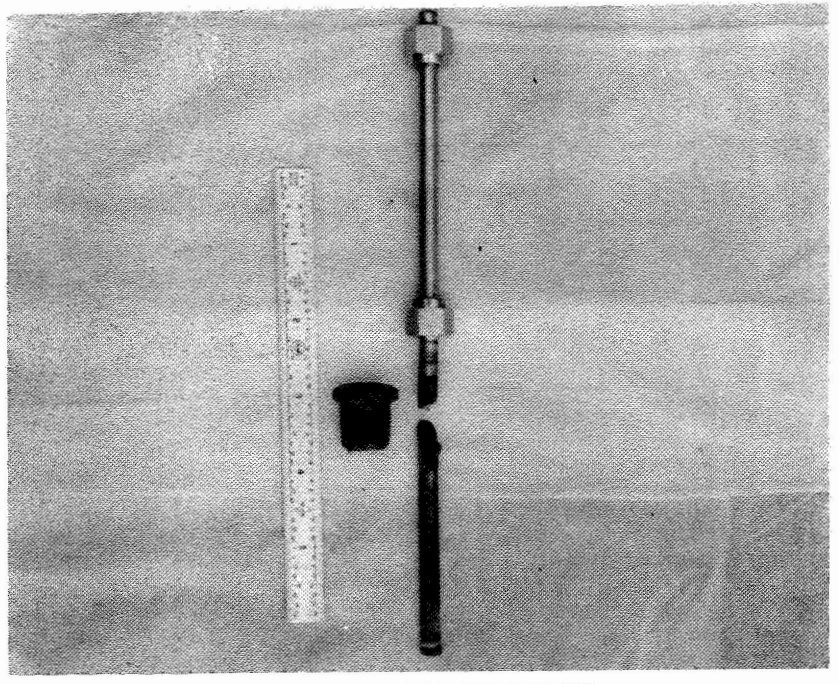

(b) A-286 NICKEL ALLOY INJECTOR

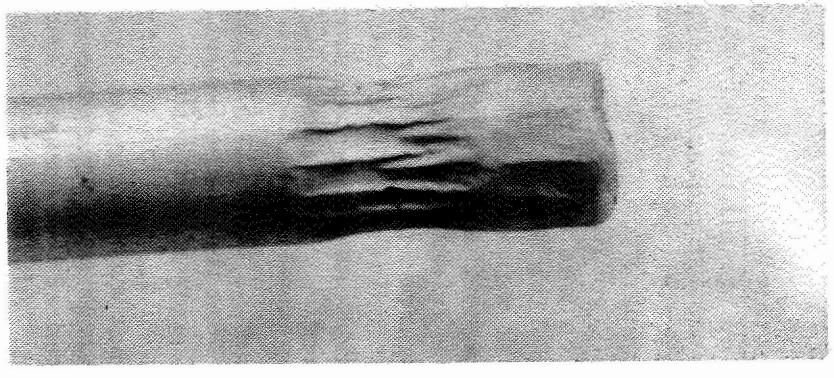

(c) 6061 ALUMINUM INJECTOR

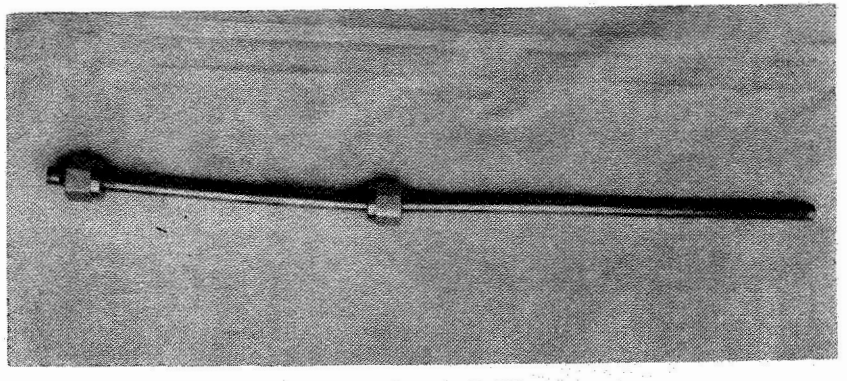

(d) COPPER INJECTOR

Figure 7. US Injector Material Comparison

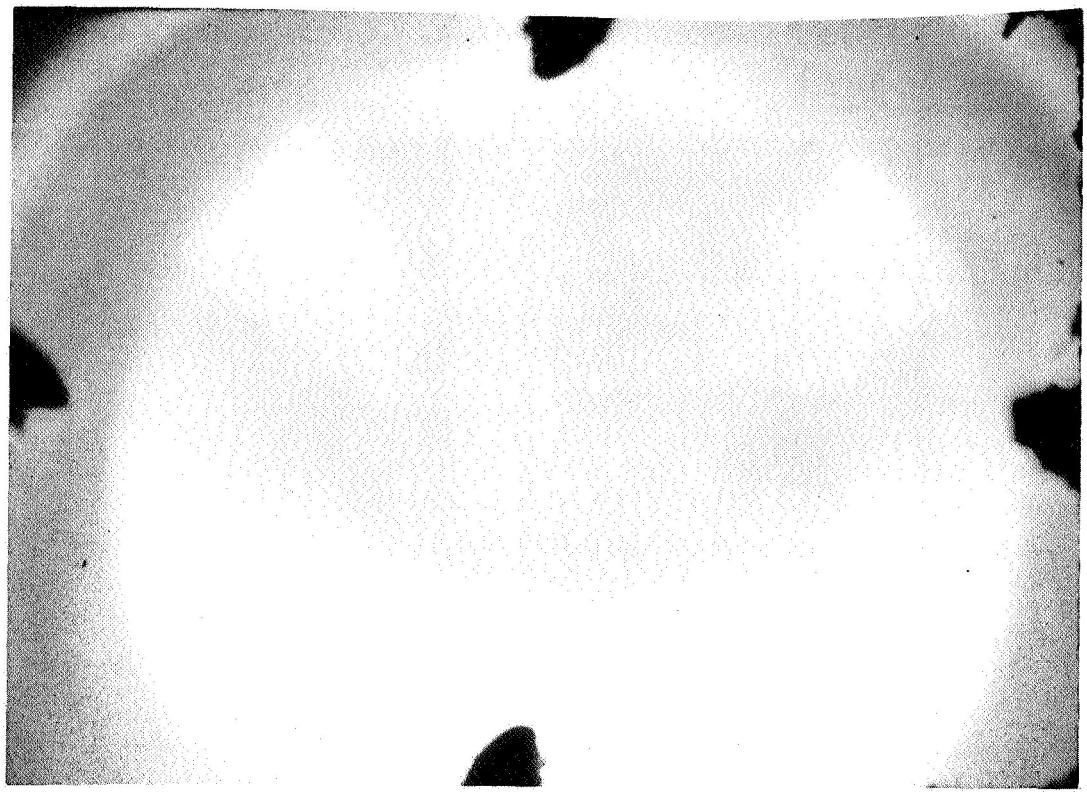

Figure 8. View into Tank During US Test

SA Injector Tests--It was originally hoped that the pyrex SA injector could be used for all tests so that the flame pattern could be observed with high-speed motion pictures; however, in the first test, this injection shattered immediately upon injection (and ignition), probably because of the thermal shock of ignition. What followed was essentially SS mode injection that, together with additional SS test data, is discussed later. Tank pressurization and expulsion was accomplished without any other incident. In the next SA test, (Test 2) the 316 stainless-steel injector was used with a high fluorine flow rate. It was originally thought that the high pressure blew the flame into the ullage, instead of allowing it to stay in the flame holder (expansion) region of the injector. This flame burned off one of the flame-deflector supports, warped the injector nozzle with heat, and corroded the test tank lid to form metal fluoride deposits. However, the injector apparently aspirated (pumped LH_2) and pressurization and expulsion was successfully accomplished.

For Test 3, the next SA test, the fluorine flow rate and pressure were reduced so that the flame would remain in the expansion region of the injector and not jump into the ullage. This gave rise to the following anomalous series of events: ignition occurred after injection and this gave a tank pressure rise that was sufficient to actuate the pressure switch and keep the injection valves open; then the reaction was extinguished. Fluorine continued to be injected and apparently froze in the injector in the vicinity of the expansion section. After 9.4 sec, the injector valve closed normally (as the timer

ran out) and the shock of valve closure apparently initiated a reaction in the frozen fluorine. It may have been a detonation, but it was certainly a rapid reaction, that gave a tank pressure rise of over 80 psi in 50 msec, and shattered the metal injector. Pressurization continued to a pressure of 110 psig and expulsion followed without further problems.

Because of these SA injector problems, the injector analysis was modified and a series of simulated propellant tests were run on the SA injector, as described in Appendix A. The results of this injector performance mapping indicated that the SA injector would run extremely oxidizer rich and would be incapable of pumping excess LH_2 (run fuel rich), keep the injector cool, and perform its desired function of vaporizing hydrogen in a predictable manner for tank pressurization. Further, the oxidizer-rich ratio could be expected to burn indeterminately throughout the length of the injector and in the ullage. The burning would be extremely hot, giving no injector heating protection and leading predictably to injector burning.

These characteristics can explain the phenomenon of ullage-space burning and injector nozzle warping in Test 2. The thesis that the high fluorine pressure blew the flame into the ullage does not satisfactorily explain the fact that the lower end of the injector got hot enough to warp. However, fluorine-rich burning throughout the injector can explain both phenomena.

To verify the oxidizer-rich performance of the SA injector, a series of full scale tests using GF_2 and LH_2 were performed, and the results are as follows.

The first SA test to verify LH_2 performance used an aluminum injector, and was not particularly successful. In this run (Test 15) the false bottom was used, as in all previous runs. Again, as in Test 3, the fairly low flow-rate fluorine froze in the injector, subsequently exploded, and destroyed the injector tube (but did not damage the top part of the injector). No further injection and expulsion was possible. Following this test, it was concluded that the use of the false bottom was imposing an unnecessarily severe environmental constraint on the submerged injector, because it required the fluorine to flow through an additional 8 in. of LH_2-temperature tubing to reach the false bottom. The false bottom was removed, and the injector tube shortened, so that the tube just penetrated the tank. In addition, to further assure elimination of the injectant freezing problem (and thus properly evaluate the SA injector performance) the injector tube was made of copper, was heated during the test (to approximately 160°F), and was purged with helium between drains. These supplemental measures were eliminated one by one in Tests 16 through 18, and there was no further freezing problem.

The remaining SA injector tests, Tests 16 and 17, gave good pressurization and expulsion despite injector problems. Pressurization in the SA mode is basically different from the US mode (fig. 9). The oscillograph for Test 17 shows that, even at fluorine driving pressure higher than for the US test, the pressure rise is much slower until draining begins at about 35 psi. The ΔP trace surges during initial LH_2 outflow. This is characteristic of low tank-pressure LH_2 expulsion. Shortly after draining begins, there is a sharp jump in tank pressure to 73 psi, which could indicate possible fluorine freezing

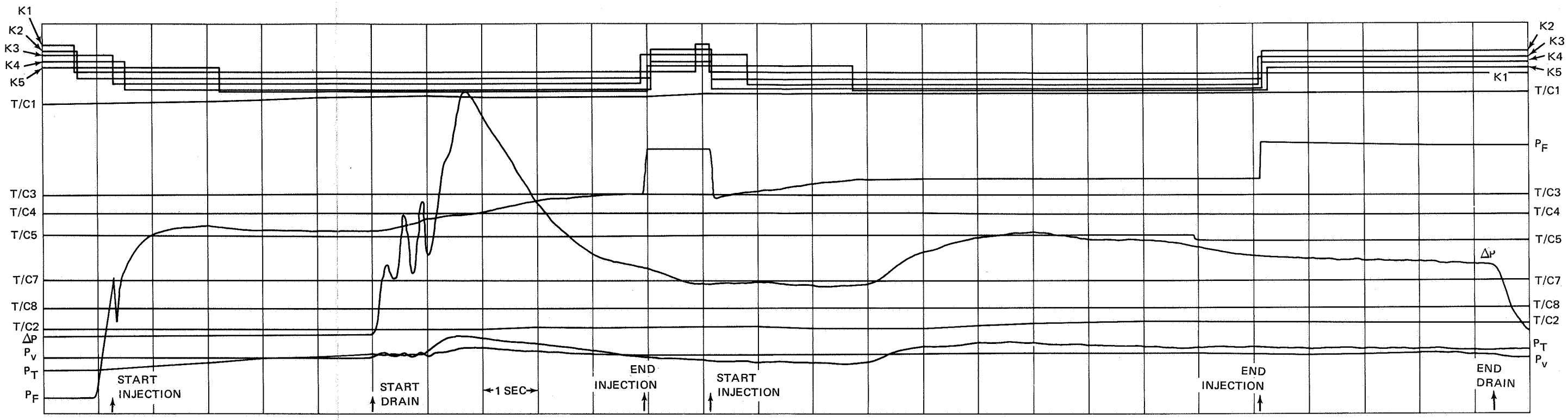

Figure 9. SA Oscillograph Record (Test 17)

Fold out FRAME I

Fold out FRAME II

followed by detonation. This phenomenon occurs again, following the second injection. Again the pressure tends to decay following the initial drain, then holds fairly steady as outflow continues, until the ullage volume gets large.

In the SA tests also, the quality of the motion pictures was generally poor. Fig. 10 shows a frame of the high-speed motion pictures during a SA mode test (Test 16). Again, a vapor cloud that was generally formed in the ullage blacked out all further viewing, until the tank was somewhat empty. In the photograph, the lower crescent is the tank wall, and the light tubes are clearly visible. Between the light tubes the injector can be seen faintly. The LH_2 level can be clearly seen on the light tubes, and the foggy appearance in the center of the tank is thought to be vapor generation in the bulk liquid from the warm injector. As in the US tests this photograph was also taken from the light of the reaction, which was occurring in the ullage at the time. The photograph was taken at the end of the first drain of Test 16 which was made with high-pressure fluorine injection. As in Test 2, the flame extended throughout the injector tube and into the ullage, burned off the flame deflector supports during the second drain, and caused injector collapse and subsequent destruction of the injector tube and aspirator nozzle. To prevent similar problems during Test 17, the flame deflector supports were protected by aluminum oxide sheaths, as shown in fig. 11. These sheaths prevented damage to the supports, although there was evidence of considerable flame deflector heating (discolorations and heat marks), and two 6-in. slits were burned in the stainless-steel injector tube just above the expansion cone. The aspirator nozzle was also damaged. The damage to the SA injectors during Tests 16 and 17 is shown in fig. 12.

In Tests 15, 16 and 17, the aspirator nozzle was set at an area ratio (β) of 1.5 to provide optimum pumping performance and maximum cooling at the fluorine driving pressures that were used. The SA tests are plotted for the test conditions in fig. A-10, Appendix A. This figure shows that the minimum O:F ratio is predicted to be 700. It is clear from the data and from examination of the injector that the SA injector, as predicted, was not pumping sufficient LH_2 and was operating extremely oxidizer-rich; this caused high flame temperatures. There was extensive injector damage despite the fact that the injector was buried in liquid hydrogen. It appeared pointless, therefore, to continue with additional SA tests, because it was believed that SS injection could provide equivalent pressurization efficiency without the risk of injector burning and potential tank damage. To demonstrate this thesis, a series of SS tests, for comparison with the SA results, was planned for Tests 18 through 21.

SS Injector Tests--Tests 18 through 21 were made with a short copper SS injector, with no injector heating, and no helium post-purge between drains. Except for Test 20, there was no further injectant freezing problem. During Test 20, the fluorine metering valve burned up, with the result that there was a very low-flow fluorine injection and the injectant froze in the SS injector. There were two explosions during injection, but there was no injector damage; however, the injector was plugged with frozen HF and neither further injection nor the planned second drain was possible. The SS mode runs gave pressurization characteristics quite similar to those of the SA mode, as shown in fig. 13 for Run 19. The pressure rise, again, is slow, requiring two

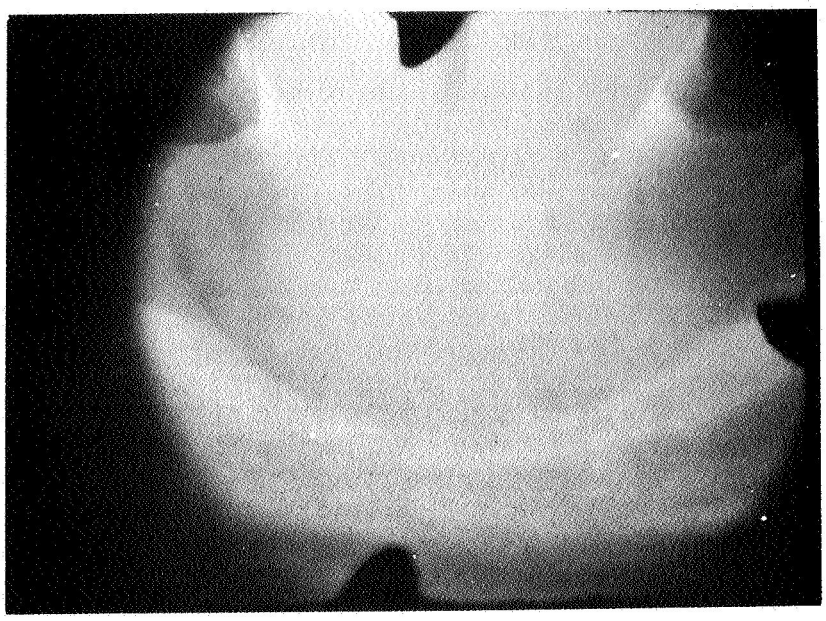

Figure 10. View into Tank During SA Test

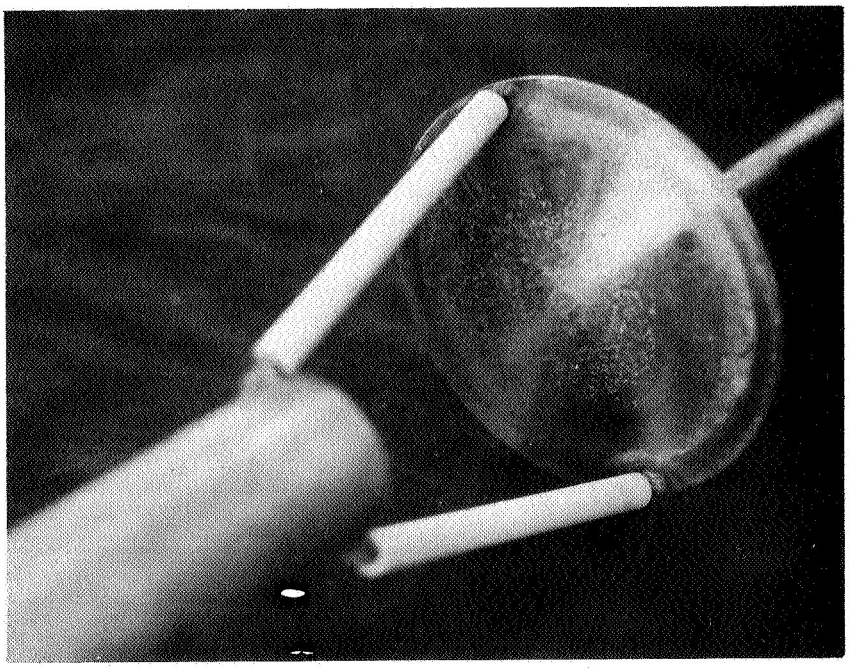

Figure 11. SA Injector Flame Deflector Modification

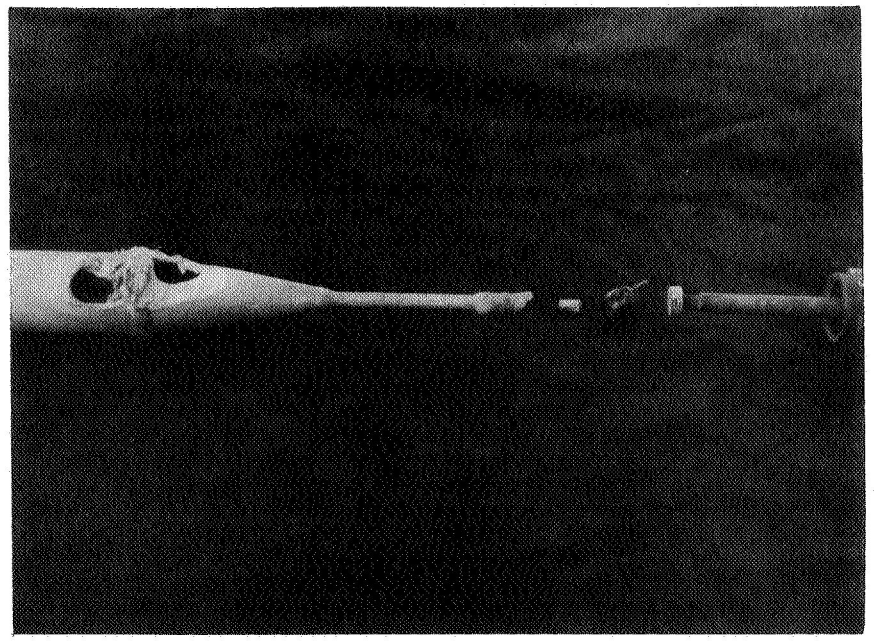

(a) TEST 16

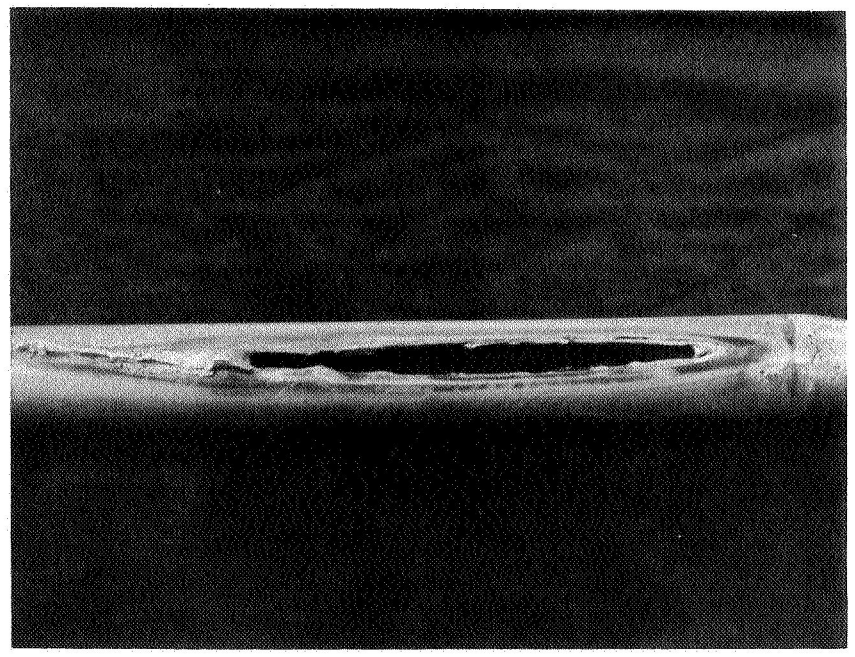

(b) TEST 17

Figure 12. SA Injector Damage

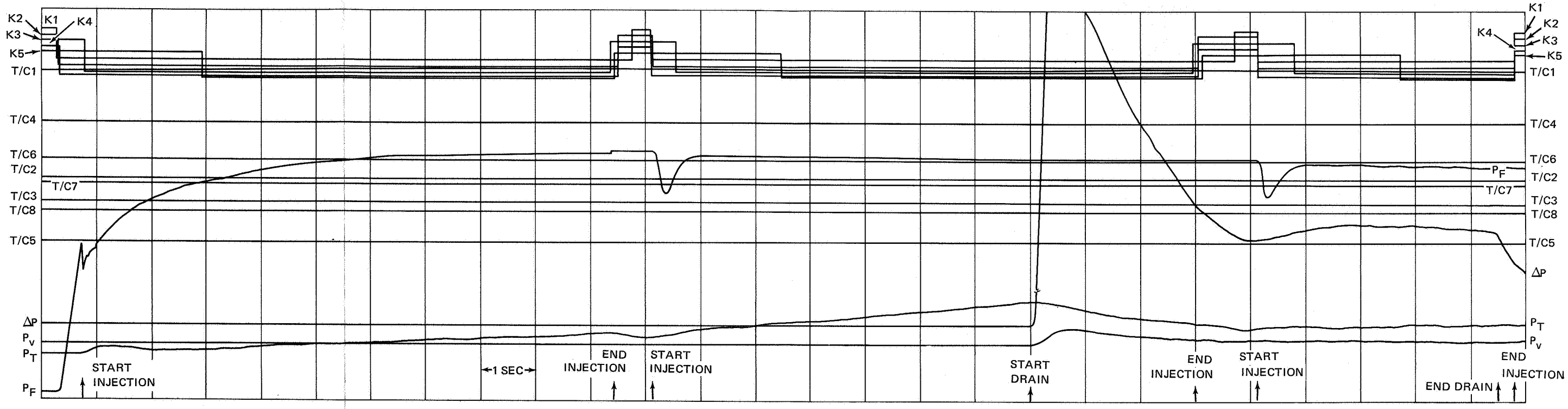

Figure 13. SS Oscillograph Record (Test 19)

Fold out FRAME I

Fold out FRAME II

injections to reach 112 psi. The pressure collapses between injections (this is discussed in detail below). As in the high pressure US run, the pressure peaks and decays rapidly during the initial drain, then pressurization keeps up with outflow. The copper SS injectors were comparable in durability to the copper US injector (fig. 14).

Injectant Freezing--For the submerged injection tests, injectant freezing was a persistent possibility. Three tests (Tests 3, 15, and 20) failed to achieve all test objectives because of injectant freezing. So that testing parameters could be defined to ensure that injectant freezing did not occur, heat transfer analysis was generated. The data correlated remarkably well with the standard forced convection heat transfer correlation

$$\frac{h\,d}{\bar{K}} = 0.023 \left(\frac{4\dot{W}}{\pi\mu d}\right)^{0.8} \left(\frac{C_p \mu}{\bar{K}}\right)^{0.3} \qquad (1)$$

The computation was based on an average injector tube internal diameter of 0.188 in., and a cooling temperature potential that was linearly averaged along the injector tube. The results are shown in fig. 15 for the length required to freeze the injectant at a given injectant flow rate.

Reaction Products (HF) Problems--With the relatively large quantities of F_2 used in the test program (Table I), large quantities of hydrogen fluoride (HF) were generated. The HF froze in the LH_2 and apparently most of it was drained along with the LH_2 during the testing, as evidenced by the severe corrosion of the drain line, drain valve, and flow control orifices; however, a considerable quantity of HF was left on the tank walls after the tests and its disposal was a nuisance. Helium purging, evacuation, and tank heating were the steps used for disposal. Corrosion and a build-up of metal fluorides inside the tank required that the tank be cleaned after every 3 or 4 tests. It is believed that the drain line and test tank corrosion was caused by the aquaeous HF solution that was formed by water vapor that leaked and condensed in the tank between tests (during the purging and heating). Pure HF attacked the pyrex camera port during the test, and this required that the window be replaced between tests.

It is apparent that HF could be a problem in a flight system, particularly if there are noncompatible materials downstream of the tank, or if the HF becomes deposited in a place where it can warm up or come in contact with water.

Wall Heating--Excessive tank wall heating was anticipated to be a potential problem during the U. S. tests with high ullage heating. During the tests, some wall heating was found, but it was not significant from a structural standpoint. From Table I, the average ullage temperature reached a maximum of 528°R, but the measured wall temperature never exceeded 100°R. Although the test tank was not flight-weight (3/16 in. walls), no wall-heating problems are anticipated for a vehicle application of the U. S. mode, because of the demonstrated insulating and heat-sink potential of the hydrogen ullage vapor.

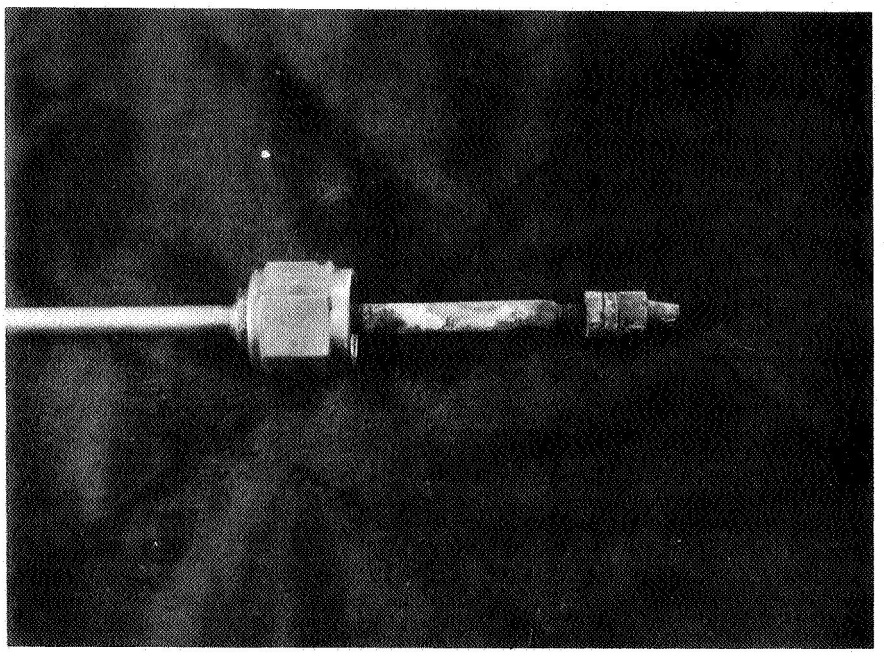

(a) SS INJECTOR FOR TESTS 18, 19 AND 20

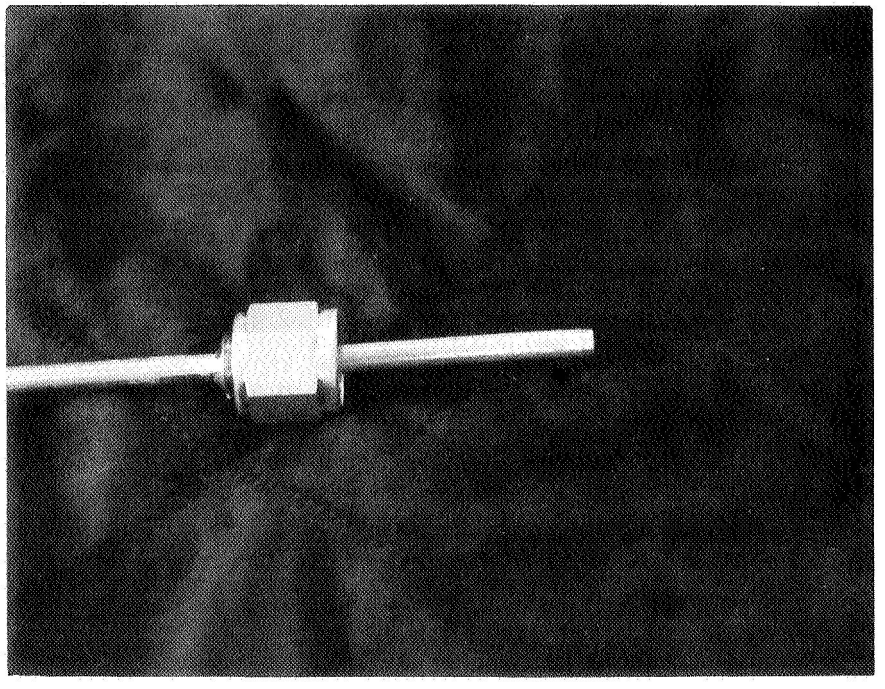

(b) SS INJECTOR FOR TEST 21

Figure 14. SS Injector Configuration

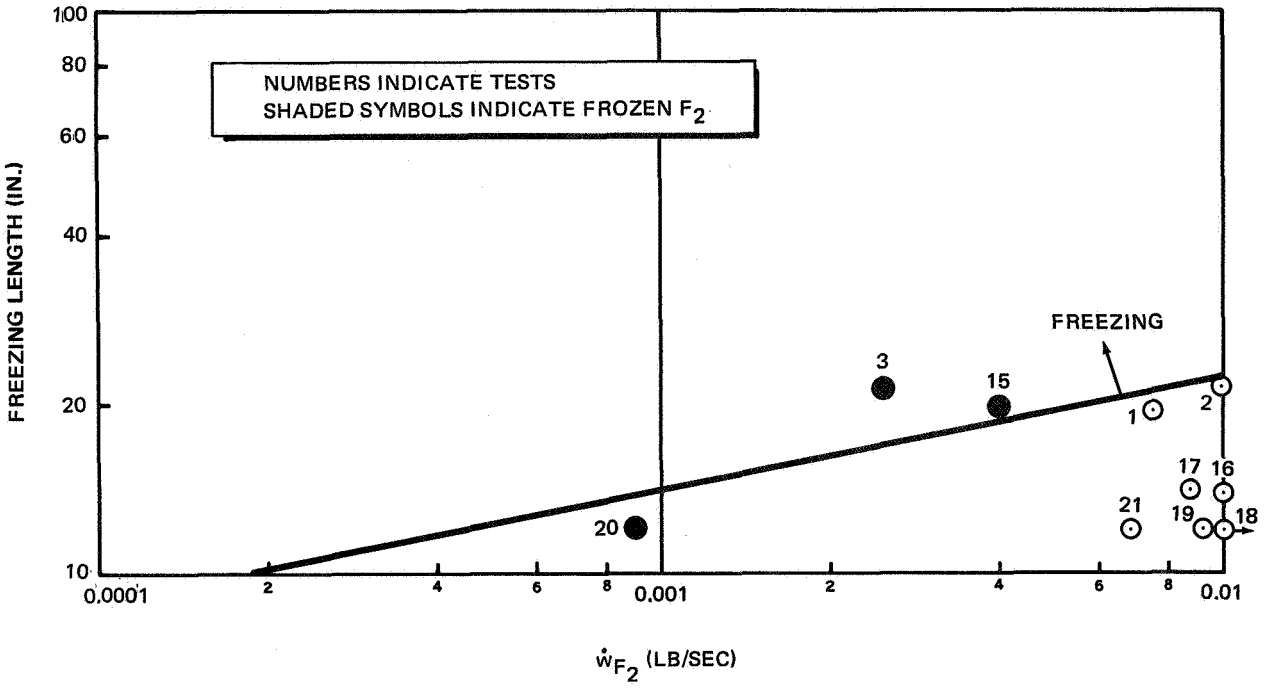

Figure 15. Injectant Freezing Correlation for Submerged Injection

Pressurization Results

Expulsion Correlation --One of the essential measurements required for analysis of the pressurization efficiency of the various injection techniques is the LH_2 drain (expulsion) rate during the tests. To measure the LH_2 drain rate, an orifice was installed in the vent/drain line downstream of the LH_2 drain valve with the twofold function of restricting LH_2 flow and providing a measurable pressure differential for flow rate calculation. It was thought that a large and a small orifice would provide two different LH_2 flow rates. To size the high- and low-flow orifices properly, it was necessary to make a compressible flow analysis of the LH_2 drain system. The basic equations for the analysis and the apporpriate flow coefficients were obtained from a Crane Company paper. *

For the compressible liquid hydrogen flow from the tank drain outlet to the orifice

$$\Delta P_L = \frac{K_L \dot{W}_L^2}{0.276\, Y^2\, d_L^4\, \rho_L} \qquad (2)$$

*Flow of Fluids through Valves, Fittings, and Pipe: Technical Paper No. 410. Crane Company, Chicago, Illinois, 1957.

If it is assumed that the liquid hydrogen will gasify at the flow orifice and in the vent stack (because these were at ambient temperature and uninsulated) the compressible gaseous hydrogen flow through the orifice is

$$\Delta P_r = \frac{\dot{W}_L^2}{0.276\ Y^2\ d_r^4\ C^2\ \rho_g} \tag{3}$$

And for compressible gaseous hydrogen flow in the vent pipe,

$$\Delta P_g = \frac{K_g\ \dot{W}_L^2}{0.276\ Y^2\ d_g^4\ \rho_g} \tag{4}$$

The total pressure drop from the tank to ambient was the sum of Equations (2), (3), and (4). If the data from the Crane paper is used, and the equations for the high-flow orifice (2 in. diam) are solved, the line marked vapor in vent is obtained in fig. 16, the high-flow LH_2 flow rate correlation. A similar calculation for the low-flow orifice (1.375 in. diam) gives the similiar line in fig. 17, the low-flow LH_2 flow rate correlation.

The assumption of vapor flow in the orifice gave results that indicated that the size variation of the orifice would give a substantial change in LH_2 flow rate, because of the sizable variation in pressure drop across the orifice. When the tests were undertaken, however, it became apparent that, from the gush of LH_2 out the vent stack during draining, there was very little boiling of the LH_2, and the LH_2 was staying liquid through the orifice and out the vent stack. Eqs. (2) and (3) were modified to reflect liquid density, and the solution showed that the orifice size change had negligible effect on the LH_2 flow rate. The results are shown as the line marked liquid in vent in figs. 16 and 17.

The strongest effect on LH_2 flow rate is the tank pressure. During the tests, the tank pressure varied continuously, and so, probably, did the LH_2 flow rate. Reduction of this great amount of continuously varying data was judged pointless; rather, the average LH_2 flow rate, over either the entire test or during chosen sections of the test, was more representative. The correlation of these average flow rates with the analytical predictions is also shown in fig. 16 and 17.

Tests 1 through 9 were run with the high-flow LH_2 orifice (2 in. ID) installed in the drain line. Flow-rate data from these runs are shown in fig. 16. Many of the data points were obtained by noting that successive thermocouples warmed up in the hot ullage during expulsion. These data were in excellent agreement with the analytical prediction as shown. When complete expulsion was used for flow-rate correlation, vapor pull-through* occurred, particularly at higher tank pressures, which made the correlation uncertain (e.g., Test 3).

*Vapor pull-through is the phenomenon of ullage gas ingestion into the tank drain line during propellant outflow.

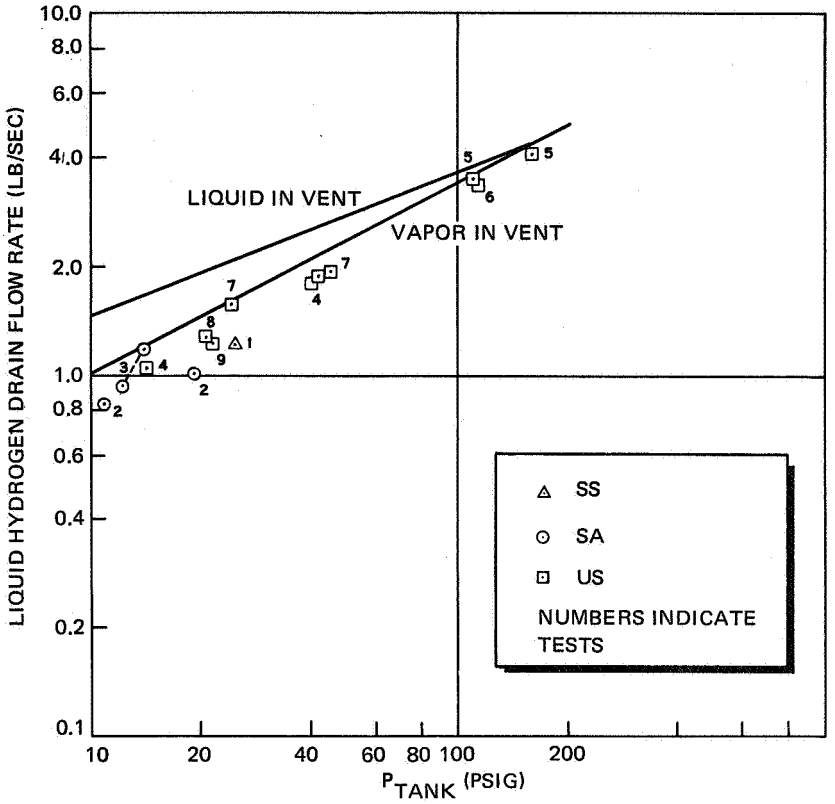

Figure 16. Liquid Hydrogen Flow Rate Correlation – Hi-Flow Orifice

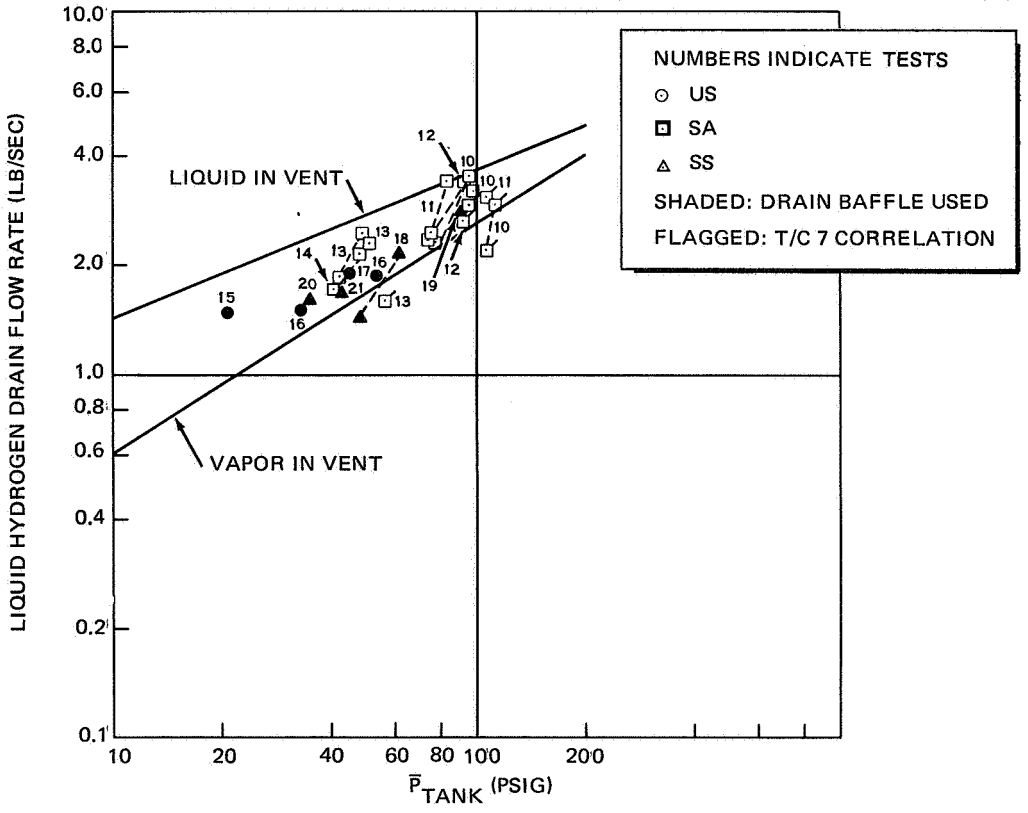

Figure 17. Liquid Hydrogen Flow-Rate Correlation – Lo-Flow Orifice

For Tests 10 through 14, the low-flow LH_2 orifice (1.375 in. ID) was used, and the correlation is shown in fig. 17. In most of these tests, total expulsion was used for correlation, and the uncertainty caused by pull-through is clearly shown. The higher point is calculated by using the time to pull-through, and the lower point is calculated by using the time to pressure blow-down following pull-through.

The uncertainty caused by pull-through led to the installation of a baffle over the LH_2 drain outlet for Tests 15 through 21. The baffle was a 3-in. -diameter metal plate centered over the 1-in. -diameter drain, and spaced 1/4-in. away from and parallel to the drain line flange. Fig. 17 shows that the addition of the drain baffle markedly reduced the uncertainty caused by pull-through and gave a correlation between the analytical lines for liquid in vent and vapor in vent, which is realistic.

Fluorine Flow Rate Correlation--Also essential to the analysis of pressurization efficiency is the knowledge of the fluorine flow rate during injection. Again the fluorine driving pressure, tank pressure, and fluorine flow rate varied continuously during the test, so the flow rate of injected fluorine was computed by monitoring the decrease in fluorine bottle pressure during the tests. The time-averaged flow-rate was determined on the basis of the actual injection time and is shown for each test in fig. 18.

Also shown is the fluorine flow rate correlation determined from the simulated propellant GN_2 and H_2O) tests described in Appendix A and shown also in fig. A-5, for the SA injector configuration. The actual SA data for

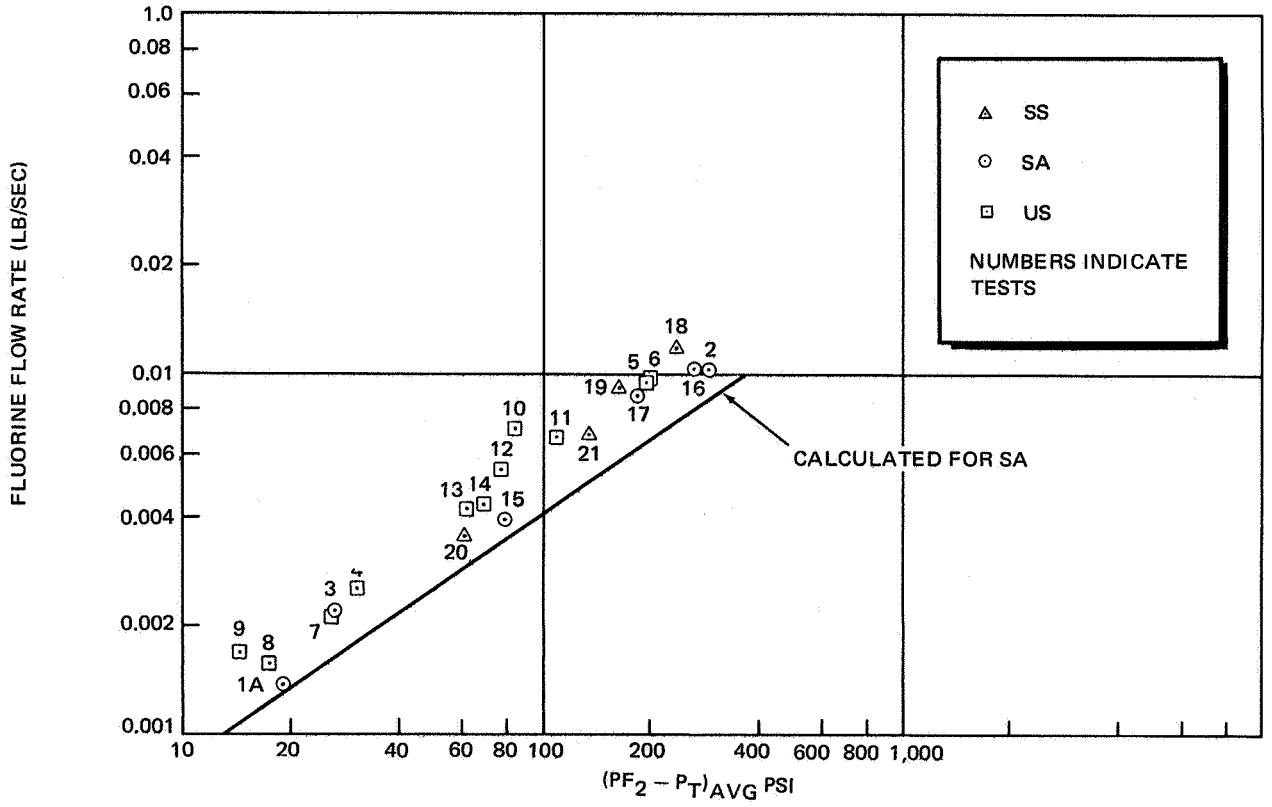

Figure 18. Fluorine Injection Flow-Rate Correlation

fluorine injection correlates quite well, although the US and SS data, which are based on a different system configuration, do not agree as well.

Tank Prepressurization--Comparison of the relative efficiency of the injection modes when used for tank pressurization prior to expulsion is of great interest from a vehicle system standpoint. This is because MTI is expected to demonstrate useful weight savings when used for prepressurization. Two simple models are useful for describing rapid prepressurization by pure heat addition to the tank. The assumption of pure heat addition is particularly appropriate for F_2/H_2 MTI, because small quantities of injectant give large quantities of heat, and the reaction products condense, giving essentially no pressurization benefit.

The first model assumes that all of the pure heat addition is used to uniformly raise the temperature (and thus the pressure) of the initial ullage gas. The analysis is shown in Appendix C. Tank pressure rise rate (for perfect gas in the ullage) as a function of injection rate and ullage volume, is

$$\frac{\dot{\Delta P}}{\dot{W}_{injectant}} = \frac{(\gamma-1)\, Q_R}{V_b} \tag{5}$$

For a nearly full LH_2 tank, the ullage may not be a perfect gas, but may consist of saturated vapor. Appendix C also shows a technique for solving for the pressure rise-rate using actual physical properties of saturated hydrogen. Actually, for low initial tank pressures (e.g., 20 psia), the computation based on saturated vapor properties (e.g., C_v), gives essentially identical results as eq. (5) (for the correct γ). For example, at 20 psia initial tank pressure, assuming a $C_v = 1.5$ gives results identical with eq. (5) assuming $\gamma = 1.73$. The assumptions for C_v and γ are quite accurate for saturated H_2 vapor at these conditions.

The second model assumes that all reaction heat is used to vaporize (but not superheat) liquid, and thus raise the tank pressure by ullage mass addition. The analytical technique that uses properties of saturated vapor is also shown in Appendix C. The results computed for this model have the same form as eq. (5)

$$\frac{\dot{\Delta P}}{\dot{W}_{injectant}} = \frac{\text{Constant}}{V_b} \tag{6}$$

Neither of the models accounts for losses of heat through heat transfer to the bulk liquid or the tank walls. Such losses merely reflect as a decrease in pressure rise-rate compared to the ideal models.

The analytical results were computed for an initial tank pressure of 20 psia and are plotted with the parameters $\dot{\Delta P}/\dot{W}$ vs V_b in fig. 19.

The prepressurization data for the small- and full-scale tests are also shown in fig. 19 with the small-scale test data in the upper left. The

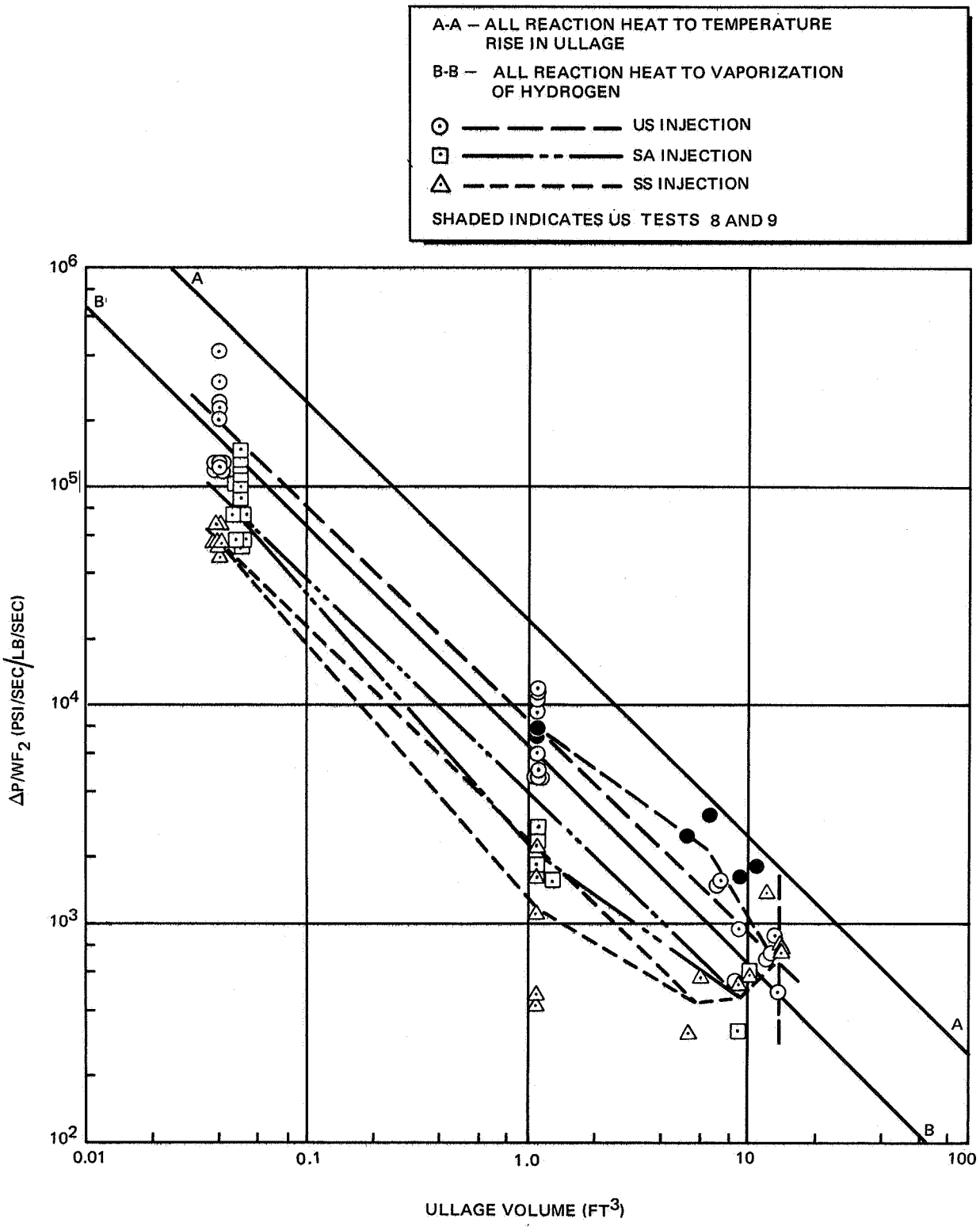

Figure 19. Prepressurization Correlation

small-scale data shown do not include all tests, but only those that were performed under similar test conditions as the full-scale tests, namely:

(1) Tests using ambient-temperature GF_2 injectant.

(2) Tests that showed vigorous reaction with no inhibition caused by oxygen content, or use of a preinjection helium purge.

The fair amount of data scatter shown may be caused by the fact that the ullage volume in the small-scale tests varied indeterminately by perhaps 20%, but all data were plotted at the estimated mean ullage volume of 0.04 ft^3.

The full-scale data are in the lower right of fig. 19. Again, there is fair scatter in the data at the small ullage volume of 1.1 ft^3; this is attributable to errors in ullage volume determination (except for the SS data scatter, which may be attributed also to the basic pressurization indeterminacy of the mode). The pressure rise-rate data were based on the longest available injection times for each run, to reduce the effect of transient surges on overall tank pressurization. Only data taken during prepressurization (at constant tank volume) were included.

The US test data correlates and follows the analytic trend very well, except that Tests 8 and 9 (shaded points) cause an upward trend in pressurization rate in the vicinity of a 7 ft^3 ullage volume. With the data from these runs ignored, the averages of the US data at each ullage volume falls on the straight dashed line shown. The anomalous behavior of Tests 8 and 9 and the reasons for the increased pressurization efficiency in these runs is discussed in detail later.

The SA test data also correlate very well from the small-scale ullage volume up to an ullage volume of about 6 ft^3. Then, the pressurization efficiency rises sharply until it is similar to the US mode at an ullage volume of 13 ft^3 (empty tank). This is because the SA (and the SS) injection mode is severely penalized by heat losses to the liquid hydrogen. As the tank empties, the losses are reduced, and all modes tend to pressurize at the same rate. This effect is clearly shown when the tank is full of liquid (ullage volume = 1.1 ft^3). The heat losses are large enough to push the pressurization rate averages down to only 57% of the predicted value; however, the dashed correlation line shown is strongly dependent on the small-scale SA data for a half-full tank, which accounts for the location of the correlation.

For the SS tests, the correlation trend is the same, and for the same reasons, except that the basic pressurization efficiency is lower than for the SA mode. This is because the SA mode (even in the small-scale tests) generally exhibited some ullage space burning, which reduces the propensity for heat transfer losses to the liquid hydrogen, with resulting increases in pressurization efficiency.

Pressurization efficiency (compared to the analytic models) vs amount of ullage is plotted in fig. 20 for selected anomalous and typical runs. Each of the points shown was for successive prepressurizations during each particular run; thus, only runs that tested with multiple drains are shown. Test 14

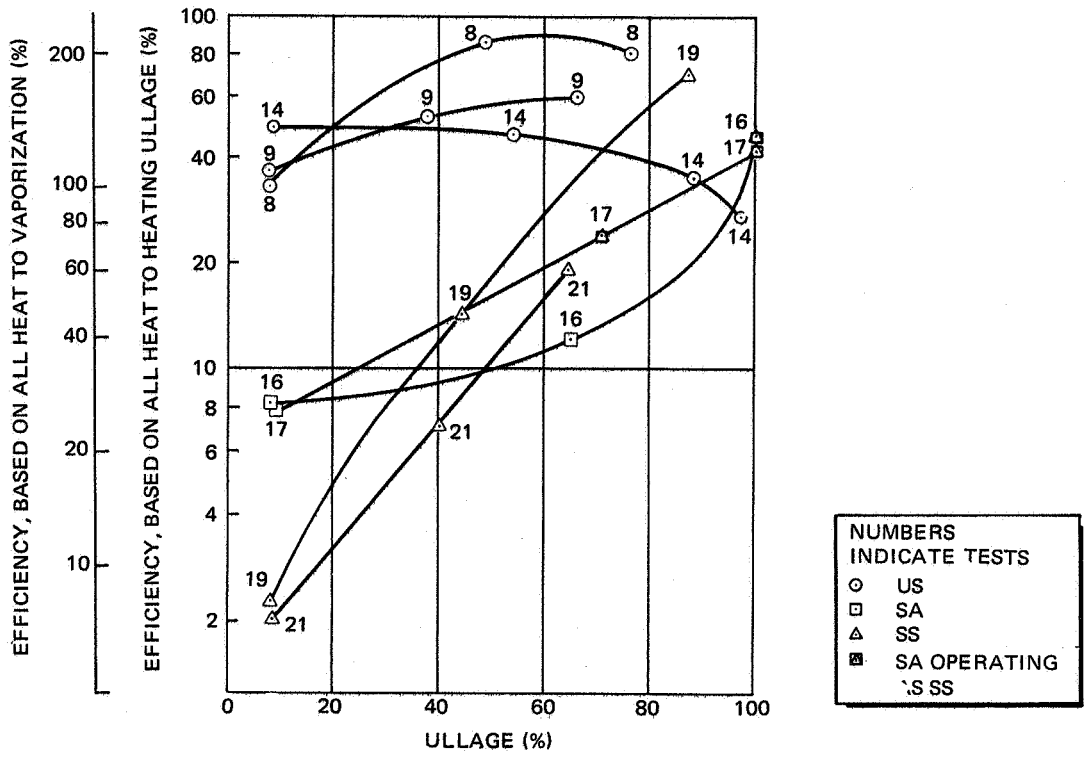

Figure 20. Prepressurization Efficiency

is a typical US mode test. The pressurization efficiency starts fairly high and remains high until the ullage volume increases to the point where the additional heat transfer losses (probably to the tank walls) take effect and drive the pressurization efficiency down. The pressurization characteristics of Tests 8 and 9 are quite different. The Test Summary, Table I, reveals that Tests 8 and 9 were different from all of the other US runs in that the fluorine driving pressure in these runs was very low (< 20 psi). This low driving pressure resulted in low fluorine injection velocity, and thus, minimum penetration of the flame into the liquid hydrogen. Initially, with the tank full, the penetration (and thus the losses) is similar for all US runs. As the tank empties, however, the efficiency of Tests 8 and 9 rises, because the low velocity flame does not penetrate the liquid hydrogen and lose heat as it did during the other US runs. Again, as the ullage volume continues to increase, the increased heat losses to the tank walls drives down the efficiency of Tests 8 and 9.

As mentioned previously, the SA tests have low efficiency with a full tank because of the long heat transfer path through the liquid hydrogen. As the tank empties, the heat losses drop, and the SA efficiency approaches that of the US injector.

The SS test pressurization efficiency is interesting in that it is extremely low (~2%) with a full tank, but increases linearly with ullage volume increase (or decrease in liquid level-heat transfer length) and also approaches the US efficiency with an empty tank.

With large ullage volume (and empty tank), all of the injection modes tend to an efficiency value of about 40% of the pressure rise rate expected based on ullage heating. Thus the ullage heating that occurs from these modes is the only way efficient pressurization can be obtained.

Expulsion Pressurization -- MTI may also be used for propellant tank expulsion pressurization for vehicle systems with pressure-fed engines (systems with pump-fed engines would probably use hydrogen bled from the engines for tank pressurization during expulsion). For this reason, it is also of interest to compare the relative efficiency of the injection modes when used for propellant expulsion pressurization. Again, two simple models are useful for describing constant pressure tank expulsion by pure heat addition, and the analyses based on these models are shown in Appendix C.

The first model assumes that all of the pure heat addition is used to uniformly heat the ullage gas so that the ullage pressure is maintained constant as the ullage volume expands (i. e. , the liquid in the tank is removed). The equation derived for perfect gas in the ullage, giving liquid outflow rate as a function of injection rate and ullage pressure is

$$\frac{\dot{W}_{LH_2}}{\dot{W}_{injectant}} = \frac{\gamma - 1}{\gamma} \frac{Q_R \rho_L}{P_b} \tag{7}$$

Again, for a saturated vapor ullage, eq. (7) gives accurate results with the correct choice of γ.

The second model assumes that all reaction heat is used to vaporize (but not superheat) liquid, and thus maintain tank pressure constant (during liquid outflow) by ullage mass addition. The resulting equation is

$$\frac{\dot{W}_{LH_2}}{\dot{W}_{injectant}} = \frac{Q_R \rho_L}{Q_V} \frac{RT_b}{P_b} \tag{8}$$

Where T_b is the saturation temperature at the ullage pressure P_b.

As in the prepressurization analyses, neither of the expulsion analyses accounts for heat losses, which reflect as a decrease in expulsion efficiency compared to the ideal models. The analytical results are plotted, together with the test data, for flow rate ratio ($\dot{W}_{LH_2}/\dot{W}_{F_2}$) vs P_b in fig. 21. The calculations for ullage heating (eq. 7) again assumed a γ = 1. 7. The full-scale test data shown (no expulsion was performed in the small-scale tests)

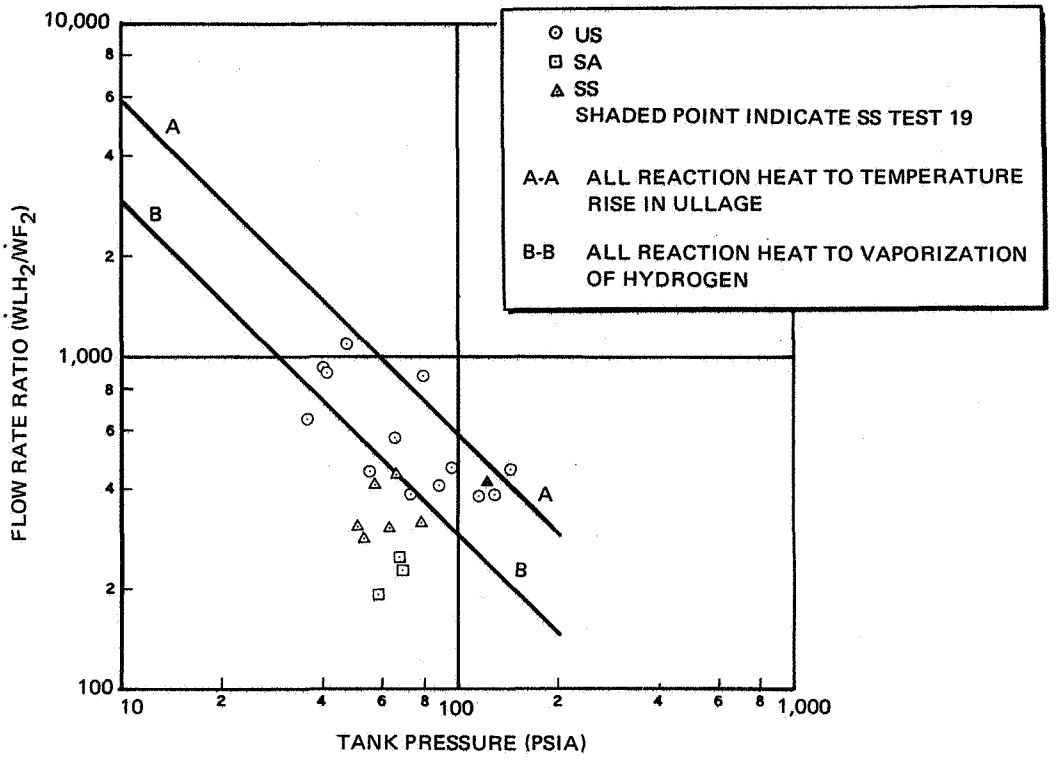

Figure 21. Expulsion Pressurization Correlation

were taken from expulsion data where the tank pressure was essentially constant during both LH_2 draining and fluorine injection. These conditions did not necessarily occur during some tests, and occurred several times on others. The data shown were computed on the basis of the average tank pressure during the selected time span. The average expulsion flow rate was computed on the basis of this average tank pressure and the correlations given in figs. 16 and 17. The average fluorine-driving pressure during the selected drain time was used to determine the fluorine-injection rate from the correlation shown in fig. 18. Further, the data were computed only for drains with ullage volume less than 90% of tank volume, for reasons that are explained below. As could be expected from the averaging technique, there is some data scatter, but it appears no worse than the scatter for the prepressurization data for which the determining variables were better controlled. The data clearly follow the trend predicted by the models, with the US data lumped in the region of the ullage heating model, but the submerged data is lower in performance, near the vaporization model. (Except for the shaded point, which represents an interesting anomalous test which is discussed in detail on page 39.)

It was found that amount of ullage volume had a strong influence on the expulsion pressurization efficiency, even though no such volume dependence appeared in the simplified analytical models. This is thought to be the result of ullage-volume-dependent heat transfer losses that are not accounted for in the analyses. The effect is not surprising because ullage-volume-dependent efficiency losses were observed in the prepressurization data discussed previously. To evaluate this ullage volume effect, the pressurization efficiency

$$\eta \equiv \frac{\left(\dot{W}_{LH_2}/\dot{W}_{F_2}\right)\ \text{Actual}}{\left(\dot{W}_{LH_2}/\dot{W}_{F_2}\right)\ \text{Heated Ullage}}$$

at the particular tank pressure, was plotted vs average ullage volume percent (during the selected drain interval) in fig. 22.

The US data drops off in efficiency with increasing ullage volume (displaying the same trend noted in the prepressurization data) up to an ullage fraction of 90%. At this point, the efficiency drops abruptly, probably due to pull-through, which occurred when the tank was nearly empty (for the US tests shown, which were made before the drain baffle was installed).

The submerged tests follow a different trend, with the efficiency remaining relatively constant but lower than the US value, until the tank is nearly empty, when the efficiency rises to match that of the US mode. This trend is similar to that found for the prepressurization efficiency.

Test 19 is shown because the test data are quite different from the other SS (or SA) data. For this test, the tank pressure remained constant at 109 psig for nearly the entire second drain. This was fortuitous, because the fluorine injection rate was just right to match exactly the LH_2 outflow rate,

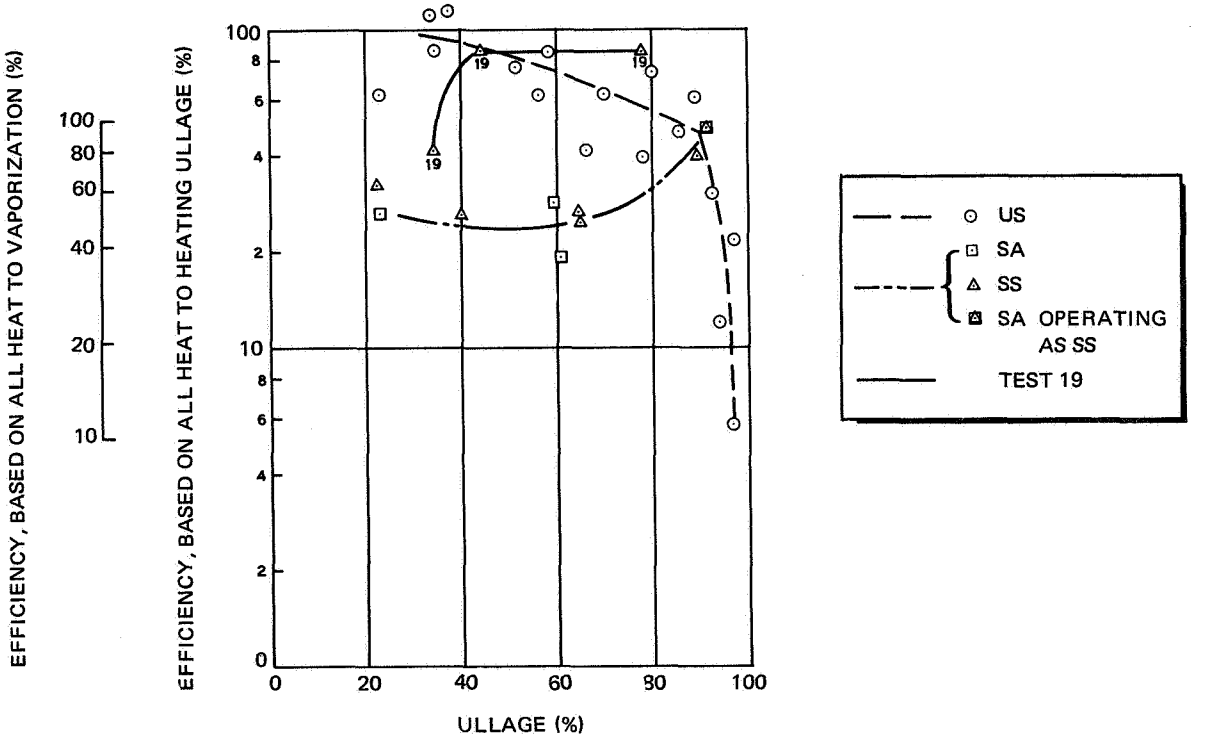

Figure 22. Expulsion Pressurization Efficiency

and thus keep the tank pressure constant (also with no apparent loss in efficiency). Further, the efficiency during this drain was very high (~86%) and very similar to the efficiencies shown for US mode injection. The reasons for this anomalous behavior appear to be that this particular submerged run was made for prepressurization and expulsion at high tank-pressure (~100 psig). Because of the planned high tank pressure, high-pressure, high flow rate, fluorine injection was used. The heavy prepressurization losses of the SS injection mode required that very long prepressurization times (~23 seconds) were required to reach 100 psig. It is believed that this long, continuous, high-velocity fluorine injection created a hole in the LH_2 that reached from the ullage to the injector along the tank centerline and that the vapor in this ullage extension was heated by injection in the same way that US mode injection heats the ullage. This would give a high initial pressurization efficiency that is comparable to that of the US mode. Further, at this high tank pressure, the LH_2 outflow rate was quite high, so that the drain from an ullage fraction of 44 to 78% (shown as the straight solid line) took place in only 6.6 seconds. This short time gives little opportunity for heat transfer and could explain the fact that efficiency remained uniform and high.

Again, with large ullage volume (and empty tank), all of the injection modes tend to an efficiency value of about 50% of the ullage heating prediction.

Pressure Collapse Correlation--The pressure collapse in the ullage that follows prepressurization injection is an important parameter in defining the efficiency of the injection modes; the proper control of this collapse may be vital for advanced missions where there is substantial delay between tank prepressurization and engine start. In the small-scale tests, it was found that the US mode tended toward substantial pressure collapse, but the submerged modes did not. This effect was thought to be caused by ullage heating (and subsequent collapse) in the US mode, and mass vaporization (without collapse) in the submerged modes. In these tests, pressure collapse occurred immediately after a single, very short injection (~100 msec) and the phenomenon was confused by scale effects (including sloshing) in the small vessel, so that an actual collapse correlation was not possible.

However, in the full-scale tests, with continuous fluorine injection and a very hot flame, pressure collapse tends to occur all the time during prepressurization and expulsion, because the potential for heat transfer to walls or liquid is always present. This collapse is reflected as an efficiency loss, as described in the preceding sections. Because collapse is basically a heat transfer phenomenon, it depends strongly on ullage temperature and, thus, heat transfer potential. In the full-scale tests, extreme temperature gradients generally occurred; with very high temperatures (burning injectors) in one part of the tank, and LH_2 temperature tank walls elsewhere. Because of the difficulty of determining the effective ullage temperatures under such conditions, the equivalent (and more reliably measured) parameter, pressure times volume, (PV) was used for collapse correlation. The pressure collapse rate in psi/sec is plotted vs the parameter PV in fig. 23. The data shown were determined for those few tests where collapse followed F_2 injection with no LH_2 draining taking place. (Many early US tests had rapid pressure rise and draining prior to the end of F_2 injection.)

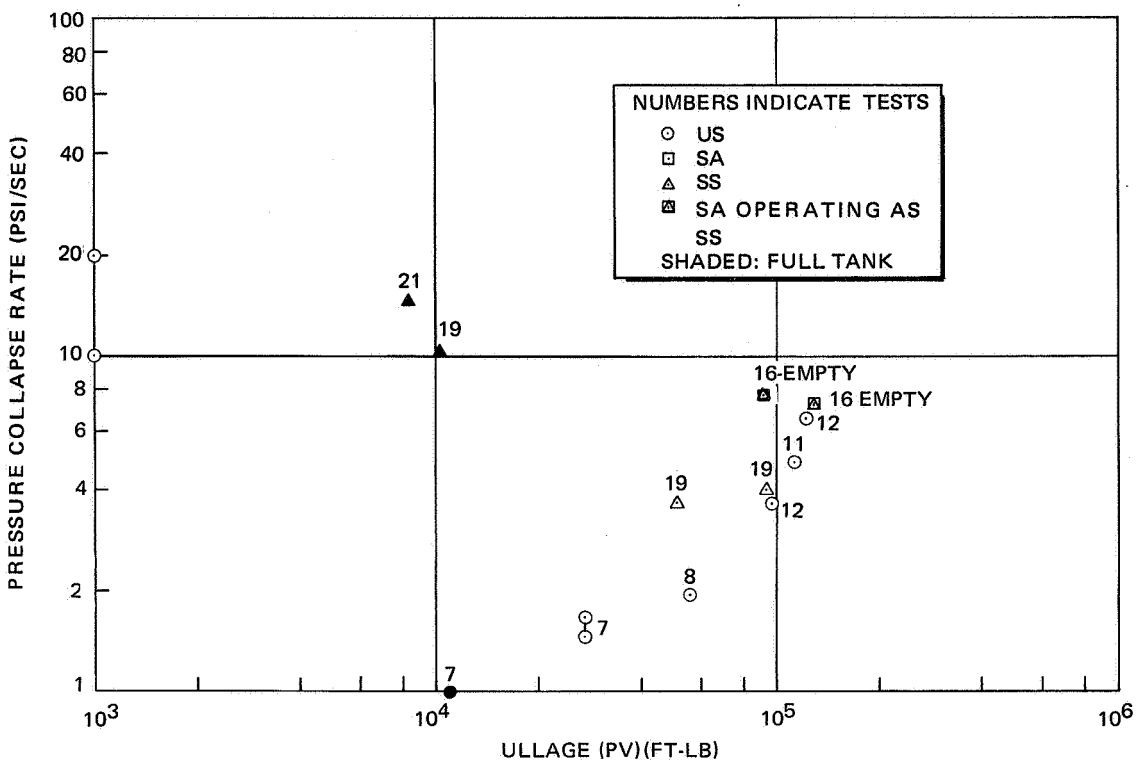

Figure 23. Pressure Collapse Correlation

The US mode shows an increase in collapse rate with PV, as would be expected from the previously mentioned prepressurization and expulsion pressurization efficiency trends that indicate higher loss (collapse) at large ullage fractions. The shaded points are for collapse with a full tank (8.3% ullage). The SS data shown have much larger collapse rates when the tank is full than the US mode. This implies that the SS mode may give pressure rise from the creation of very hot vapor bubbles, which then lose heat in the surrounding liquid (and collapse) once injection ceases. This collapse happens rapidly. For Tests 19 and 21 (shown shaded) the initial collapse took only 0.5 second; then there was no further collapse. In fact, in Test 21, the pressure rose 3 psi during the next 24 seconds (due, likely, to heat leak into the tank.) Other submerged tests also displayed no further collapse after the initial sharp drop.

In Test 19, however, collapse is quite pronounced, because, as described previously, the mode was performing as the US mode, and the trend for this test approaches the US mode trend. Further, the SA mode, when it operated into an empty tank, also tended to behave like the US mode--with equivalent collapse rate.

The trends shown again reinforce the results shown previously for trends of efficiency loss, demonstrated by pressure collapse, in all of the injection modes.

CONCLUSIONS

As a result of the full-scale injector test program it has been found that fluorine-hydrogen MTI is a feasible pressurization technique for a liquid hydrogen tank; however, tank pressurization can be efficiently attained only by ullage heating, rather than by vaporization of hydrogen. Manual control of the tank pressure during prepressurization and expulsion was demonstrated, and the extension to an automatic tank pressure control system appears straightforward. The MTI technique can be made to perform in a reliable and repeatable fashion, as evidenced by the following specific conclusions:

(1) Reliable ignition and re-ignition was demonstrated in all injection modes (US, SA, and SS). In the submerged modes, injectant freezing and detonation was an occasional problem. The injector configuration criteria that are necessary to eliminate the problem were developed.

(2) An injector burning problem in the US mode was solved by the use of a copper injector. The high thermal conductivity eliminated hot spots leading to injector destruction. Tank pressurization was not significantly affected by injector burning.

(3) The US injector mode demonstrated efficient and rapid tank pressurization by ullage heating and required minimum fluorine for tank prepressurization and propellant expulsion.

(4) The SA injector did not operate satisfactorily: It was unable to pump (by aspiration) sufficient hydrogen for vaporization and injector cooling. The injector always operated extremely oxidizer (fluorine)--rich and very hot, which resulted in severe damage to the injector as the tank emptied.

(5) The SS injection mode has very low pressurization efficiency when it is operating into a full tank because of large heat losses to the liquid, but the efficiency improves as the tank empties, and approaches the US mode, in operation and efficiency, with a nearly empty tank. With high-pressure fluorine injection, the SS mode approaches the operation and efficiency of the US mode for a half-full tank.

(6) The generation of large quantities of HF in the course of the program was an annoyance as far as disposal was concerned, but did negligible damage to the tank interior. However, the HF is drained along with the hydrogen and, in sufficient quantities, could cause vehicle subsystem problems, particularly if allowed to warm up and contact water.

(7) Wall heating during the US mode tests was not a significant problem, and some pressure collapse, probably due to heat transfer to the walls, was observed during the US mode tests with a nearly empty tank.

(8) The test program generated much valuable MTI system design data that included:

(A) Correlation of prepressurization trends with simple models and determination of relative injection mode efficiency.

(B) Pressurization during expulsion showed similar efficiency trends that also correlate well with simple models.

It is recommended that more detailed and sophisticated models, which would include provisions for heat transfer modes, be developed to predict injection losses and more exactly correlate the data, so that more confident extrapolation from the existing test data to arbitrary tank sizes and liquid levels is possible.

This test program has demonstrated sufficient confidence in the Fluorine-Hydrogen MTI system reliability and controllability to allow consideration of MTI system development and application to a flight vehicle.

Appendix A

SA INJECTOR ANALYSIS AND DEVELOPMENT

PRELIMINARY ANALYSIS

The configuration for the preliminary analysis is shown in fig. A-1, and the symbols are defined in Nomenclature. The analysis assumes compressible, perfect-gas, isentropic flow of the fluorine and incompressible flow of the LH_2. It is also assumed that there is no heat transfer or shear force across the fluid interface. The momentum equation for the system is

$$\frac{\dot{W}_L}{g} U_{L_2} + P_2 A_{L_2} - \frac{\dot{W}_L}{g} U_{L_1} - P_1 A_{L_1} = \int_o^L P dA_L$$

for the configuration shown,

$$\int_o^L P dA_L \doteq \frac{1}{2}(P_1 + P_2)(A_{L_2} - A_{L_1}) \qquad \text{and} \qquad P_2 = P_b$$

The continuity equation for the liquid is

$$\dot{W}_L = \rho_L A_{L_1} U_{L_1}$$

Combining and rearranging gives the expression for the entering and exiting liquid area ratio:

$$\frac{A_{L_2}}{A_{L_1}} = \frac{\frac{2\rho_L U_{L_1}^2}{g}\left[\left(\frac{U_{L_2}}{U_{L_1}}\right) - 1\right]}{P_1 - P_b} - 1 \qquad \text{(A-1)}$$

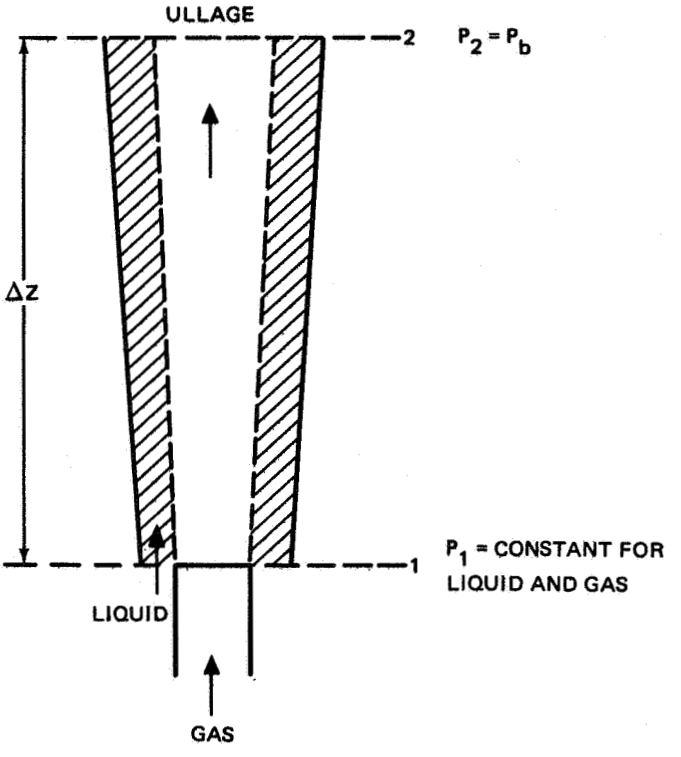

Figure A-1. SA Analysis Model

The continuity equation for the gas is

$$\rho_{g_1} U_{g_1} A_{g_1} = \rho_{g_2} U_{g_2} A_{g_2}$$

and the equation of state is

$$\rho_{g_1} = \frac{P_1}{RT_{g_1}} \quad ; \quad \rho_{g_2} = \frac{P_b}{RT_{g_2}}$$

Combining and rearranging gives

$$\frac{A_{g_2}}{A_{g_1}} = \left(\frac{P_1}{P_b}\right)\left(\frac{T_{g_2}}{T_{g_1}}\right)\left(\frac{U_{g_1}}{U_{g_2}}\right) \qquad \text{(A-2)}$$

Also

$$\frac{A_2}{A_1} = \frac{A_{L_2} + A_{g_2}}{A_{L_1} + A_{g_1}} = \frac{\frac{A_{L_2}}{A_{L_1}} + \left(\frac{A_{g_2}}{A_{g_1}}\right)\left(\frac{A_{g_1}}{A_{L_1}}\right)}{1 + \frac{A_{g_1}}{A_{L_1}}} \tag{A-3}$$

From Bernoulli's equation for the liquid:

$$U_{L_1} = \left\{2g\left[\frac{(P_b - P_1)}{\rho_L} + \Delta Z\right]\right\}^{1/2} \tag{A-4}$$

Also, the following equations apply to the gas flow:

$$\left.\begin{aligned}
P_1 &= \frac{P_{o_g}}{\left(1 + \frac{\gamma - 1}{2} M_{g_1}^2\right)^{\gamma/\gamma-1}} \\
T_{g_1} &= \frac{T_{o_g}}{1 + \frac{\gamma - 1}{2} M_{g_1}^2} \\
U_{g_1} &= M_{g_1} \sqrt{\gamma g R T_{g_1}} \\
T_{g_2} &= \frac{T_{o_g}}{1 + \frac{\gamma - 1}{2} M_{g_2}^2} \\
M_{g_2} &= \sqrt{\frac{2}{\gamma - 1}\left[\left(\frac{P_{o_g}}{P_b}\right)^{\gamma-1/\gamma} - 1\right]} \\
U_{g_2} &= M_{g_2} \sqrt{\gamma g R T_{g_2}}
\end{aligned}\right\} \tag{A-5}$$

Equations (A-1) through (A-5) were programmed in Intercom Language for the RCA 70-45 digital computer and were solved for

$$\lambda = \frac{\dot{W}_{L(H_2)}}{\dot{W}_{g(F_2)}} \quad \text{and} \quad \beta = \frac{A_{L_1}}{A_{g_1}}$$

Because of the form of the equations, with all variables floating, and no closed-form solution, assumptions had to be made for many of the pertinent variables. The small-scale testing indicated that the injectant Mach number in these tests varied between about 0. 1 and 0. 5, and thus, these values were assumed to be the range of Mg_1. Appropriate assumptions were made for P_o, P_b, T_o, ΔZ, and Ag_1 on the basis of the anticipated full-scale test configuration. The input values of β were 1/3, 1, and 3.

An additional assumption was needed for the ratio U_{L2}/U_{L1} because in the initial analysis, the ratio A_2/A_1 was allowed to vary. Because of the model configuration, the selected ratio U_{L2}/U_{L1} was quite small. Further, as the results were generated, it was found that the parameter $(P_o - P_b)$ had to be of a low-value ($\sim$0. 5 psi) to achieve good pumping performance. The initial results of this simplified analysis are shown in fig. A-2. The pumping ratio (λ) decreases with a decrease in pumping area ratio (β) and an increase in back pressure. With a constant pressure fluorine supply, an increase in back pressure will decrease the incoming Mach number and also cause a decrease in λ, as shown. This trend is significant because a decrease in λ is equivalent to an increase in oxidizer-fuel (O:F) ratio and therefore, an increase in flame temperature. $\lambda = 4$ gives an equilibrium flame temperature of 500°R, which is the maximum recommended for normal pressurization. Fig. A-2 shows that a $\beta = 1$ gives a $\lambda \doteq 4$ even with increases in back pressure. A $\beta = 3$ gives much larger values of λ.

It appears that some of the assumptions of the analysis, particularly the assumptions of one-dimensional flow and $P_g = P_{L1}$, break down at large values of β. This was observed experimentally with the original small-scale aspirator design when, with a $\beta = 5$, there was reverse flow in the pumping area.

An SA injector that was designed from this preliminary analysis and the small-scale test data gave problems during the injector testing with F_2 and LH_2, as discussed in Results. Because of these SA injector problems, it was decided that simulated propellant tests would be performed on an identical spare SA injector and that H_2O and gaseous nitrogen would be used to simulate the LH_2 and GF_2. The purpose of these tests was to verify and map injector pumping (aspiration) performance and then to compare the results with the preliminary (or a modified) analysis and extrapolate the results to predict injector performance with LH_2 and GF_2; the test parameters such as the required GF_2 driving pressure could then be redefined.

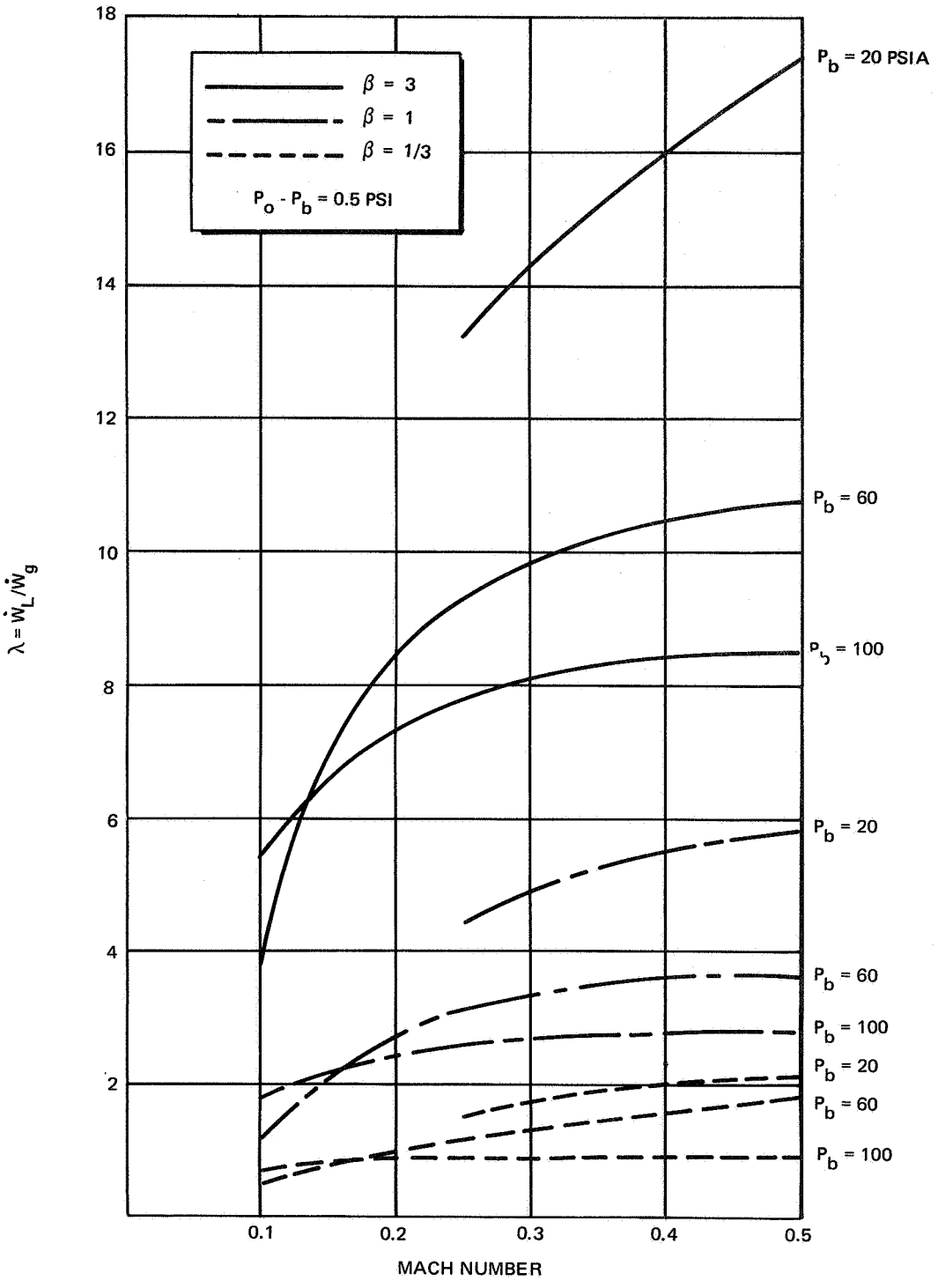

Figure A-2. Preliminary SA Injector Performance

SIMULATED PROPELLANT TESTING

The test apparatus that was used in the simulated propellant tests is shown schematically in fig. A-3. The injector was assembled in a 2-ft-diam by 4-ft tank. The injector tube extended out of the tank and the penetration through the tank wall was sealed, both at the top and bottom of the tank. The tank was filled with water to a level of 1.27 ft above the injector nozzle. A 1-in.-diam collector tube was fastened to the injector tube; this tube extended down to a graduated cylinder where the pumped water was collected and measured. The overall water test facility is shown in fig. A-4.

During each run, the tank was vented to the atmosphere by a 1/4-in.-diam vent line that penetrated the bottom of the tank and extended up to the liquid level. The liquid level was maintained by filling the tank slightly above the vent line level and then allowing the tank to drain through the vent. The vent line was also used to check the reverse flow through the aspirator during each run. This check was accomplished by using leak detection soap solution at the vent exit. GN_2 was supplied by a bank of cylinders that were regulated to the desired pressure. The GN_2 flow rate was measured by a calibrated turbine flowmeter and pulse rate converter. Static pressures were measured at two positions downstream of the injector valve (P''_2 and P''_1). The total pressure upstream of the injector valve (P'_o) was measured in a total pressure chamber. When the injector valve was opened a surge of water (~100 cc) was delivered to the graduated cylinder. This was, primarily, the water that was contained in the injector tube. So as not to include transient starting conditions, the test measurements began after the collector flow appeared to be steady. The test duration for each run was 5 min. At the beginning and end of each run, the GN_2 flow rate, the pressures, and the water level in the graduated cylinder were recorded. Table A-1 shows the data obtained in the 31 runs during which the total driving pressure P'_o, and the injector area ratio (β = liquid flow area/gas flow area) were varied for each run. β was varied by the adjustment build into the injector. The back pressure, P_b, was kept constant at 14.7 psia by the tank vent.

The static pressure measurements made downstream of the injector valve (P''_2 and P''_1), together with the GN_2 flow rate, provided the information necessary for the computation of the total pressure at this location (P''_{o2} and P''_{o1}). Further, it was shown that

$$\frac{(\dot{W}_g)_{N_2}\sqrt{T_o R}}{P''_o A''_g} = \text{constant} = 3.88\, C_d$$

throughout the pressure (P'_o) range from 80 to 250 psig.

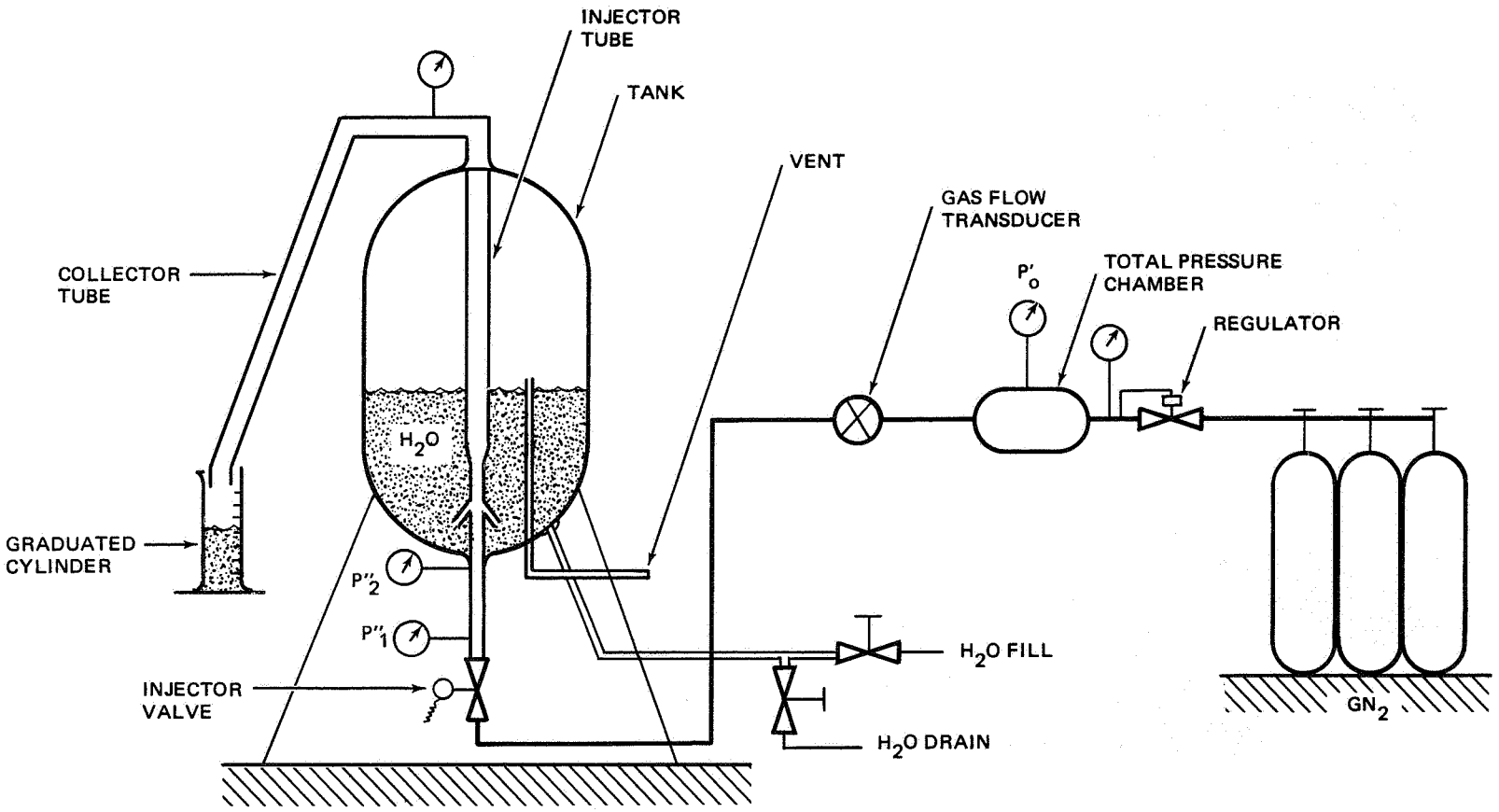

Figure A-3. Simulated Propellant Injector Test Apparatus Schematic

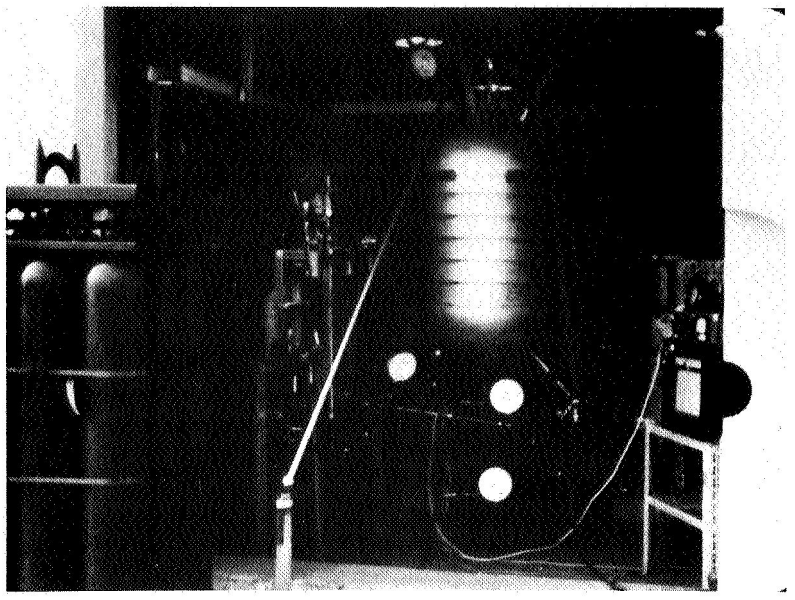

Figure A-4. Injector Water Test Facility

A total pressure of 80 psig was the lowest practical value for the full-scale MTI tests, because this corresponded to a fluorine driving-pressure downstream from the injector valve of about 30 psig (which was equal to the lowest tank pressure tested).

The form of the equation shows that the flow is choked, and the data are matched by a discharge coefficient (C_d) of 0.73, as shown in fig. A-5. This discharge coefficient corresponds to that of a choked-sharp-edged orifice given by Shapiro. * This discharge coefficient now defines the total pressure (P''_o), in the injector that is required to analyze the pumping performance. This curve was also extrapolated for GF_2 flow by merely multiplying the GN_2 flow by the square root of the molecular weight ratio

$$\sqrt{\frac{m_{F_2}}{m_{N_2}}}$$

*Shapiro, A. H. : The Dynamics and Thermodynamics of Compressible Fluid Flow. Ronald Press, 1953.

TABLE A-I

SIMULATED PROPELLANT TEST SUMMARY

	Run No.	P_o'	$(P'')_1$	$(P'')_2$	$\dot{W}_{GN_2}$		$\dot{W}_{H_2O}$	
		psig	psig	psig	SCFM	lb/sec	ml H_2O	lb/sec
$\beta = 1.45$	1	250	62	57	5.40	0.00682	60	0.000441
	2	200	50	44	4.60	0.00580	95	0.000698
	3	150	36	30	3.70	0.00470	232	0.00171
	4	100	23	17	2.42	0.00330	280	0.00206
	5	80	17	12	2.05	0.00261	305	0.00224
	6	30	7	2	1.20	0.00152	210	0.00155
	7	15	5	0	0.80	0.00102	155	0.00114
	8	60	11.5	8	1.75	0.00222	282	0.00207
	9	7	0	0	-	0.00025	75	0.000552
$\beta = 3.15$	10	250*	63	56	5.40	0.00682	5	0.0000368
	11	200*	48	43	4.60	0.00580	30	0.000221
	12	150	35	30	3.70	0.00470	145	0.001065
	13	100	21.5	17	2.60	0.00340	176	0.001295
	14	80	16	12	2.05	0.00261	190	0.00140
	15	60	12	8	1.70	0.00219	185	0.00136
	16	30	7	2	1.20	0.00152	160	0.001175
	17	15	4	0	0.80	0.00102	109	0.00080
$\beta = 0.4$	18	248	63	56	5.40	0.00682	112	0.000823
	19	200	51	43.5	4.60	0.00580	167	0.001225
	20	150	34	30	3.80	0.00480	222	0.00163
	21	100	20	17	2.52	0.00319	208	0.00153
	22	80	15	11	2.10	0.00266	170	0.00125
	23	60	10	7	1.75	0.00222	131	0.000963
	24	30	5	1	1.25	0.00158	65	0.000478
$\beta = 4.65$	25	104	20	17	2.42	0.00306	149	0.001095
	26	150*	33	30	3.60	0.00456	120	0.000882
	27	202*	47	43	4.50	0.00569	49	0.000360
	28	250*	61	56	4.60	0.00558	10	0.0000735
	29	60	13	8	1.65	0.00208	168	0.001235
	30	40	8	4	1.40	0.00177	161	0.001180
	31	30	4	2	1.20	0.00152	136	0.001000

* Backflow

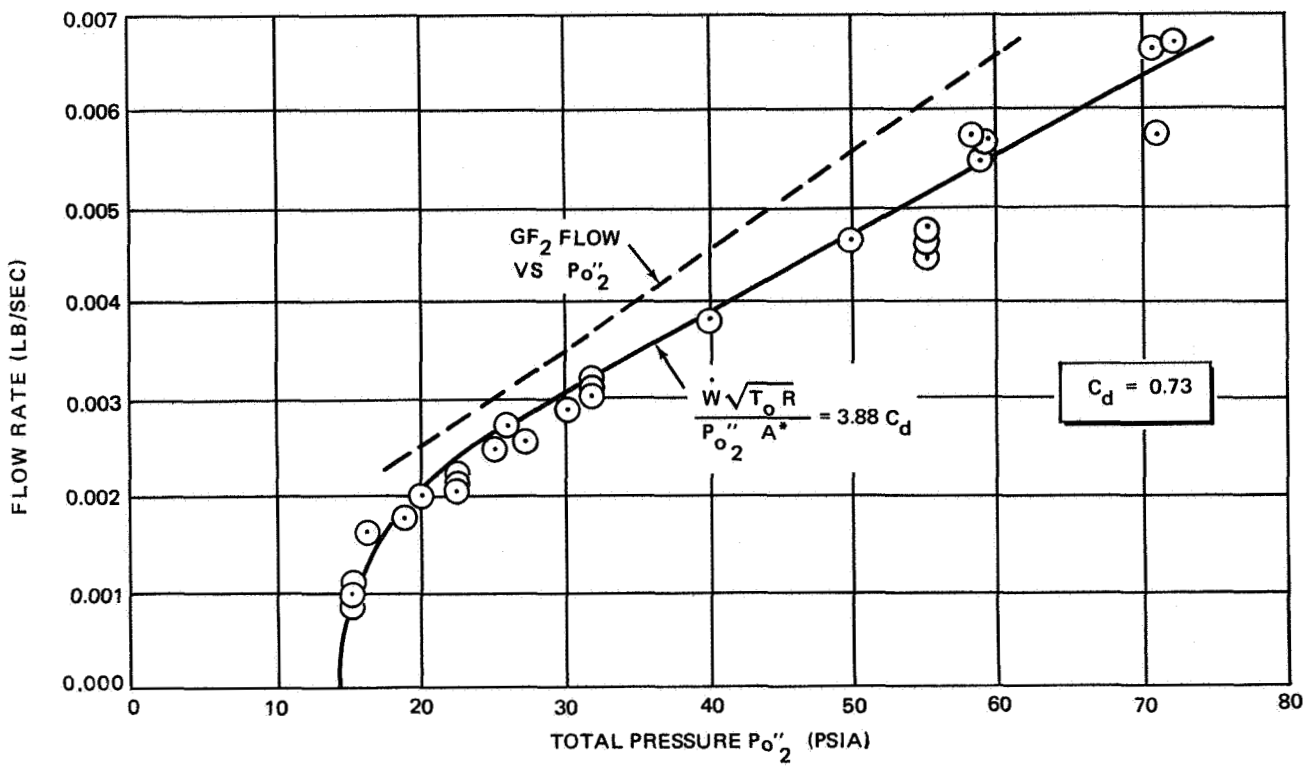

Figure A-5. GN_2 Flow Rate Vs. Total Pressure

The actual water pumping performance of the injector is mapped in fig. A-6. Here, the flow rate ratio (λ) in lb/sec of water per lb/sec of GN_2 is plotted as a function of the pumping area ratio (β) with P'_o as a parameter. The pumping performance (λ) increases with β to a maximum, then falls off with further increase in β. λ also increases as the driving pressure (P'_o) decreases. At high β and high P'_o, there is reverse flow in the aspirator; this was experimentally observed at the five points shown. The points of maximum λ, although not exactly determined, are bracketed by the experimental data, which allow for extrapolation of the calculated (solid) lines by the dashed lines shown.

MODIFIED ANALYSIS

The preliminary analysis was modified to conform to the actual injector configuration. The preliminary analysis was for the injector configuration shown in fig. A-7a, but the actual configuration is shown in fig. A-7b. In the process of the modification of the analysis, some of the equations were rewritten to conform better to the model and revised assumptions; e. g. , the aspirator was a constant-diameter tube; and the entering gas flow was sonic or near-sonic. The revised equations were as follows:

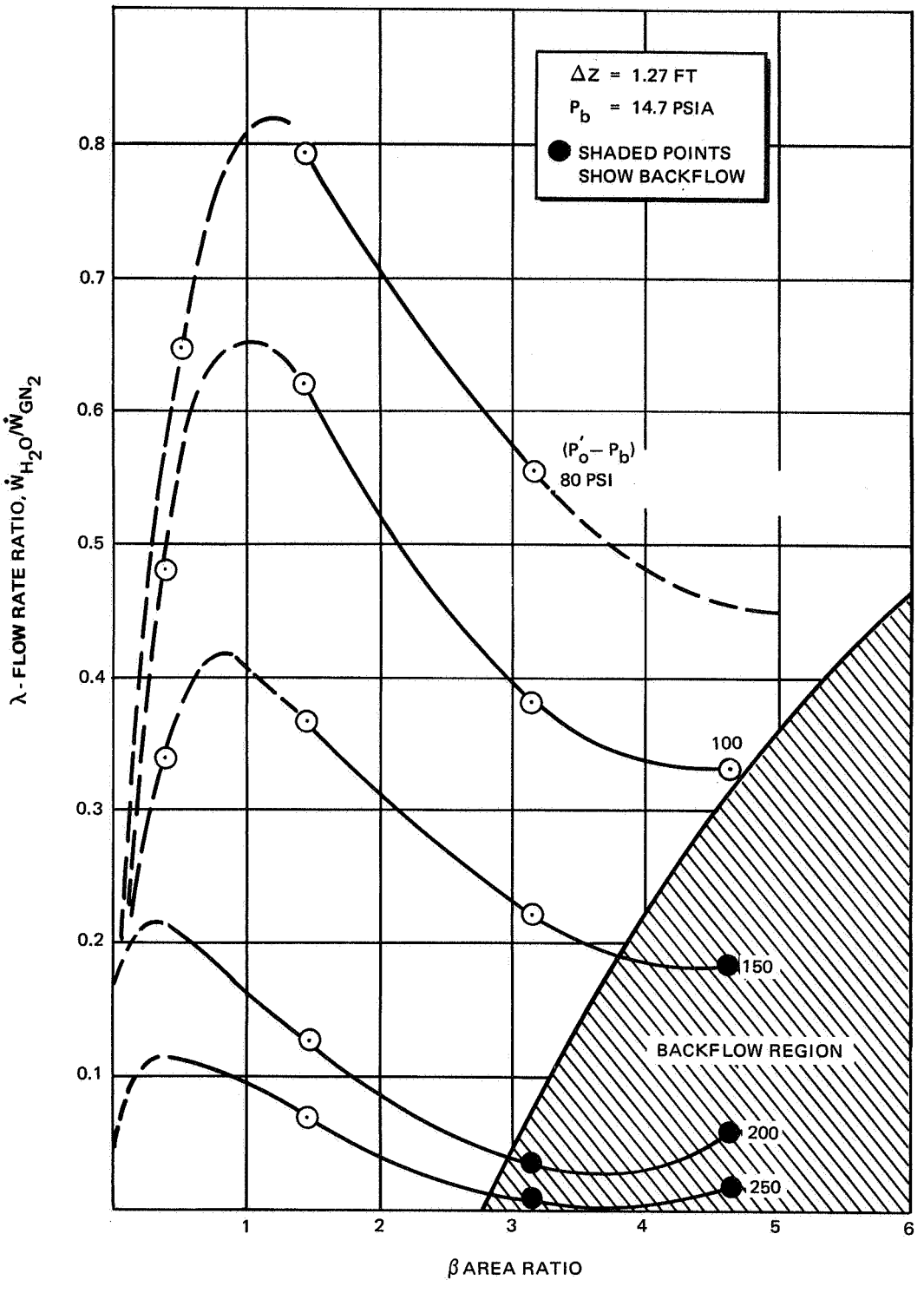

Figure A-6. Water Pumping Performance for SA Injector

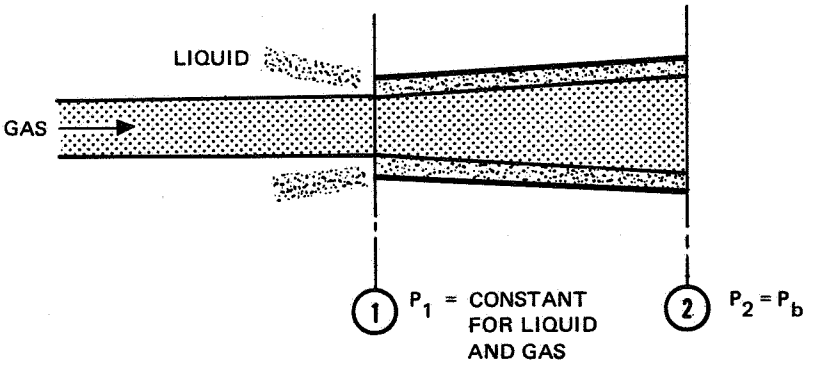

(a) SIMPLIFIED MODEL

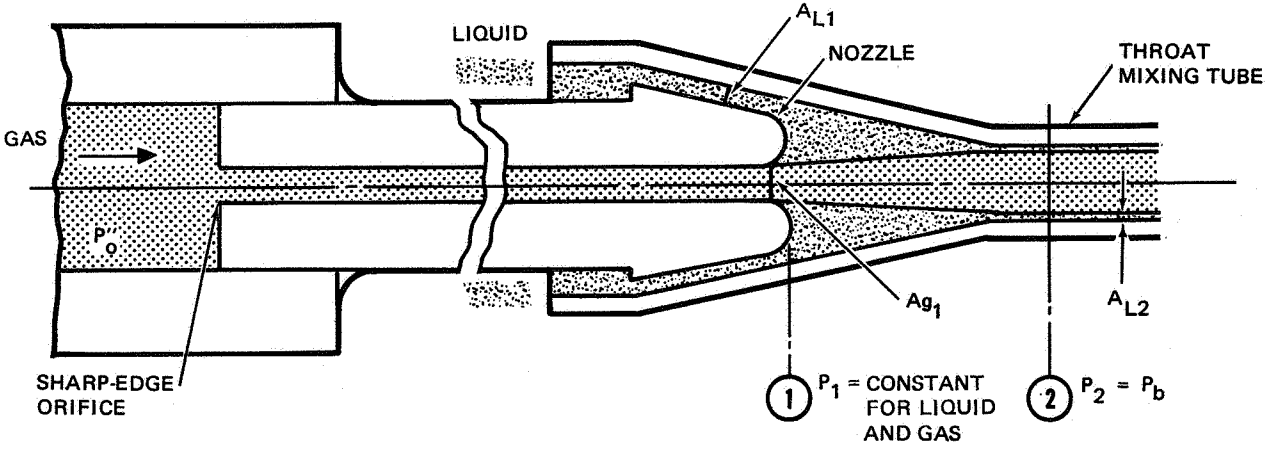

(b) ACTUAL CONFIGURATION

Figure A-7. Analytical Models for SA Injector

The momentum equation for the system is still

$$\frac{\dot{W}_L}{g} U_{L_2} + P_2 A_{L_2} - \frac{\dot{W}_L}{g} U_{L_1} - P_1 A_{L_1} = \int_o^L P dA_L \qquad (A-6)$$

and for the configuration shown,

$$\int_o^L P dA_L = \frac{1}{2}(P_1 + P_2)(A_{L_2} - A_{L_1}) \qquad \text{with} \qquad P_2 = P_b$$

The continuity equation for the liquid is written as

$$\dot{W}_L = \rho_L \beta A_{g_1} U_{L_1} \qquad (A-7)$$

From Bernoulli's equation the velocity of the liquid at station 1 is

$$U_{L_1} = \left\{ 2g \left[\frac{P_b - P_1}{\rho_L} + \Delta Z \right] \right\}^{1/2} \qquad (A-8)$$

Also, the following equations still apply to the gas flow:

$$\left.\begin{aligned} P_1 &= \frac{P_{o_g}}{\left(1 + \frac{\gamma - 1}{2} M_{g_1}^2\right)^{\gamma/\gamma - 1}} \\ T_{g_1} &= \frac{T_{o_g}}{1 + \frac{\gamma - 1}{2} M_{g_1}^2} \\ U_{g_1} &= M_{g_1} \sqrt{\gamma g R T_{g_1}} \\ M_{g_2} &= \sqrt{\frac{2}{\gamma - 1}\left[\left(\frac{P_{o_g}}{P_b}\right)^{\gamma - 1/\gamma} - 1\right]} \end{aligned}\right\} \qquad (A-9)$$

The difference between these and the original equations is that the conditions at Station 2 and the variable A_2/A_1 are no longer required. Because of this simplification, an explicit solution can now be obtained in terms of the input parameters. Again, the equations were programmed in Intercom Language for the RCA 70-45 digital computer and were solved for

$$\lambda = \frac{\dot{W}_{L(H_2)}}{\dot{W}_{g(F_2)}}$$

in terms of geometric and fluid parameters.

The performance from the water tests, however, was not predictable with this model, because of the actual injector nozzle-throat configuration shown in fig. A-7b. Here, the liquid flow encounters a sudden contraction at the annular entrance, followed by a gradual contraction to Station 1, a sudden expansion, and then gradual contraction to Station 2.

The flow losses caused by these expansions and contractions combine to cause a net head (pressure) loss. Further, the liquid area at Station 1, A_{L_1}, is not equal to βA_{g_1}, as was the case for the sharp-edged nozzle in the simple model, fig. A-7a. To account for this area difference and head loss, a discharge coefficient C_{d_L} was incorporated into the continuity equation as follows:

$$\dot{W}_L = P_L \beta A_{g_1} U_{L_1} C_{d_L} \qquad \text{(A-10)}$$

where

$$C_{d_L} \equiv C_{W_L} C_A$$

With the experimental data from the water tests, solution of eqs. (A-6), (A-8), (A-9), and (A-10), resulted in values of C_{d_L} as a function of β, as shown in fig. A-8. The dotted lines shown are extrapolated to zero (corresponding to $C_A = 0$).

To use the discharge coefficient (C_{d_L}) for prediction of the performance of the SA injector when it is operating with LH_2 and GF_2, it is necessary to determine the dependence of C_{d_L} on Reynold's number, which is the applicable similarity parameter. Based on the Reynold's number form

$$Re = \frac{Wd}{A\mu}$$

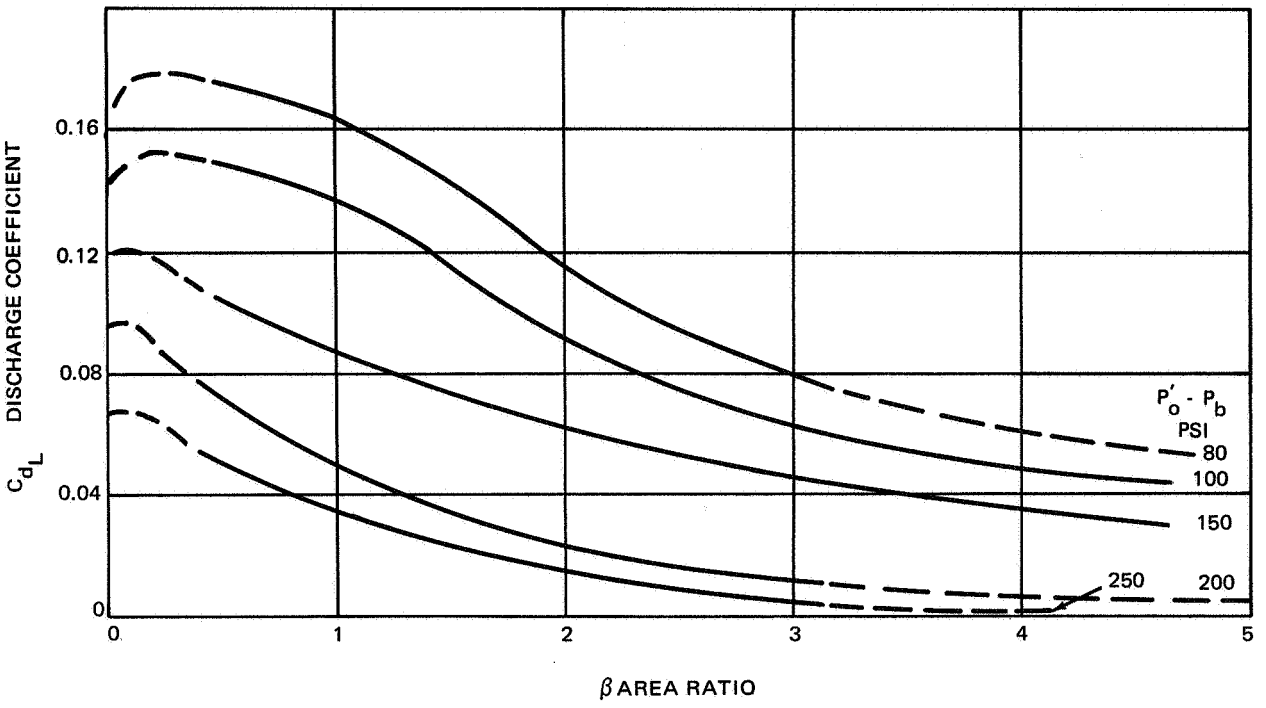

Figure A-8. Water Discharge Coefficient for SA Injector

where $\dot{W}$ is the actual water flow rate and d is the actual flow gap distance (at a particular β); C_{d_L} is plotted versus Reynolds number in fig. A-9. The points at which there was backflow are not included, and the points for β = 0.4 are not included, because they are over the hump in the λ - β curve (fig. A-6) and are not represented by the same configuration and flow model as the remaining points. Actually, the region between β = 0 and β = PEAK conforms to the analytical λ - β variation, but past the peak, the analytical assumptions break down and the C_{d_L}'s begin to take effect. The flow is very laminar: it may be assumed that the C_{d_L} curve bends to the horizontal at higher Reynold's numbers. In the range of Reynold's numbers from 10 to 100, the correlation

$$C_{d_L} = 0.0018\ Re$$

fits the data well.

Applying the C_{d_L} correlation, and solving eqs. (A-6), (A-8), (A-9), and (A-10) for the LH_2 and GF_2 system gives the results shown in fig. A-10. Here, the inverse of the pumping ratio, $1/\lambda$ (which is identical to the oxidizer-fuel, O:F, ratio), in the injector is plotted versus β, and driving pressure $(P'_o - P_b)$. The injector is always operating at an O:F ratio far above stoichiometric, because of the low pumping efficiency. Much of this low

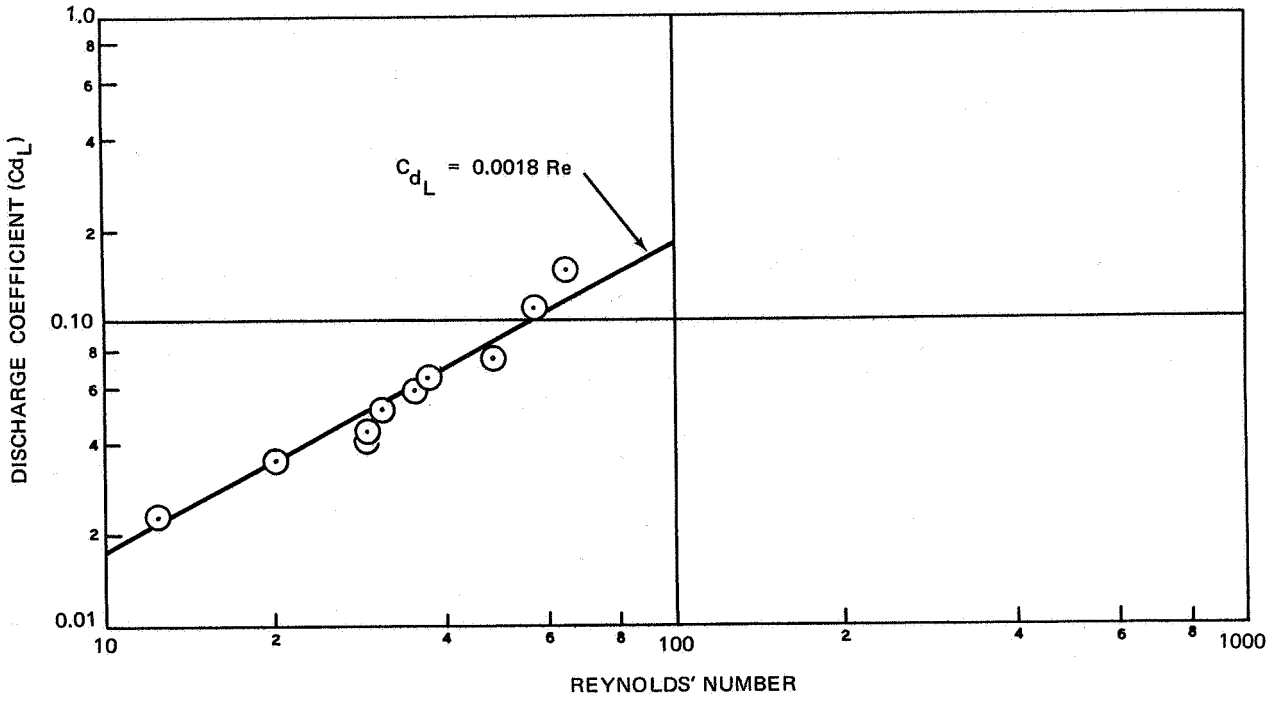

Figure A-9. Liquid Discharge Coefficient vs Reynolds' Number

efficiency and low C_{d_L} can be blamed on the small scale of the injector that, due to adjustability, included sharp edges and expansions that could be eliminated by revised design and different manufacturing techniques. However, even with ideal (C_{d_L} = 1.0) flow, the injector usually operates oxidizer-rich as shown in fig. A-11. Here the pressure parameter is (P_{o2} - P_b) for comparison with the original analytical pressure parameter, (P_o - P_b) with which it is identical. The original performance prediction is shown at the bottom of fig. A-11. Even at low values of (P_o - P_b), this prediction is considerably different from the revised prediction (shown at the top of fig. A-11). This variation is caused by the different form of the equations in the original analysis, including the floating parameter A_2/A_1 and the assumptions that are required to define the flow conditions at Station 2. In addition, such low values of (P_o - P_b) are not physically realizable, even ideally, because a larger value of this parameter is required for the choked flow that actually occurs.

The actual performance with this injector is even worse, which is not too surprising, because even well designed gas-gas pumps have fairly low efficiencies (<24%) and pumping capacities.* Gas-liquid pumps could be expected to be even less efficient. Worse yet, an increase in the pumping efficiency drives the injector closer to stoichiometric with a resultant increase in flame temperature, as shown in fig. A-10.

*Stephanoff, A. J.: Centrifugal and Axial Flow Pumps, Theory, Design, and Application. John Wiley and Sons, Inc., 1948.

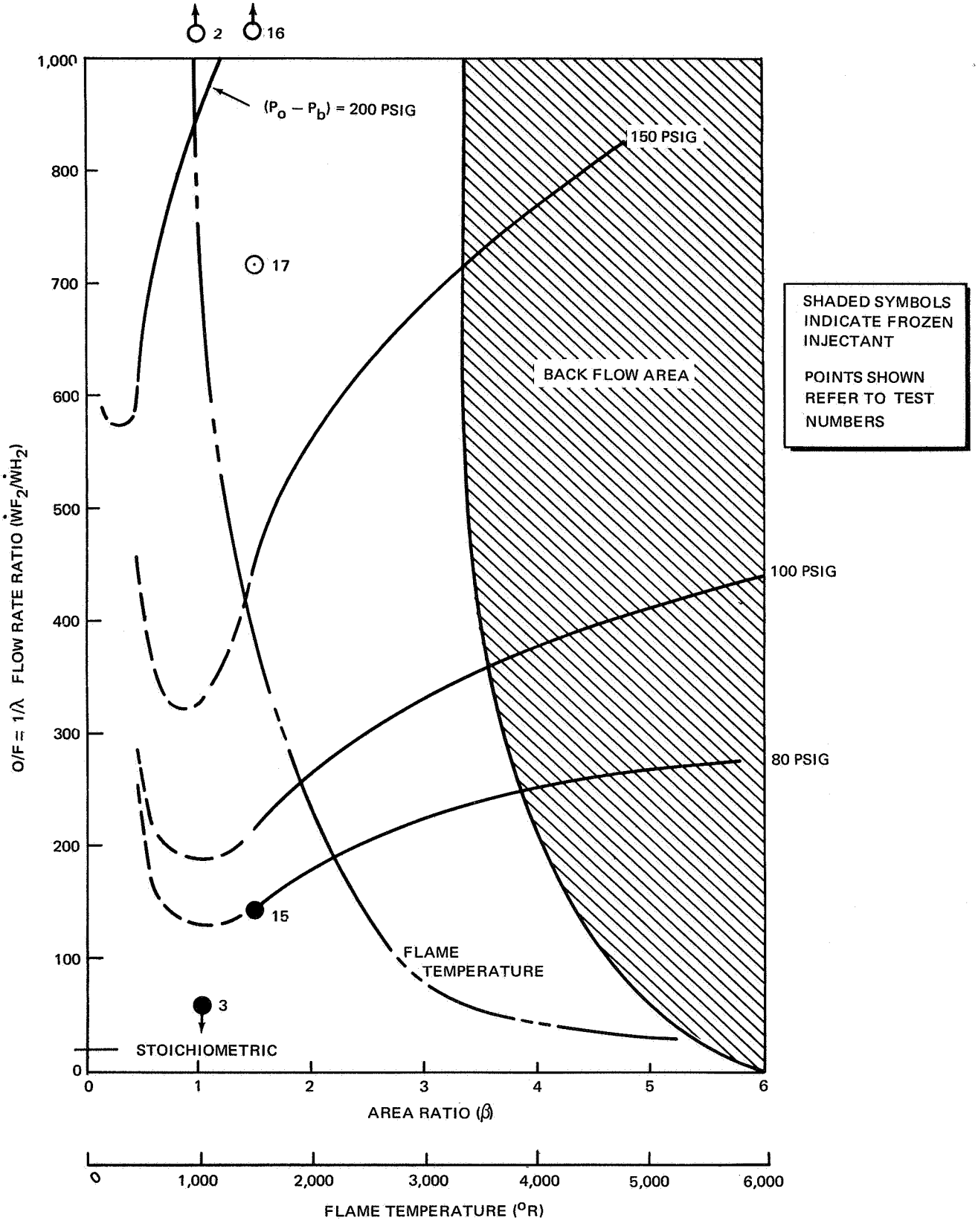

Figure A-10. Predicted Liquid Hydrogen/Gaseous Fluorine Performance for SA Injector

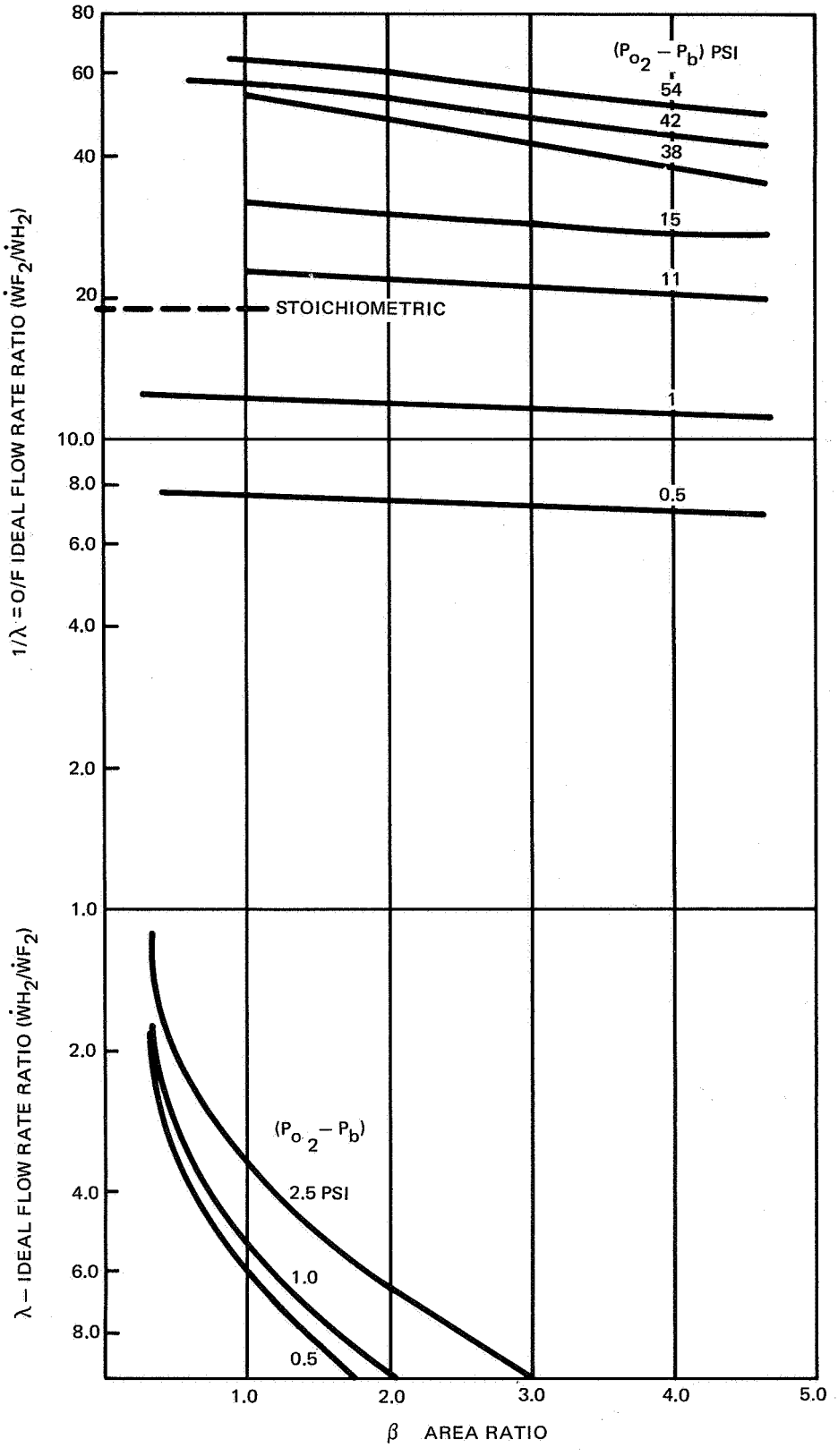

Figure A-11. Ideal Liquid Hydrogen/Gaseous Fluorine Performance for SA Injector

The implications of this characteristic on the utility of the SA injector are profound:

(1) The SA injector is incapable of pumping excess LH_2 to run fuel-rich, keep the injector cool, and perform its desired function of vaporizing hydrogen in a predictable manner for tank pressurization.

(2) The oxidizer-rich ratio burns indeterminately throughout the length of the injector and in the ullage. The burning is also extremely hot; it gives no injector heating protection and it leads predictably to injector burning.

Appendix B
TEST FACILITY DESCRIPTION AND PROCEDURES

TEST APPARATUS

The injector testing apparatus and facility are shown schematically in fig. B-1. There were two basic loops: (1) the LH_2 fill, drain, and vent system and (2) the GF_2 supply and injection systems; the only contact of the two loops was at the injector valve. LH_2 was supplied from an Air Products CLCH-60 storage tank through a hand-operated valve mounted on the storage tank (V18) (Table B-I contains valve nomenclature) to the remotely operated fill valve (H1). It then flows into a 1-in. vacuum-jacketed fill line to the test tank. The test tank was evacuated through the fill line and valve (H1) and the vacuum valve (H2). A calcium-hydroxide scrubber was situated upstream of the H_2 vacuum pump to remove any HF that might have remained in the tank after a test. The LH_2 was drained through a 1-in. vacuum-jacketed line to the drain valve (H6), through the flow orifice, and out the vent stack. The test tank was vented through a 2-in. insulated line to the vent valve (H7) and then through a 2-in. uninsulated line to the vent stack.

The GF_2 control loop supplied fluorine from a standard supply cylinder through the prevalve (F9). The cylinder pressure was monitored by the gage (GF1). The injection system downstream of the prevalve was evacuated and F_2-scrubbed through the vacuum valve (F10) and another calcium hydroxide scrubber. A compound gage (GF2) monitored the pressure upstream of the flow throttling valve (F12). The injection system was purged with nitrogen (or helium) through F13.

The point of contact of the two loops was the injector valve (F14). This valve was a solenoid-actuated, pneumatically (helium) operated valve made by the Fox Valve Development Company; it had a copper-to-stainless-steel seat and was compatible with both liquid and gaseous fluorine. This valve (together with many of the other valves shown) was used on the small-scale test program; it gave excellent performance then and in this program as well.

The auxiliary loops shown were used to pressurize the test tank with helium through H5, and monitor the test tank pressure at the gage (GH). The LH_2 that remains in the test tank and that could not be drained through the normal drain line to H6 was drained through the auxiliary drain valve (H6A).

All valves were remotely operated, except the metering valves and the propellant supply hand-operated valves. The facility was designed to give completely remote operation, from the operation of flowing LH_2 into the test tank, through injection, to reaction pressurization and LH_2 expulsion.

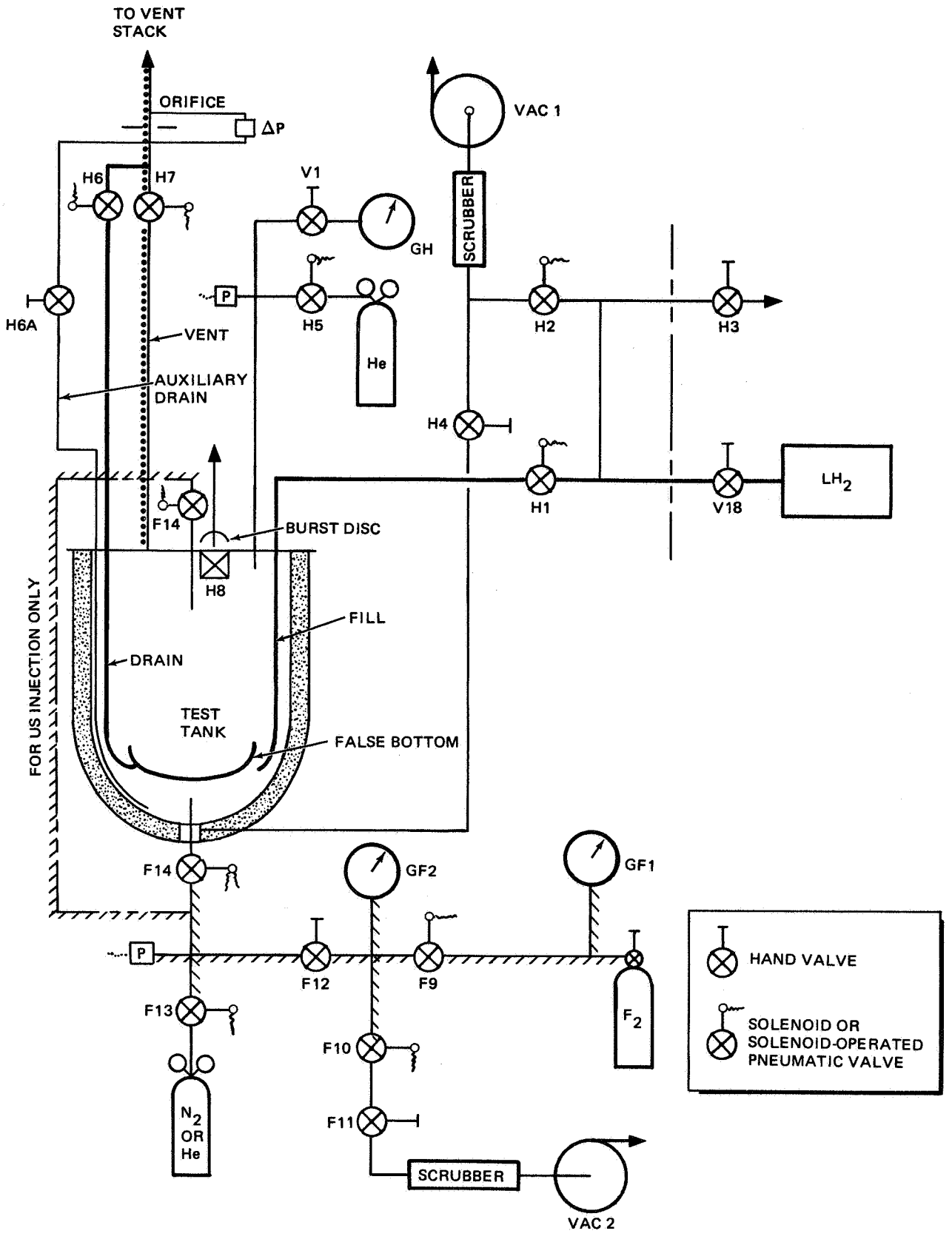

Figure B-1. MTI Injector Test Facility Schematic

TABLE B-I

VALVE IDENTIFICATION

Number	Function	Vendor	Part Number
H1	H_2 Fill	CVI Corporation	V-1070-100J w/SOV
H2	H_2 Vacuum	Control Components, Inc.	CE 3008T w/4-way sol.
H3	H_2 Relief	Control Components, Inc.	ES 3008T
H4	Penetration Vacuum	Control Components, Inc.	ES 3004T
H5	Helium Pressure	Control Components, Inc.	CE 3008T w/4-way sol.
H6	H_2 Drain	CVI Corporation	V-1070-100J w/SOV
H6A	H_2 Auxiliary Drain	Control Components, Inc.	MV 3004T
H7	H_2 Vent	CVI Corporation	V-1070-200 w/SOV
H8	Burst-Disc Shut-off	Hannifin	66-200-25-24 DC
F9	F_2 Prevalve	Control Components, Inc.	CE 3008T w/4-way sol.
F10	F_2 Vacuum	Control Components, Inc.	CE 3008T w/4-way sol.
F11	F_2 Vacuum Throttle	Control Components, Inc.	MV 3004T
F12	F_2 Metering	Control Components, Inc.	MV 3004T
F13	F_2 Purge	Control Components, Inc.	CE 3008T w/4-way sol.
F14	F_2 Injector	Fox Valve Development Corp.	610851
V1	H_2 Gage Shut-off	Control Components, Inc.	MV 3004T
V18	H_2 Pre-fill	Air Products Tank Valve	4-921-07-0126

The test tank used for the full-scale testing was a specially made stainless-steel, vacuum-jacketed, and superinsulated LH_2 Dewar. The tank internal dimensions were 24 in. diam by 60 in. deep. The inner vessel was built to ASME code specifications for a working pressure of 200 psig. A bottom penetration was provided (for injection) through the vacuum jacket. The penetration itself was sealed and evacuated through valve H4 to prevent cryopumping of air into the penetration. Except for this small (~3/8 in.) bottom penetration, all penetrations into the tank were through the test tank cover, which was made from a stainless-steel, 150-lb, ASA blind flange. This cover was bolted to a mating flange on the tank and sealed with a 1100-0 aluminum gasket that was encapsulated in a tongue and groove.

The cover penetrations included fill, drain, vent, and pressurization lines; light and camera ports; thermocouple and other sensor lead penetrations; and a rupture disc. If the rupture disc had burst while the tank was full of LH_2, a pneumatically operated burst orifice shutoff valve (H8) would have been used to allow the tank to be pressurized with helium before it was drained. A 3-in. rupture disc would vent the tank in less than 1 sec: a Continental disc set at 250 psig ±4% (with a vacuum support) was used. The burst head assembly and all lines were bolted to the cover with high strength stainless-steel bolts (A-286) and sealed with flat gaskets fabricated from a 1/4-in. sheet of low temperature silicone rubber (specification MIL-R-5847D Class I, Grade 32). These seals showed no detectable leakage even with a helium pressure of 100 psig.

The light and camera ports were 3 in. in diam and were originally made of 3/4-in.-thick polished pyrex; however, during the initial checkout tests, the intense heat from the lights cracked the thick pyrex. New windows were made from three laminations of 1/4-in.-thick Vycor; these windows proved to be much more heat resistant and were unharmed throughout the remainder of the testing.

To comply with safety requirements, the motion-picture camera and lights, as well as the vacuum pumps, were enclosed in purge boxes that were continuously pressurized and purged with inert GN_2 during operation to prevent deflagration of any leaking hydrogen from these potential ignition sources.

The internal configuration of the test apparatus is shown in fig. B-2. A stainless-steel false bottom, 18 in. in diam, was used to provide many design benefits:

(1) A normal bottom drain configuration, so that the effect of draining on SA injector operation could be studied.

(2) An effective baffle to dampen slosh during filling (the fill line reaches below the false bottom).

(3) A polished (and dimensionally indexed) surface that reflects light and aids in internal tank illumination, but is easily removed for recleaning.

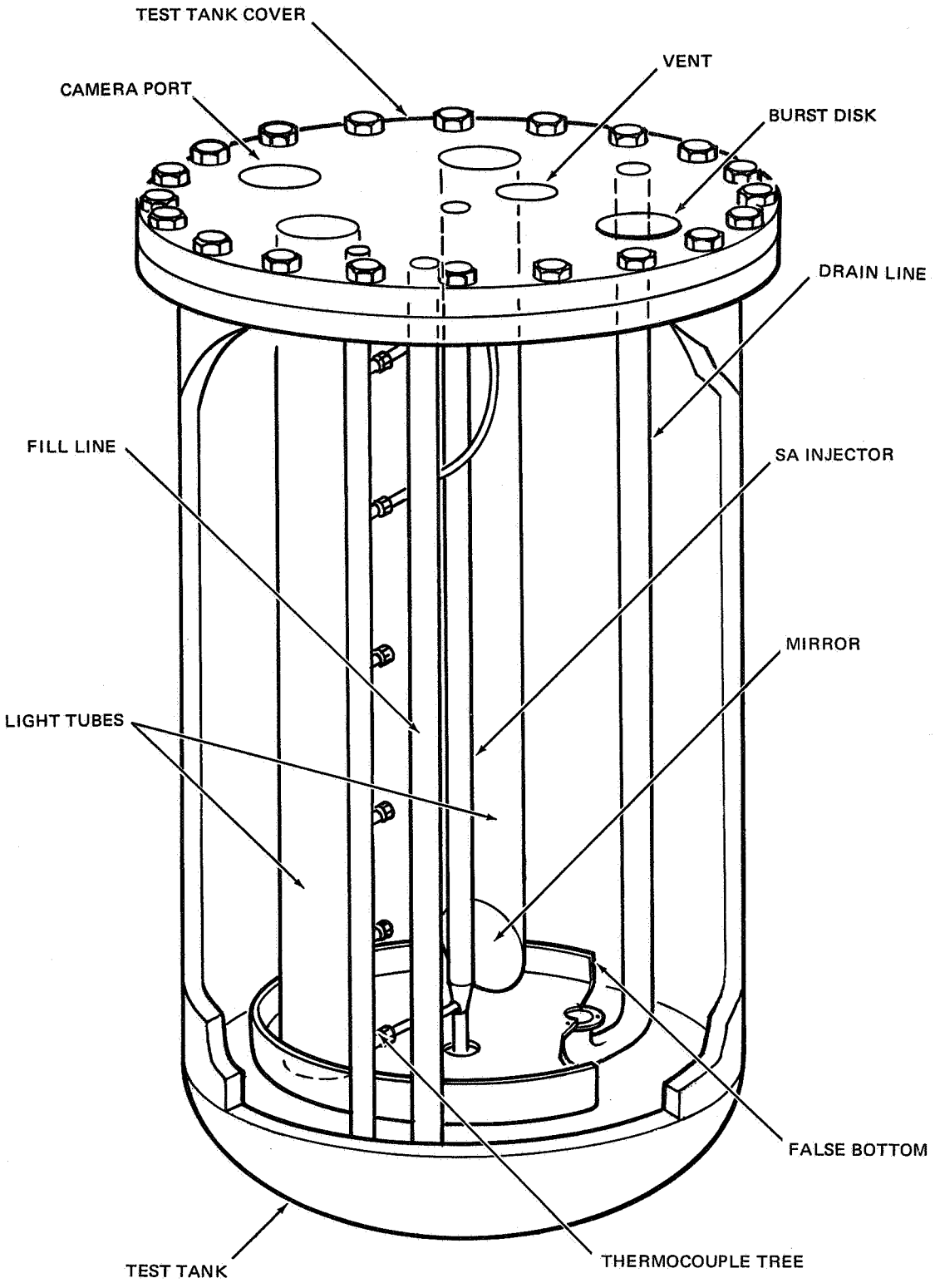

Figure B-2. Test Apparatus Internal Configuration

Light transmission tubes guide light from the lighting ports in the cover to the false bottom where it is reflected and used to backlight the injector region. These tubes are made from 3-in. -diam stainless-steel pipe, with stainless-steel mirrors in the scarfed tube bottoms. Tests in water with a similar tankage configuration showed that this technique eliminated surface reflection and glare.

INSTRUMENTATION

The basic instrumentation requirements for the full-scale testing provided for visual test coverage (by high-speed motion pictures) of the test tank interior and recorded pressures and temperatures at points of interest inside and outside of the tank. The motion-picture camera was a Milliken DBM5B with a 400-ft film capacity and a Kern Switar 10mm f/1.6 lens. The chosen framing rate represented a compromise between framing speed and motion-picture duration, because it was impractical to reload the camera during testing. The framing rate that was selected was 250 pictures/sec; this allowed about 60 sec of coverage, which was sufficient for virtually all of the tests. Lighting was provided by two General Electric type DVY 650-W quartz-bromide lamps; this was regarded as the maximum practical amount of illumination that could be put into the test tank through the cover and light tubes, but the lighting was generally inadequate. As expected, the motion pictures that were taken during the full-scale tests were generally inferior to the quality of those taken during the small-scale tests in the glass apparatus. The specific viewing problems encountered during the tests are discussed in detail in Results.

Since any instrumentation or transducers placed inside the test tank are subject to potential damage from the F_2-H_2 flame as well as possible corrosive attack by HF and F_2, expensive and fragile ultra-high-response instrumentation was not used. Rather, temperatures were measured with thermocouples of 36-gage copper-constantan wire with the reference junction contained in a liquid nitrogen bath. Many of the initial thermocouples were unshielded and had a response time of about 100 msec. Some of these were damaged by burning and HF attack in the initial testing and were replaced with stainless-steel shielded thermocouples with a response time of about 500 msec to 1 sec. This slow response time was permissable for most of the temperatures that were measured. The pressures were measured with ordinary bridge-type stainless-steel-diaphragm transducers. SA injector test transducer and thermocouple locations, functions, and identities are shown in fig. B-3.

A thermocouple tree was fabricated to provide support for the thermocouple junctions within the tank and to route the wiring through the tank cover. The main trunk of the thermocouple tree was fabricated of 1-in. -diam stainless-steel tubing welded shut at the bottom and connected at the top to a special connector that mated to a pin-type penetration welded into the cover. The thermocouple junctions were extended to their positions in the tank via 1/8-in. -diam stainless-steel tubing sealed at the junction end with Swagelok

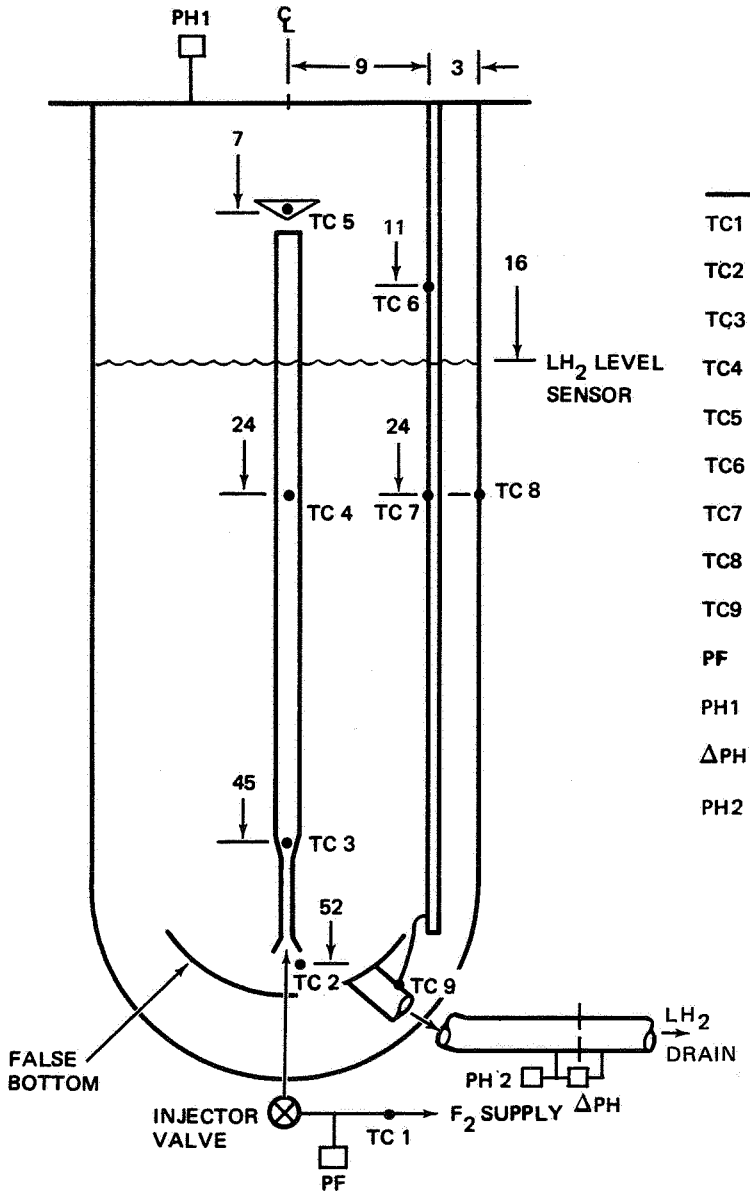

	PARAMETER	TYPE	PART NO.	RANGE
TC1	GF_2 TEMPERATURE	Cu-CN		500°R
TC2	SA INJECTION NOZZLE	Cu-CN		40 TO 600°R
TC3	SA INJECTION EXPANSION CONE	Cu-CN		40 TO 600°R
TC4	SA INJECTION TUBE	Cu-CN		40 TO 600°R
TC5	SA INJECTION FLAME DEFLECTOR	Cu-CN		40 TO 600°R
TC6	H_2 ULLAGE	Cu-CN		40 TO 600°R
TC7	LH_2 TEMPERATURE	Cu-CN		40 TO 600°R
TC8	DEWAR WALL TEMPERATURE	Cu-CN		40 TO 600°R
TC9	LH_2 DRAIN TEMPERATURE	Cu-CN		40 TO 100°R
PF	GF_2 PRESSURE	TRANSDUCER	GP-46M-500-7019	0 TO 500 PSIG
PH1	DEWAR PRESSURE	TRANSDUCER	GP-46M-300-7016	0 TO 300 PSIG
ΔPH	LH_2 PRESSURE DIFFERENTIAL	STATHAM	PM80TC-25-350	0 TO 25 PSID
PH2	LH_2 FLOW ORIFICE PRESSURE	STATHAM	PG246TCB-300-350	0 TO 300 PSIG

NOTE: ALL DIMENSIONS ARE IN INCHES
DIMENSIONS ARE DISTANCE FROM LID

Figure B-3. SA Injector Test Instrumentation Location and Identification

fittings with Teflon ferrules and into other Swagelok fittings welded to the 1-in. trunk. The tubing had enough spring force to hold the thermocouple junctions in place against the injector at the position shown, and the junction was not fastened to the injector. This allowed the injector to be removed from the tank independently of the thermocouple tree. The same thermocouple tree was used for the US injector configuration, but the junctions were situated at different points, as shown in fig. B-4. A United Control 2641-1-1 level sensor was mounted on the tree at the position shown as LH_2 level to provide remote indication of LH_2 fill, but the level-sensing system failed to function properly, so the tank was filled by a different technique, as described in the Experiment Technique section. Although all joints in the thermocouple tree were sealed as tightly as possible with Teflon gaskets to keep LH_2 out of the tree, LH_2 still leaked into the tree, and the chilling cycles so damaged the thermocouple wiring that the tree had to be completely rebuilt during the test program (after Test 14).

The test tank ullage pressure (PH) and the fluorine driving pressure (PF) were measured at the positions shown. A calibrated orifice (two different sizes were used) was installed in the LH_2 drain line to control and measure the LH_2 flow rate. The recorded pressure upstream of the orifice and the pressure drop across the orifice, together with the LH_2 temperature and orifice size, could be used to calculate the LH_2 flow rate.

The thermocouple and transducer signals were fed to Douglas-manufactured balance panels and, together with various control relay signals, were recorded on a direct writing 18-channel CEC oscillograph. A permanent oscillograph record was made of each test. (Typical oscillographs are given in Results.)

CONTROL SYSTEM DESIGN

Because the full-scale testing could have been hazardous, all functions during the test run were controlled remotely from a blockhouse situated 350 ft from the test area. To allow control of the various valves and to monitor the test, a blockhouse control panel was designed and built to satisfy the following requirements:

(1) To operate all remote valves from the panel, with a signal light indication to show valve-actuation power. (For the tank vent valve, microswitches were used to show the open and closed positions of the valve.)

(2) To program the operation of the injection loop so that automatic safeguards will stop injection if ignition does not occur and to provide one-switch shutdown if there is a malfunction or a detonation.

A control system to satisfy these requirements was designed and is shown schematically in fig. B-5. Each valve has its own circuit, with panel lights to indicate power to the valve. In addition, the fluorine prevalve (F9) and

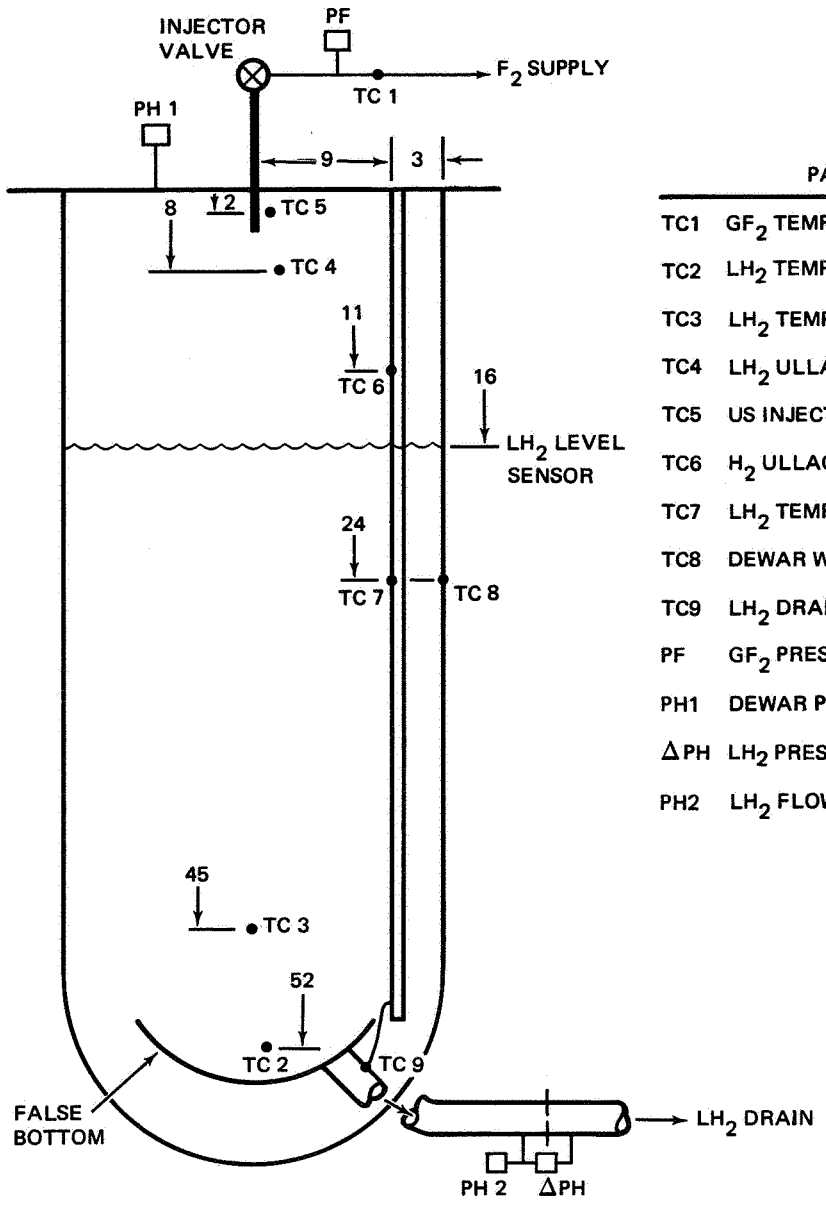

	PARAMETER	TYPE	PART NO.	RANGE
TC1	GF_2 TEMPERATURE	Cu-CN		500°R
TC2	LH_2 TEMPERATURE	Cu-CN		40 TO 600°R
TC3	LH_2 TEMPERATURE	Cu-CN		40 TO 600°R
TC4	LH_2 ULLAGE (ℓ_L)	Cu-CN		40 TO 600°R
TC5	US INJECTOR NOZZLE	Cu-CN		40 TO 600°R
TC6	H_2 ULLAGE	Cu-CN		40 TO 600°R
TC7	LH_2 TEMPERATURE	Cu-CN		40 TO 600°R
TC8	DEWAR WALL TEMPERATURE	Cu-CN		40 TO 600°R
TC9	LH_2 DRAIN TEMPERATURE	Cu-CN		40 TO 100°R
PF	GF_2 PRESSURE	TRANSDUCER	GP-46M-500-7019	0-500 PSIG
PH1	DEWAR PRESSURE	TRANSDUCER	GP-46M-300-7016	0-300 PSIG
ΔPH	LH_2 PRESSURE DIFFERENTIAL	STATHAM	PM80TC-25-350	0-25 PSID
PH2	LH_2 FLOW ORIFICE PRESSURE	STATHAM	PG246TCB-300-350	0-300 PSIG

NOTE: ALL DIMENSIONS ARE IN INCHES
DIMENSIONS ARE DISTANCE FROM LID

Figure B-4. US Injector Test Instrumentation Location and Identification

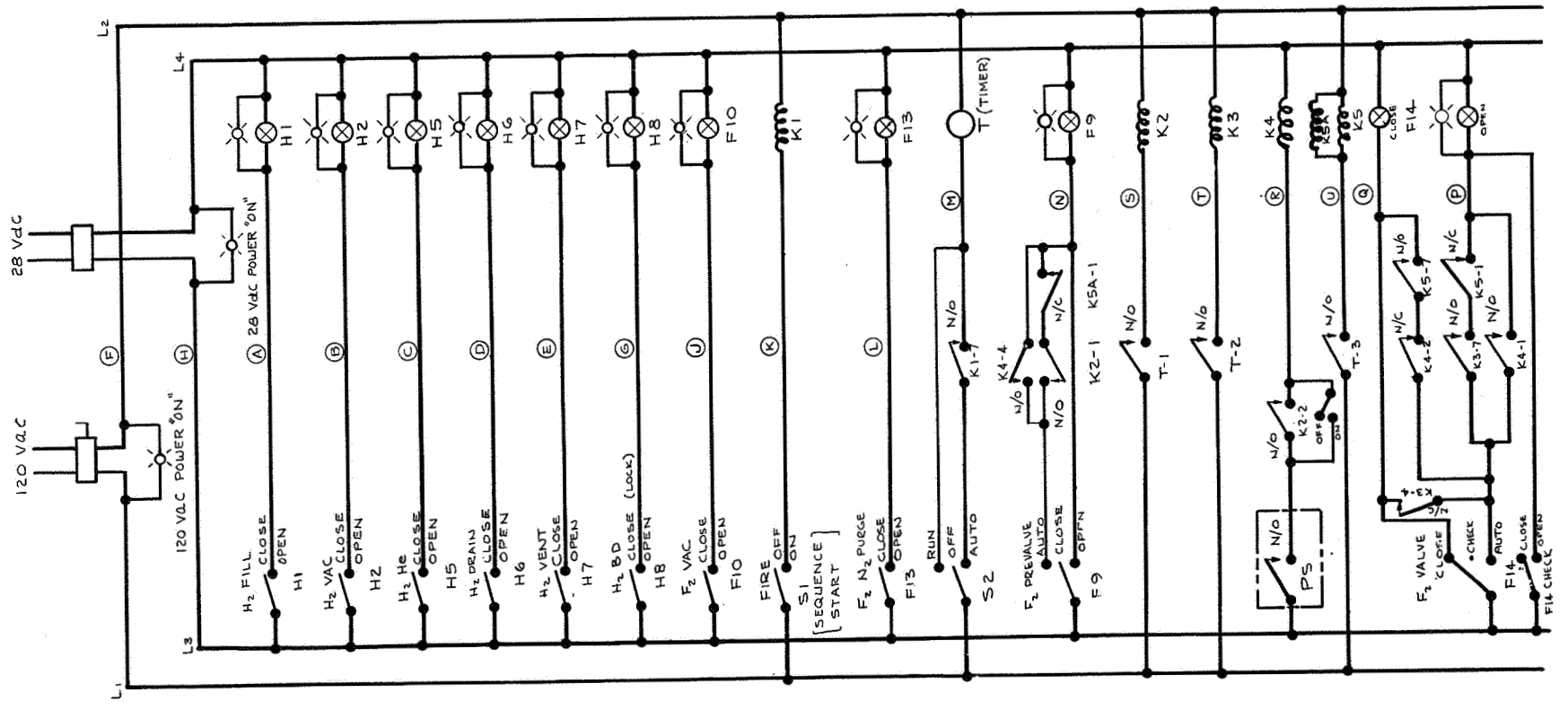

SEQUENCE OF OPERATION:

1. CIRCUIT BREAKERS CONTROL 120 VAC & 28 VDC POWER.
2. REMOTE VALVES H1, H2, H5, H6, H7, H8, F9, F10, F13, & F14 CAN BE OPENED & CLOSED BY MANUAL SWITCH.
3. PHOTO PANELS & CAMERAS ARE TURNED ON MANUALLY.
4. CLOSING "FIRE" SWITCH PULLS IN K1 RELAY, WHICH STARTS TIMER T (S2 ON AUTO). AFTER DELAY, T-1 PULLS IN K2, WHICH OPENS F9 (ON AUTO). AFTER DELAY, T-2 PULLS IN K3, WHICH OPENS F14 (ON AUTO).
5. AFTER DELAY, T-3 PULLS IN K5 TO CLOSE F14 UNLESS PRESSURE SWITCH PS HAS PULLED IN K4 TO KEEP F14 OPEN.

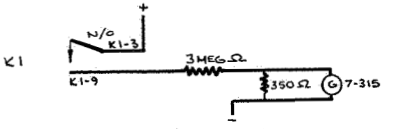

K2, K3, K4, K5 SAME AS K1

Figure B-5. MTI Injector Test Control Schematic

the injector valve (F14) have circuits marked AUTO that provide automatic operation of the injection loop. With these valves, and the enabling switch (S2) in the AUTO position, the automatic operation proceeded as follows:

(1) When the SEQUENCE START (FIRE) switch is closed, relay (K1) starts the timer (T).

(2) After time delay (T1), relay (T-1) operates relay (K2), which opens the prevalve (F9) and enables the pressure switch circuit (see below).

(3) After time delay (T2), relay (T-2) operates relay (K3), which opens the injector valve (F14).

(4) After time delay (T3), relay (T-3) operates relays (K5 and K5A), which close the injector valve (F14) and the prevalve (F9) simultaneously.

This would be the sequence if there were nonignition (and thus no tank pressure rise) following injection; however, if ignition occurs, a pressure rise in the tank would actuate a pressure switch (PS) that senses the tank ullage pressure. If the pressure switch relay is energized by a pressure rise, it operates a relay (K4) that, through parallel circuits, keeps the prevalve (F9) and the injector valve (F14) open, even though the circuit through K5 closes. [In practice, the pressure switch was set at 10 psig, and the time (T3) was set at 2 sec.] There must be a pressure rise of 10 psi in 2 sec for the injector valves to stay open. Opening the FIRE switch de-energizes all relays and closes F9 and F14, thus providing single-switch shutdown. As a further safety measure, the timer (T) runs out after about 10 sec, shutting valves F9 and F14; manual reoperation of the FIRE switch is then required to restart the sequence. Each of the relays signals the time at which it is energized on the oscillograph record through the circuit shown. The blockhouse control room is shown in fig. B-6. The control panel is on the right, and the oscillograph and balance panels for thermocouples and pressure transducers are on the left.

EXPERIMENT TECHNIQUE

A standard Operational Procedure (Douglas Drawing 1T31900) was prepared and followed in the preparation, the operation, and the shutdown for each test. The general steps of procedure were as follows:

(1) Fill the thermocouple reference bath with LN_2, vent the test tank and fluorine injection loop to atmosphere, and calibrate and zero the pressure transducers and thermocouples.

(2) Select the tank pressure for the test (low pressure, 30 psig; medium pressure, 100 psig; or high pressure, 170 psig) and mark the oscillograph with a pointer at that pressure as an approximate guide.

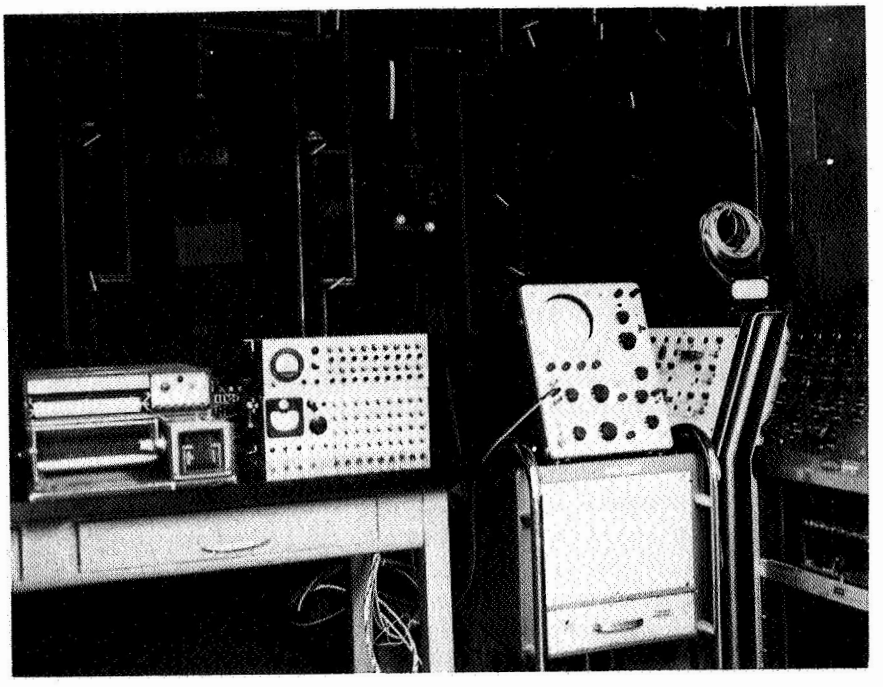

Figure B-6. MTI Injector Test Control Room

(3) Check the operation of all system valves, (except F14 to save wear and tear, and H8 - emergency only) and, with all valves closed, start the vacuum pumps and the purge to the pumps; open the H_2 and F_2 vacuum valves H4, H2, H1, and F10, and evacuate the test tank and injection loop. Evacuate for 1/2 to 1 hr until GH and GF2 show hard vacuum (~30 in. Hg).

(4) Close the H_2 vacuum valve(H2), and pressurize the test tank to 20 psig with helium.

(5) Close the H_2 fill valve(H1), (leave H4, and F10 open) and recheck seal leakage.

(6) Install the lights and camera. [Check camera operation and lights. Put thin film of alcohol on camera port to prevent frosting (heat from the lamps keeps the light ports frost free). Install the camera purge box and connect the purge line.]

(7) Set F_2 metering valve, (F12); open F_2 cylinder valve, and observe and record cylinder pressure.

(8) Open the LH_2 storage tank valve, (V18). Evacuate the test area and return to the blockhouse.

(9) Fill the test tank with LH_2: open fill valve(H1), and vent valve(H7). Record fill on oscillograph at slow paper speed, 0.25 in./sec

(Filling takes about 6 min. The level sensor did not function, so the tank was filled to within about 4 in. of the top by listening through a speaker system to the test area for the surge of LH_2 in the vent. Repeated trials with this fill technique gave LH_2 levels in the tank consistent from run to run within 1/2 in.)

(10) After the fill, wait a few minutes until no vapor is seen at the vent stack, then proceed with countdown.

(11) Ensure that AUTO switches are set correctly, then close F_2 vacuum valve, (F10), and tank vent valve, (H7). Count down from 5.

(12) On 3, start oscillograph at a paper speed of 4 in./sec.

(13) On 2, start the camera (and lights). On fire, actuate the FIRE switch.

(14) When the tank pressure oscillograph trace reaches the preset point, either stop the injection to observe pressure collapse or open drain valve (H6). Maintain tank pressure by cycling the FIRE switch. If a partial drain is required, the injection, the drain, the camera, and possibly the oscillograph are shut down between drains, then the sequence is repeated until the tank is emptied. Other variations can also be performed.

(15) Following the test, open vent valve (H7), return F9 and F14 to CLOSE, open F_2 vacuum valve (F10), and purge injection loop with GN_2 through F13 and F10.

(16) After returning to the test area, close V18, open H3, record F_2 cylinder pressure, close F_2 cylinder valve, and open auxiliary drain valve(H6A).

(17) With personnel in a protected position, close vent valve (H7) and pressurize the tank to about 30 psig with helium to complete the drain operation. This procedure removes the propellant below the drain outlet in the false bottom.

(18) After the drain, close drain valve (H6A), close H3, and open H1 and H2 to evacuate the test tank. (The fluorine trapped upstream of F9 is removed by cycling F9 with F10 open to the F_2 vacuum pump.)

(19) Remove the camera and lights. (After the tank is evacuated, it is inerted and purged with helium to remove any HF still in the tank.)

PROPELLANTS

The propellants used in the tests were commercially obtained. The liquid hydrogen was 99.995% pure hydrogen obtained from Union Carbide Corp., Linde Division, Sacramento, California.

The fluorine was obtained from Air Products, Inc. and was supplied as gas in standard 400 psig cylinders. The manufacturer's specification (based on cylinder analysis) was as follows:

Fluorine	98.0% (minimum)
Oxygen	0.2% (maximum)
Nitrogen	1.0% (maximum)
HF	0.1% (typical)
CF_4	200 ppm (typical)
SF_6	100 ppm (typical)

The helium used as a pressurant for the hydrogen and the fluorine was commercial water-pumped (12 ppm H_2O) and was obtained in standard 2500-pisg cylinders from Air Products, Inc.

Appendix C

ANALYTICAL MODELS FOR TANK PRESSURIZATION

Pressurization of Perfect Gas Ullage by Heat Addition

Assuming constant volume pure heat addition, and no mass addition

$$dQ = \overline{M}_b \, C_v \, dT \tag{C-1}$$

For perfect gas

$$\overline{M}_b = \text{constant} = \left(\frac{PV}{RT}\right)_b \tag{C-2}$$

Thus, since $\frac{C_v}{R} = \frac{1}{\gamma - 1}$;

$$dQ = \frac{1}{\gamma - 1} \, P_b \, V_b \, \frac{dT}{T} \tag{C-3}$$

For constant volume pressurization

$$\frac{dP}{P} = \frac{dT}{T} \tag{C-4}$$

Thus:

$$dQ = \frac{V_b}{\gamma - 1} \, dP \tag{C-5}$$

For pressurization time (t)

$$\frac{\Delta Q}{t} = \frac{V_b}{\gamma - 1} \, \frac{\Delta P_b}{t} \tag{C-6}$$

For a reaction

$$\frac{\Delta Q}{t} = Q_R \dot{W}_{injectant} \tag{C-7}$$

Thus:

$$Q_R \dot{W}_{injectant} = \frac{V_b}{\gamma - 1} \Delta \dot{P}_b \tag{C-8}$$

$$\therefore \Delta P_b / \dot{W}_{injectant} = \frac{(\gamma - 1) Q_R}{V_b} \tag{C-9}$$

Pressurization of Saturated Vapor Ullage by Heat Addition

Again, for constant volume

$$\Delta Q = \overline{M}_b C_v \Delta T \tag{C-10}$$

The ΔT from Equation (9) is computed based on ΔQ for injected mass

$$\Delta Q = Q_R \dot{W}_{injectant} t \tag{C-11}$$

and actual $\overline{M}_b$ and C_p for saturated H_2 vapor from Mollier diagram and H_2 properties.

From initial conditions (assumed at 20 psia saturated) ΔT will give pressure rise (ΔP) from Mollier diagram with constant ullage density (assuming no mass addition.)

Pressurization of Saturated Vapor Ullage by Mass Addition Through Liquid Vaporization

For pure heat addition, for time, t

$$Q_R \dot{W}_{injectant} t = \Delta \overline{M}_{b_v} Q_V \tag{C-12}$$

From the initial ullage conditions of volume and pressure, the initial mass, $\overline{M}_{b_i}$ of saturated vapor can be determined from a Mollier phase diagram.

The new ullage mass $\left(\overline{M}_{b_i} + \overline{M}_{b_v}\right)$ will give a new ullage density, and this will give a new ullage pressure (P_b) at saturated conditions. The new pressure, less the critical pressure, gives ΔP per unit time, (t) or ΔP.

Expulsion Pressurization of Perfect Gas Ullage by Heat Addition

Assuming constant pressure, pure heat addition, and no mass addition

$$dQ = \overline{M}_b \, C_p \, \Delta T \tag{C-13}$$

For perfect gas

$$\overline{M}_b = \text{constant} = \left(\frac{PV}{RT}\right)_b \tag{C-14}$$

Thus:

$$dQ = \frac{\gamma}{\gamma - 1} \, P_b \, V_b \, \frac{dT}{T} \tag{C-15}$$

For constant pressure expansion

$$\frac{dV}{V} = \frac{dT}{T} \tag{C-16}$$

Thus:

$$dQ = \frac{\gamma}{\gamma - 1} \, P_b \, dV \tag{C-17}$$

For expulsion time (t)

$$\frac{\Delta Q}{t} = \frac{\gamma}{\gamma - 1} \, P_b \, \frac{\Delta V}{t} \tag{C-18}$$

For reaction and outflow

$$\frac{\Delta Q}{t} = Q_R \, \dot{W}_{\text{injectant}} \qquad \frac{\Delta V}{t} = \frac{\dot{W}_{LH_2}}{\rho_L} \tag{C-19}$$

Thus:

$$Q_R \dot{W}_{injectant} = \frac{\gamma}{\gamma-1} \frac{P_b}{\rho_L} \dot{W}_{LH_2} \qquad \text{(C-20)}$$

$$\therefore \dot{W}_{LH_2}/\dot{W}_{injectant} = \frac{\gamma-1}{\gamma} \frac{Q_R \rho_L}{P_b} \qquad \text{(C-21)}$$

Expulsion Pressurization of Saturated Vapor Ullage by Mass Addition Through Liquid Vaporization

$$dQ = d\overline{M}_b Q_V \qquad \text{(C-22)}$$

and

$$\frac{d\overline{M}}{\overline{M}} \doteq \frac{d_V}{V} \qquad \text{(C-23)}$$

Thus:

$$dQ = \frac{M_b}{V_b} dV Q_V \qquad \text{(C-24)}$$

For expulsion time (t)

$$\frac{\Delta Q}{t} = Q_R \dot{W}_{injectant} = \frac{M_b}{V_b} Q_V \frac{\Delta V}{t} \qquad \text{(C-25)}$$

Thus:

$$Q_R \dot{W}_{injectant} = \frac{M_b}{V_b} Q_V \frac{\dot{W}_{LH_2}}{\rho_L} \qquad \text{(C-26)}$$

Equation (C-26) can be solved for M_b/V_b, which, together with the initial ullage conditions will give the ullage density, can be converted to saturated vapor pressure, or approximately

$$\frac{M_b}{V_b} \doteq \frac{P_b}{RT_b} \tag{C-27}$$

Thus:

$$Q_R \dot{W}_{injectant} = \frac{Q_V}{\rho_L RT_b} P_b \dot{W}_{LH_2} \tag{C-28}$$

$$\therefore \dot{W}_{LH_2}/\dot{W}_{injectant} = \frac{Q_R \rho_L}{Q_V} \frac{RT_b}{P_b} \tag{C-29}$$

DISTRIBUTION LIST FOR FINAL REPORT, NASA CR72408

"AN INVESTIGATION OF FLUORINE-HYDROGEN MAIN TANK INJECTION PRESSURIZATION"

CONTRACT NAS3-7963

		Copies
National Aeronautics and Space Administration Lewis Research Center 21000 Brookpark Road Cleveland, Ohio 44135		
Attention:	Contracting Officer, MS 500-210	1
	Liquid Rocket Technology Branch, MS 500-209	8
	Technical Report Control Office, MS 5-5	1
	Technology Utilization Office, MS 3-16	1
	AFSC Liaison Office, MS 4-1	2
	Library	2
	Office of Reliability and Quality Assurance, MS 500-203	1
	D. L. Nored, MS 500-209	1
	E. W. Conrad, MS 100-1	1
National Aeronautics and Space Administration Washington, D. C. 20546		
Attention:	Code MT	1
	RPX	2
	RPL	2
	SV	1
Scientific and Technical Information Facility P. O. Box 33 College Park, Maryland 20740		
Attention:	NASA Representative Code CRT	6

	Copies
National Aeronautics and Space Administration Ames Research Center Moffett Field, California 94035 Attention: Library	1
National Aeronautics and Space Administration Flight Research Center P. O. Box 273 Edwards, California 93523 Attention: Library	1
National Aeronautics and Space Administration Goddard Space Flight Center Greenbelt, Maryland 20771 Attention: Library	1
National Aeronautics and Space Administration John F. Kennedy Space Center Cocoa Beach, Florida 32931 Attention: Library	1
National Aeronautics and Space Administration Langley Research Center Langley Station Hampton, Virginia 23365 Attention: Library	1
National Aeronautics and Space Administration Manned Spacecraft Center Houston, Texas 77001 Attention: Library	1
National Aeronautics and Space Administration George C. Marshall Space Flight Center Huntsville, Alabama 35812 Attention: Library	1
Keith Chandler, R-P&VE-PA	1
Jet Propulsion Laboratory 4800 Oak Grove Drive Pasadena, California 91103 Attention: Library	1
Office of the Director of Defense Research & Engineering Washington, D. C. 20301 Attention: Dr. H. W. Schulz, Office of Asst. Dir. (Chem. Technology)	1

	Copies
Defense Documentation Center Cameron Station Alexandria, Virginia 22314	1
RTD (RTNP) Bolling Air Force Base Washington, D. C. 20332	1
Arnold Engineering Development Center Air Force Systems Command Tullahoma, Tennessee 37389 Attention: AEOIM	1
Advanced Research Projects Agency Washington, D. C. 20525 Attention: D. E. Mock	1
Air Force Missile Test Center Patrick Air Force Base, Florida Attention: L. J. Ullian	1
Air Force Systems Command (SCLT/Capt. S. W. Bowen) Andrews Air Force Base Washington, D. C. 20332	1
Air Force Rocket Propulsion Laboratory (RPR) Edwards, California 93523	1
Air Force Rocket Propulsion Laboratory (RPM) Edwards, California 93523	1
Air Force FTC (FTAT-2) Edwards Air Force Base, California 93523 Attention: Col. J. M. Silk	1
Air Force Office of Scientific Research Washington, D. C. 20333 Attention: SREP, Dr. J. F. Masi	1
Office of Research Analyses (OAR) Holloman Air Force Base, New Mexico 88330 Attention: RRRT	1
U. S. Air Force Washington 25, D. C. Attention: Col. C. K. Stambaugh, Code AFRST	1

	Copies
Commanding Officer U. S. Army Research Office (Durham) Box CM, Duke Station Durham, North Carolina 27706	1
U. S. Army Missile Command Redstone Scientific Information Center Redstone Arsenal, Alabama 35808 Attention: Chief, Document Section	1
Bureau of Naval Weapons Department of the Navy Washington, D. C. Attention: J. Kay, Code RTMS-41	1
Commander U. S. Naval Missile Center Point Mugu, California 93041 Attention: Technical Library	1
Commander U. S. Naval Ordnance Test Station China Lake, California 93557	1
Attention: Code 45	1
Code 753	1
W. F. Thorm, Code 4562	1
Commanding Officer Office of Naval Research 1030 E. Green Street Pasadena, California 91101	1 1
Director (Code 6180) U. S. Naval Research Laboratory Washington, D. C. 20390 Attention: H. W. Carhart	1
Picatinny Arsenal Dover, New Jersey Attention: I. Forsten, Chief Liquid Propulsion Laboratory	1
U. S. Atomic Energy Commission Technical Information Services Box 62 Oak Ridge, Tennessee Attention: A. P. Huber, Code ORGDP Box P	1

	Copies
Air Force Aero Propulsion Laboratory Research & Technology Division Air Force Systems Command United States Air Force Wright-Patterson AFB, Ohio 45433 Attention: APRP (C. M. Donaldson)	1
Aerojet-General Corporation P. O. Box 296 Azusa, California 91703 Attention: Librarian	1
Aerojet-General Corporation 11711 South Woodruff Avenue Downey, California 90241 Attention: F. M. West, Chief Librarian	1
Aerojet-General Corporation P. O. Box 1947 Sacramento, California 95809 Attention: Technical Library 2484-2015A	1
Aeronutronic Division of Philco Corporation Ford Road Newport Beach, California 92600 Attention: Technical Information Department	1
Aeroprojects, Incorporated 310 East Rosedale Avenue Westchester, Pennsylvania 19380 Attention: C. D. McKinney	1
Aerospace Corporation P. O. Box 95085 Los Angeles, California 90045 Attention: Library-Documents	1
Arthur D. Little, Inc. Acorn Park Cambridge 40, Massachusetts Attention: A. C. Tobey	1
Astropower, Incorporated Subs. of Douglas Aircraft Company 2121 Cambus Drive Newport Beach, California 92663	1

	Copies
Astrosystems, Incorporated 1275 Bloomfield Avenue Caldwell Township, New Jersey Attention: A. Mendenhall	1
ARO, Incorporated Arnold Engineering Development Center Arnold AF Station, Tennessee 37389 Attention: Dr. B. H. Goethert Chief Scientist	1
Atlantic Research Corporation Shirley Highway & Edsall Road Alexandria, Virginia 22314 Attention: Security Office of Library	1
Battelle Memorial Institute 505 King Avenue Columbus, Ohio 43201 Attention: Report Library, Room 6A	1
Beech Aircraft Corporation Boulder Facility Box 631 Boulder, Colorado Attention: J. H. Rodgers	1
Bell Aerosystems, Inc. Box 1 Buffalo, New York 14205 Attention: W. M. Smith	1
Bendix Systems Division Bendix Corporation Ann Arbor, Michigan Attention: John M. Bureger	1
The Boeing Company Aero Space Division P. O. Box 3707 Seattle, Washington 98124 Attention: Ruth E. Peerenboom (1190) J. D. Alexander	1 1
Chemical Propulsion Information Agency Applied Physics Laboratory 8621 Georgia Avenue Silver Spring, Maryland 20910	1

	Copies
Chrysler Corporation Missile Division Warren, Michigan Attention: John Gates	1
Chrysler Corporation Space Division New Orleans, Louisiana Attention: Librarian	1
Curtiss-Wright Corporation Wright Aeronautical Division Woodridge, New Jersey Attention: G. Kelley	1
University of Denver Denver Research Institute P.O. Box 10127 Denver, Colorado 80210 Attention: Security Office	1
Douglas Aircraft Company, Inc. Santa Monica Division 3000 Ocean Park Blvd., Santa Monica, California 90405 Attention: J.L. Waisman R.W. Hallet G.W. Burge	1 1 1
Fairchild Stratos Corporation Aircraft Missiles Division Hagerstown, Maryland Attention: J.S. Kerr	1
General Dynamics/Astronautics P.O. Box 1128 San Diego, California 92112 Attention: Library & Information Services (128-00)	1
Convair Division General Dynamics Corporation P.O. Box 1128 San Diego, California 92112 Attention: Mr. W. Fenning Centaur Resident Project Office	1
General Electric Company Flight Propulsion Lab. Department Cincinnati 15, Ohio Attention: D. Suichu	1

	Copies
Grumman Aircraft Engineering Corporation Bethpage, Long Island, New York Attention: Joseph Gavin	1
Hercules Powder Company Allegheny Ballistics Laboratory P. O. Box 210 Cumberland, Maryland 21501 Attention: Library	1
IIT Research Institute Technology Center Chicago, Illinois 60616 Attention: C. K. Hersh, Chemistry Division	1
Kidde Aero-Space Division Walter Kidde & Company, Inc. 675 Main Street Belleville 9, New Jersey Attention: R. J. Hanville, Director of Research Engineering	1
Lockheed Missiles & Space Company P. O. Box 504 Sunnyvale, California Attention: Technical Information Center	1
Lockheed-California Company 10445 Glen Oaks Blvd., Pacoima, California Attention: G. D. Brewer	1
Lockheed Propulsion Company P. O. Box 111 Redlands, California 92374 Attention: Miss Belle Berlad, Librarian	1
Lockheed Missiles & Space Company Propulsion Engineering Division (D. 55-11) 1111 Lockheed Way Sunnyvale, California 94087	1
Marquardt Corporation 16555 Saticoy Street Box 2013 - South Annex Van Nuys, California 91404 Attention: Librarian	1

	Copies
Martin-Marietta Corporation Martin Division Baltimore 3, Maryland Attention: John Calathes (3214)	1
McDonnell Douglas Corporation P. O. Box 6101 Lambert Field, Missouri Attention: R. A. Herzmark	1
North American Aviation, Inc. Space & Information Systems Division 12214 Lakewood Boulevard Downey, California 90242 Attention: Technical Information Center, D/096-722 (AJ01)	1
Northrop Space Laboratories 1001 East Broadway Hawthorne, California Attention: Dr. William Howard	1
Purdue University Lafayette, Indiana 47907 Attention: Technical Librarian	1
Radio Corporation of America Astro-Electronics Division Defense Electronic Products Princeton, New Jersey Attention: S. Fairweather	1
Republic Aviation Corporation Farmingdale, Long Island New York Attention: Dr. William O'Donnell	1
Rocket Research Corporation 520 South Portland Street Seattle, Washington 98108	1
Rocketdyne Division of North American Aviation, Inc. 6633 Canoga Avenue Canoga Park, California 91304 Attention: Library, Department 596-306	1
Rohm and Haas Company Redstone Arsenal Research Division Huntsville, Alabama 35808 Attention: Librarian	1

	Copies
Space-General Corporation 777 Flower Street Glendale, California Attention: C.E. Roth	1
Stanford Research Institute 333 Ravenswood Avenue Menlo Park, California 94025 Attention: Thor Smith	1
Thiokol Chemical Corporation Alpha Division, Huntsville Plant Huntsville, Alabama 35800 Attention: Technical Director	1
Thiokol Chemical Corporation Reaction Motors Division Denville, New Jersey 07834 Attention: Librarian	1
Thiokol Chemical Corporation Redstone Division Huntsville, Alabama Attention: John Goodloe	1
TRW Systems, Incorporated 1 Space Park Redondo Beach, California 90200 Attention: STL Tech. Lib. Doc. Acquisitions	1
TRW, Incorporated TAPCO Division 23555 Euclid Avenue Cleveland, Ohio 44117 Attention: P.T. Angell	1
United Aircraft Corporation Corporation Library 400 Main Street East Hartford, Connecticut 06118 Attention: Dr. David Rix Erle Martin	1 1
United Aircraft Corporation Pratt & Whitney Division Florida Research & Development Center P.O. Box 2691 West Palm Beach, Florida 33402 Attention: Library	1

	Copies
United Aircraft Corporation United Technology Center P. O. Box 358 Sunnyvale, California 94088 Attention: Librarian	1
Vought Astronautics Box 5907 Dallas 22, Texas Attention: Warren C. Trent	1